Centro de Investigación y de Estudios Avanzados del Instituto Politécnico Nacional

DEPARTAMENTO DE FÍSICA

Factor de forma de transición de $\pi°$ con dos multipletes de resonancias de mesones vectoriales dentro de la teoría de resonancias quirales y sus contribuciones a la parte de dispersión luz por luz hadrónica del $\alpha\mu$

Tesis que presenta

Emilio José Estrada González

para obtener el Grado de

Maestro en Ciencias

en la Especialidad de

Física

Director de tesis: **Dr. Pablo Roig Garcés**

Ciudad de México   Marzo, 2023

CENTRO DE INVESTIGACION Y DE ESTUDIOS AVANZADOS DEL INSTITUTO POLITECNICO NACIONAL

PHYSICS DEPARTMENT

"π° transition form factor with two multiplets of vector meson resonances within the resonance chiral theory and its contribution to the hadronic light by light piece of αµ"

Thesis submitted by

Emilio José Estrada González

In order to obtain the

Master of Science

degree, speciality in

Physics

Supervisor: **Dr. Pablo Roig Garcés**

Mexico City

March, 2023.

CINVESTAV

PHYSICS DEPARTMENT

PARTICLE PHYSICS GROUP

π^0 TRANSITION FORM FACTOR WITH TWO MESON RESONANCE MULTIPLETS WITHIN THE RESONANCE CHIRAL THEORY, AND ITS CONTRIBUTION TO THE HADRONIC LIGHT BY LIGHT PIECE OF a_μ.

Emilio José Estrada González

Advised by Dr. Pablo Roig Garcés

Ciudad de México, March of 2023

CINVESTAV

PHYSICS DEPARTMENT

π^0 TRANSITION FORM FACTOR WITH TWO MESON RESONANCE MULTIPLETS WITHIN THE RESONANCE CHIRAL THEORY, AND ITS CONTRIBUTION TO THE HADRONIC LIGHT BY LIGHT PIECE OF a_μ.

MASTER THESIS
PRESENTED TO THE HEAD OF
THE PHYSICS DEPARTAMENT
BY

EMILIO JOSÉ ESTRADA GONZÁLEZ
ADVISED BY DR. PABLO ROIG GARCÉS

TO BE GIVEN THE DEGREE OF
MASTER OF SCIENCE IN THE SPECIALITY OF PHYSICS

CIUDAD DE MÉXICO, MARCH OF 2023

ACKNOWLEDGMENTS

To Sandra, Rodolfo, José y Majo, for being my fortitude in every hardship that I have faced during the years far from you and my happy place where I have gone every time I have accomplished something.

To my grandparents, for the hard work and sacrifice in educating my parents, and the love you have shared with your grandchildren.

To my family, for being a constant in this world of variables, through the hard and the good times.

To Dr. Pablo Roig Garcés, for his invaluable advice since 2019, specially during this work and his dedication to his research and his students. And all of things I have learned from your passion and hard work.

To Ms. Mariana Del Castillo, for her help with all administrative matters which became even harder during the pandemic.

To all my professors at Cinvestav, for the commitment with our formation and all the academic and professional advice.

To the Physics Departament at Cinvestav, for their fidelity to excellence in research.

To Conacyt, for the systematic construction of a robust public education system in Mexico, both for nationals and foreigners.

To all my friends, (which I will not name one by one as the list of people who have lend me a hand during these years is large) for being there for me in the good and the hard times far from home.

To Dino, for all the love and complicity in this beautiful time we have shared.

To my undergraduate professors, who taught me well so I could be a good student and researcher in my further career.

To my Tae Kwon Do professors, for teaching me more than just kicking and screaming, but discipline and that day to day work sums up tremendously.

To all the scientists, because is your passion and your hard work which allows us, the young researches, to desire, one day, become scientists.

To Muno, Tita and Lucía.

Contents

Resumen

En este trabajo se abordó la contribución del polo de π^0 a la parte de dispersión luz por luz hadrónica de la anomalía a_μ. Esto a través del cálculo del factor de forma de transición de π^0 dentro del marco de teoría de resonancias quirales ($R\chi T$) con dos multipletes de resonancias vectoriales. Esto con el fin de reproducir los correctos comportamientos asintóticos predichos por cromodinámica cuántica (QCD por sus siglas en inglés). Uno de estos límites no es posible reproducirlo únicamente con un multiplete de resonancias vectoriales. El factor de forma de transición en $R\chi T$ queda expresado en terminos de los paramétros de los multipletes y combinaciones lineales de las constantes de acoplamiento de la teoría efectiva. Los parámetros se tomaron de trabajos previos y de la información disponible de las partículas involucradas (del PDG). Además se encontraron relaciones entre las constantes de acoplamiento a partir de las condiciones de corta distancia de QCD. Quedaron tres constantes de acoplamiento libres, de las cuales 2 estaban restringidas a valores específicos por los límites a altas energías y la otra fue ajustada a información experimental del factor de forma de π^0 con un fotón virtual (no existe información para dos fotones virtuales en el caso del π^0). Con esto se obtuvieron, de manera preliminar, cotas para el valor de $a_\mu^{HLbL:\pi-\text{pole}}$: $4.60 \pm 0.06 \leq a_\mu^{\pi^0-\text{pole},HLbL} \times 10^{10} \leq 6.26 \pm 0.09$. Este valor no es competitivo con las mejores determinaciones actuales dada la gran incerteza de nuestro resultado, pero se espera que esto mejore al realizar el mismo cálculo para $\eta - \eta'$. Estos casos sí poseen información para dos fotones virtuales, además de ser más sensibles a los datos (la supresión quiral es proporcional a la masa al cuadrado de los mesones pseudoescalares).

Abstract

In this work, the π^0-pole contribution to the hadronic light by light(HLbL) piece of the a_μ was addressed. This through the calculation of the π^0 transition form factor within the framework of Resonance Chiral Theory ($R\chi T$) with two multiplets of vector resonances. This was done with the purpose of reproducing the correct asymptotic behavior predicted by Quantum Chromodynamics (QCD). One of these limits could not be reproduced by a single multiplet of vector meson resonances. The transition form factor in $R\chi T$ is expressed in terms of the parameters that characterize the multiplets and linear combinations of the of the coupling constants of the effective field theory. The parameters were taken from previous work and from available information of the particles involved (from PDG). Besides, relations between the coupling constants were found by imposing the short distance constraints from QCD. Three constants remained free, which 2 of them were constrained to specific values for the high energy limits and the other one was fitted to available data of 1 virtual photon π^0-TFF (there is no information for doubly virtual photons in the π^0 case). Given this, in a preliminary way, bounds for the value of $a_\mu^{HLbL:\pi-\text{pole}}$: $4.60 \pm 0.06 \leq a_\mu^{\pi^0-\text{pole},HLbL} \times 10^{10} \leq 6.26 \pm 0.09$. This value is not competitive with the best accepted values given the big uncertainty of our result, but it is expected to improve after the same procedure for $\eta - \eta'$ is performed. These cases do have information for doubly virtual photons, also, they are more sensitive to data (the chiral suppression is proportional is proportional to the squared mass of pseudoscalar mesons).

List of Figures

List of Tables

Introduction

Particle Physics has described the fundamental interactions of nature with great success based on a construction made in the late 70's. This is the Standard Model of elementary particles (SM), which incorporates features from quantum field theory (QFT) and Group Theory. However, new challenges have emerged as high-energy physics faces a new precision era. These defiances come from different places: dark matter, matter-antimatter asymmetry of the universe, origin of neutrino masses and observables which differ significantly from the SM predictions.

In the latter is where this research comes into place. Since the beginning of this century, measurements of the gyromagnetic ratio of the muon (g_μ) indicated a discrepancy with the SM prediction. The first measurement of the 2000s was done at BNL [1], this resulting in a deviation of $2.6\,\sigma$ with respect to the SM, which was not enough for the anomaly to be confirmed. Because of this, both theoretical and experimental efforts were done in order to improve their precision. Two years ago, FNAL [2] improved the measurement, increasing the tension between theory and experiment to slightly more than 4 standard deviations. The precision of the experiment was so good, that it forced the theoretical efforts to go even further. This is the current stage of the muon g-2 research.

The main source of the theoretical error in g-2 comes from the hadronic contributions, since in contrast with electroweak (EW) interactions, QCD (for Quantum Chromodynamics, the gauge theory of strong interactions) is non-perturbative at low $(2m_\pi \leq E \leq 1$ GeV) and intermediate energies $(1$ GeV $\leq E \leq 2$ GeV). Because of this, an alternative description, valid in this regime, must be implemented. Due to confinement of the theory and the running of its coupling (giving rise also to asymptotic freedom) [3], gluons and quarks are not the degrees of freedom in nature, but the hadrons instead. Because of this, an effective field theory (EFT) for low and intermediate energies is implemented using hadrons as the interacting

fields. One approach is the so-called Chiral Perturbation Theory[4] (χPT) for low energies, and Resonance Chiral Theory[5] ($R\chi T$) for low and intermediate energies, which are based on the underlying symmetries of the fundamental QCD and the concept of EFT.

Among the two main hadronic contributions there is the hadronic light-by-light scattering (HLbL) and hadronic vacuum polarization (HVP). Within the first one, lays this research. The main contribution to HLbL is the one coming from the pseudoscalar-poles, which were previously calculated as pseudoscalar particle exchanges (see e. g. [6]). Later, the most important contribution to this process, was understood as the pseudoscalar-pole contribution (see, for instance, [7]). Both of them used the Transition Form Factor (TFF) of the pion within the framework of χPT (Chiral Perturbation Theory) with resonances (RχT).

In the last work mentioned, one multiplet of vector boson resonances was included as active fields. However, the form factor was underestimated at high energies, since the asymptotic behavior did not coincide with the one predicted by QCD at short distances (in one of the two relevant regimes). This can be fixed including two vector meson resonance multiplets as active fields. Performing this calculation is the aim of this work.

Computational methods were used for the development of this work. Our EFT, has infinite terms, so some of them must be truncated, and the mathematical structure of matter multiplets is non trivial, so the symbolical processing of expressions for obtaining the truncated Lagrangian up to the required accuracy, was performed in Wolfram Mathematica. The Feynman rules were obtained by this method too, but the kinematics for obtaining the amplitude were performed by hand. Latter, short distance constraints were applied by symbolical processing using the same tool and finally, the fit to experimental data and the numerical integration described in Chapter 6 were performed in Python 3.

The tools for calculation in this thesis are EFT, specifically χPT and RχT. As a consequence, concepts about the underlying fundamental theory (QCD) must be developed before proceeding with the calculation of the π pole contribution to the HLbL piece of a_μ. These are the first two chapters of the thesis, the first one deals with the basic concepts of QFT, symmetries and Gauge Theories, so the basis

are set for the construction of the SM, which is worked our in the latter chapter. The third and fourth chapters develop the theory and methods of the EFTs used in this work. The fifth chapter describes the calculation to be computed and the methods previously used. The sixth chapter addresses the calculation of the π-pole contribution, and develops the methodology for LMD+V computation on ref. [7]. The last chapter describes in detail the calculation of π-TFF with two multiplets of vector meson resonances and preliminary bounds for a_μ in this scheme were found. The bounds found are $4.60 \pm 0.06 \leq a_\mu^{\pi^0-\text{pole},HLbL} \times 10^{10} \leq 6.26 \pm 0.09$, consistent with previous calculations [6, 7, 8, 9, 10, 11, 12] but with too large error for the moment.

The obtained value for the π-pole contribution to the HLbL piece of a_μ is still preliminary, since only one parameter was fitted from the 5 unfixed. Furthermore, the calculation for $a_\mu^{\pi^0-\text{pole},HLbL}$ is not complete in this thesis, as the computation of $\eta - \eta'$-TFFs are required for the calculation of coupling constants which cannot be obtained reliably from the π-TFF, because of chiral suppression and lack of experimental data issues which are going to be solved in the $\eta - \eta'$ case.

1. Theoretical Background

The calculations to be performed in this work are constructed based on the symmetries of QCD, so, in order to understand how this is done, theoretical basis must be set for this thesis to be understandable. For this purpose, a pedagogical example is worked out, QED. Then, concepts which will be used in more complicated theories, are explained within the theory of electromagnetic interactions. Later, the relevant concepts of symmetries are mentioned and connected with physics of fundamental interactions. Finally, with all this explained, Gauge Theories (the cornerstones for the construction of fundamental interactions, based on symmetry principles) are developed.

1.1   QED: a simple QFT

All the physics of an interaction is described by its Lagrangian density. In the case of QED, this Lagrangian contains matter fields (fermions) and interaction bosons (the photon)[13].

$$\mathcal{L} = \bar{\psi}(x) \left(i\slashed{D} - m \right) \psi(x) - \frac{1}{4} F^{\mu\nu}(x) F_{\mu\nu}(x), \tag{1.1}$$

where $\psi(x)$ and $\bar{\psi}(x)$ are the fields annihilating fermions and anti-fermions (and creating the corresponding antiparticles), with mass m and unit charge (like the electron), the photonic field is A^{μ}, which appears both in D_{μ} and in $F^{\mu\nu}$ in the following way:

$$D_{\mu} = \partial_{\mu} - ieA_{\mu}, \ \ F^{\mu\nu} = \partial^{\mu} A^{\nu} - \partial^{\nu} A^{\mu} . \tag{1.2}$$

The Lagrangian in eq. (1.1), gives rise to the kinetic terms for both the photon and the fermions, and the interactions between fermions and photons. This can be summarized in the Feynman diagrams for propagators and the vertex of QED:

(a)   **(b)**   **(c)**
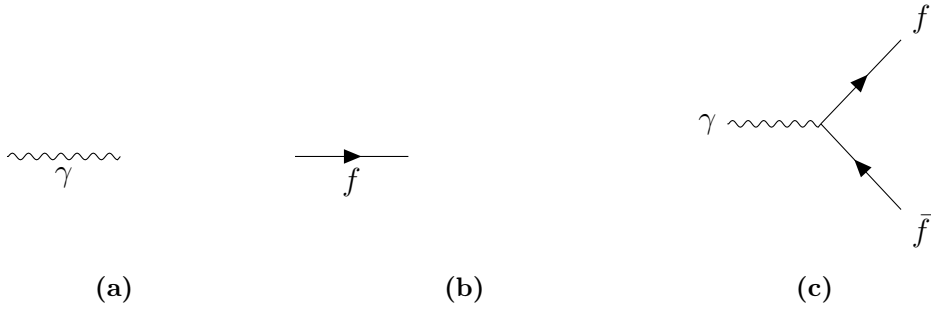
Figure 1.1. Feynman diagrams for QED: **(a)** is the photon propagator, **(b)** is the fermion propagator and **(c)** is the interaction vertex.

This is enough to construct a quantum theory for electromagnetic interactions. Its study gives rise to understanding different processes, some of the most important ones are:
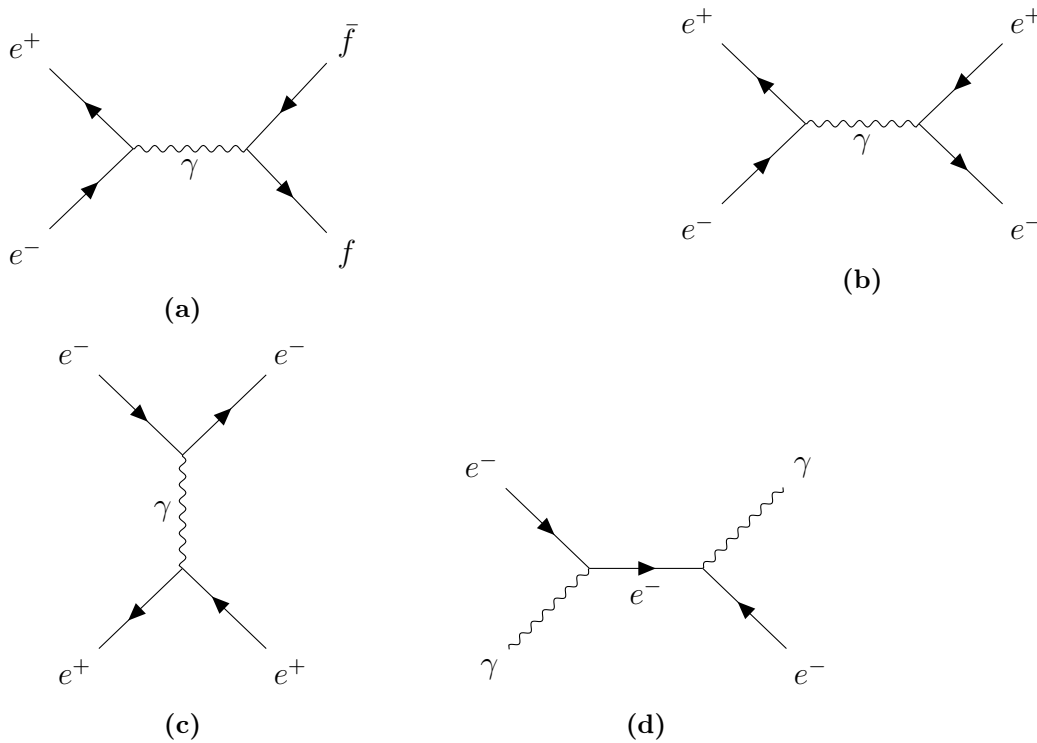
Figure 1.2. Feynman diagrams for simple QED processes: **(a)** is a general pair annihilation $e^+e^- \to f\bar{f}$ for $f \neq e$, **(b)** and **(c)** are the contributions at tree level for the Bhabha scattering, being these in the s and u channels, and **(d)** is the known Compton scattering.

These are the basics for QED, in the next sections, important concepts for the construction of a fundamental and an EFT theory will be developed from this pedagogical example.

1.1.1 Second Quantization in QED

The second quantization of QED [1] is given by raising the electromagnetic fields for electrons and photons to operators:

$$\psi(x) \to \hat{\psi}(x), \quad A_\mu(x) \to \hat{A}_\mu(x). \tag{1.3}$$

After this promotion, commutation relations can be constructed for the fields similar to the ones between $\vec{x}$ and $\vec{p}$ in quantum mechanics. For this construction, two features lead the procedure: the resulting Hamiltonian has to be bounded from below, and the commutation relations have to respect the spin-statistics theorem [14] (actually causality leads to the spin-statistics theorem in quantum field theory). This can be achieved by the following fields in terms of the creation and annihilation operators:

$$\hat{\psi}(x) = \int \frac{d^3\mathbf{k}}{(2\pi)^3 \sqrt{2\omega}} \sum_{s=1,2} \left[\hat{c}_s(k) u(k,s) e^{-ik\cdot x} + \hat{d}_s^\dagger(k) v(k,s) e^{ik\cdot x} \right], \tag{1.4}$$

where u and v are the spinorial solutions for particle and antiparticle and $\hat{c}_s^\dagger(k)$ and $\hat{d}_s^\dagger(k)$ are the creation operators of fermionic particles and antiparticles of polarization s and momentum k. For the spin-statistics connection to be obeyed, anti-commutation relations are constructed between creation and annihilation operators for both particles and antiparticles. This leads to anti-commutation relations between the field operator and its conjugated momenta. We will not go further into this discussion since all the development of the theory leads to the widely known Feynman rules of QED.

For the electromagnetic mediator, the photon, the degree of freedom is the field $\hat{A}_\mu$ which obeys commutation relations and it is described by:

$$\hat{A}^\mu = \int \frac{d^3\mathbf{k}}{(2\pi)^3 \sqrt{2\omega}} \sum_\lambda \left[\varepsilon^\mu(k,\lambda) \hat{\alpha}(k,\lambda) e^{-ik\cdot x} + \varepsilon^{*\mu}(k,\lambda) \hat{\alpha}^\dagger(k,\lambda) e^{ik\cdot x} \right], \tag{1.5}$$

where ε^μ is te polarization vector and $\hat{\alpha}^{(\dagger)}$ is the creation (annihilation) operator. With this description constructed, Feynman rules can be obtained. The building blocks for the computation of the amplitudes of different processes are the Feynman rules for incoming and outgoing particles, propagators and for the vertex in Figure

---

[1]This is a historical, although bad (as it can be misleading, unless one reminds it came from the transition from Quantum Mechanics) name. From the point of view of quantum field theory there is only one quantization.

1.1. Many processes as the ones in Figure 1.2 can be addressed with this formalism which has shown to be highly precise and accurate.

1.1.2 Form Factors in QED

For the diagrams of processes in Figure 1.2 Feynman rules give us their contributions, however, the diagrams shown are just the dominant part of the amplitude. There are more contributions to them, which are suppressed as the coupling constant is much less than 1. These suppression can be arranged by number of loops (which is equivalent to an expansion in powers of the coupling). For example, in the pair annihilation of Figure 1.2, 1 loop corrections to this process are shown in Figure 1.3(the loop in one of the external fermions appears in any of the 4 external particles).

Form factors can be understood from this example, since all different contributions can be summed up into a blob, as it is observed in Figure 1.4. Form factor in this case, describes the interactions of the process $e^+e^- \to \bar{f}f$ considering all possible contributions. In the case of QED, since it is a perturbative quantum field theory, all contributions can be computed, and the sum of all contributions will give us the expression for the blob vertex. However, as the problem becomes harder for other QFTs (non perturbativity, diversity of structures in different diagrams), symmetries can be used to predict the different structures appearing in the blob and experimental data can be used to get the coefficients for each contribution.

1.2 Lie Groups, Lie Algebras and Symmetries

Lie groups, algebras and symmetries are tightly related, and they are the building blocks for the systematic construction of any quantum field theory, which is why it is important to mention some important properties of them. First of all, a group G is a set of elements $g \in G$ which fulfills the following conditions [13]:

- the group has an associative multiplication law $\circ$, under which $g_1 \circ g_2 = g_3$, such that $g_1, g_2, g_3 \in G$ and is associative under that multiplication law: $g_1 \circ (g_2 \circ g_3) = (g_1 \circ g_2) \circ g_3$.

- the group has an identity element $I \in G$ under the multiplication law, such that $I \circ g = g \circ I = g$, $g \in G$.
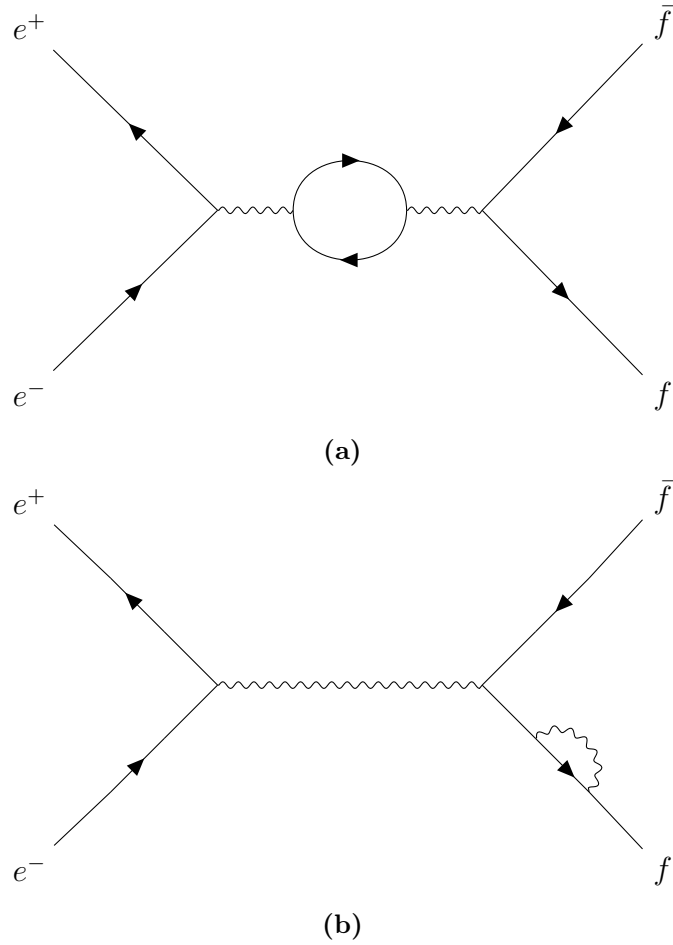
Figure 1.3. Feynman diagrams for simple two types of QED corrections to pair annihilation: **(a)** a fermion loop in the photon propagator, **(b)** a photon-fermion loop in one of the external particles.
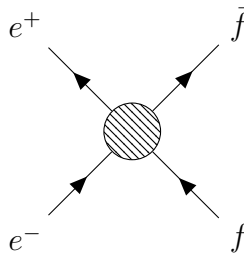
Figure 1.4. Effective interactions (including possible form factor) of $e^+e^- \to \bar{f}f$.

- there is an unique inverse element $g^- \in G$ for each $g \in G$ under the multiplication law, such that $g^- \circ g = I$.

The group does not require commutativity under the multiplication law, but if the group does satisfy it, it is called an abelian group. In case it does not, it is called a

5

non-abelian group. Also, the groups can be separated in discrete and continuous.

1.2.1 Lie Groups and Algebras

A Lie group is a continuous group for which the multiplication law involves differentiable functions of the parameters which label the group element. This characteristic, allows us to connect all elements of the group to the identity trough infinitesimal transformations (which can be connected by adding up those into finite transformations). The infinitesimal transformations are linear combinations of the basis, which are called *Generators of the group*. The generators of the group define both infinitesimal transformations and the algebra of the group itself, which is described by the generators and its commutation relations. Some example of groups are:

- N-Dimensional Special Orthogonal Group ($SO(N)$): the group of real orthogonal N×N matrices ($O \times O^T = \mathbb{1}$) with determinant 1. This group is $N(N-1)/2$ dimensional.

- one dimensional unitary group (U(1)): the group of all phase shifts of module 1. This group is one dimensional.

- N-Dimensional Special Unitary Group ($SU(N)$): this is the most used group in physics, the algebra of any angular momenta is described by SU(2). This is the group of complex unitary N×N matrices of determinant one. This group is of dimension $N^2 - 1$.

Another concept that will become handy is that of a representation of the group. A representation of the group is a map between all elements of the group into matrices, such that the matrix multiplication between the elements in the representation reproduces the multiplication table obtained from the multiplication law ∘ given in the definition of the group.

1.2.2 Symmetries

Symmetries in physics can be split in continuous and discrete. Continuous symmetries are related with Lie groups and Lie algebras, since matter is written in different representations of diverse symmetry groups. This allows us to relate symmetries of nature to group structures. This means that if we impose a symmetry on a system, its dynamics is defined by which singlets (or higher-dimensional representations) we can construct with the different representations of matter. Symmetries can be

6

global (independent of space-time parameters) or local (functions of space-time parameters).

1.3   Gauge Theories

Gauge Theories are based on a local symmetry. The general procedure for constructing a gauge theory is to impose a global symmetry, construct the most general Lagrangian compatible with the symmetries and then promote it to a local symmetry by absorbing the remaining terms of the local transformation(usually coming from the derivative of the local parameters) into gauge bosons, which will now mediate the interactions. In a simple sense, if we get the symmetry and the matter, we get the interactions and the mediators, which means, we get the dynamics. This can be performed systematically for the construction of any quantum field theory (sometimes the procedure is not straightforward and may require the spontaneous symmetry breaking of the gauge symmetry, in such a way that the symmetry of the vacuum is a sugbroup of the Lagrangian symmetry).

1.3.1   Abelian Gauge Theories

An abelian gauge theory is the easiest way to introduce the topic, and we have done so already. In eq. (1.1), the Lagrangian is already gauged, as the covariant derivative $\slashed{D}$ is a transformation of the derivative $\slashed{\partial}$. This Lagrangian is an U(1) symmetric one, if we transform the fermionic field by

$$\psi \to e^{i\alpha}\psi, \tag{1.6}$$

the Lagrangian is invariant, but if instead of α, we use $\alpha(x)$, the Lagrangian is only invariant under this transformation when the electromagnetic field A_μ as in eq. (1.2) and transforms in such way that absorbs the terms coming from the derivative of $\alpha(x)$.

1.3.2   Non-Abelian Gauge Theories

Non-abelian gauge theories in general have a more complicated structure than just a phase transformation. Examples of them are the most commonly used in physics, SU(2) and SU(3). About SU(3) we will talk about in further chapters so we will focus for this short discussion on SU(2).

SU(2) is the algebra that defines all angular momenta. As already mentioned, SU(2) has 3 generators, which obey the commutation relations (with structure constants proportional to the Levi-Civita symbol):

$$[T_i, T_k] = i\varepsilon_{ijk}T_k. \tag{1.7}$$

Furthermore, The Standard Model of Elementary Particles which is split in 3 fundamental interactions, has an SU(2) part, which is the one that combined with U(1) becomes the Electroweak Theory.

Another important feature of non-abelian gauge theories is that -as it was proved by ref. [3]- just these theories can reproduce the asymptotic freedom behavior observed in strong interactions.

2. The Standard Model, $SU(3)_C \otimes SU(2)_L \otimes U(1)_Y$

In this chapter, we give a brief description of the Standard Model of elementary particles with emphasis on the relevant pieces of it for this work. In the first section, we will mention the Electroweak Theory and some of its main features: an EFT for electroweak processes, the gauge group of the theory, and a short example complement the discussion on form factors from the first chapter. In the second section, we will introduce the Higgs mechanism and develop the most relevant characteristics for χPT and RχT. In the third section, we will discuss QCD, the fundamental theory of strong interactions, which are of the main interest for our work. QCD has a lone candidate for describing the phenomenology, $SU(3)_C$. Within this phenomenology lies the asymptotic freedom, which can be described with the beta function. As in EW theory, form factors are found in QCD (mostly here than anywhere else), so we will mention them briefly in the context of QCD. Finally, some words about loop calculation are mentioned, which will be helpful for the development of future chapters.

2.1 Electroweak Theory

Electroweak interactions are the ones responsible for the radioactive decay of some elements in nature in the process known as beta decay (or β-decay). This process was first observed by Henri Becquerel in 1896. Later observations came which gave intuition of a different kind of interactions which was not electromagnetism. The discovery of neutron and proton opened a gate into these interactions, a deeper understanding of it could be awaited since protons and neutrons were the components of the decaying nuclei in radioactive decays. With more fundamental particles to study these decays, non-conservation of energy and momentum arose, which was inconsistent with all developed physics till that point of history. For the purpose of avoiding this problem, Wolfgang Pauli proposed in 1932 the existence of a new particle, the neutrino (ν), which was responsible of the missing energy and momentum

(and of restoring the spin-statistics connection). 21 years later, in 1953, Reines and Cowan reported experimental evidence of its existence. With this discovery, β-decay was understood with the Fermi theory as the process sketched in Figure 2.1.
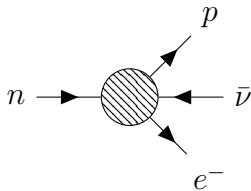
Figure 2.1. Fermi theory diagram for β-decay: $n \to pe^-\bar{\nu}$.

New observations lead to successful modifications, such that the theory was compatible with them: parity violation, V-A theory, lepton decays, strangeness violation, the quark model, quark mixing (CP violation). However, violation of unitarity at high energies lead to the idea that the Fermi theory was an effective theory and that, inside the blob, there was more information. Therefore, the theory of the intermediate vector boson (IVB) emerged (see fig. 2.2).
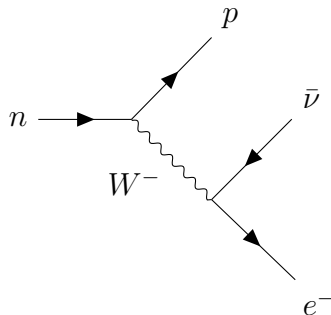
Figure 2.2. IVB diagram for β-decay: $n \to pe^-\bar{\nu}$.

However, the unitarity violation persisted. There was a way out, if an electrically neutral massive boson W^0 (today called Z^0) was added, the bad energy behavior could be canceled. The algebra of the currents (including the new neutral current) was the one of $SU(2)$, so a gauge invariant theory could be written, which, with the help of the Higgs mechanism, could be compatible with observations. At the same time, there was no room for QED, so the theory was extended to $SU(2) \times U(1)$. Finally, charged weak current processes were measured, so the result was a successful theory for weak and electromagnetic interactions [13].

2.1.1 An EFT for the nuclear β decay

As we mentioned before, the nuclear beta decay suggested the necessity of a complementary theory which described the β decay. This process corresponded to the ejection of electrons from an atomic nucleus [15] $(N, Z) \to (N - 1, Z + 1)e^-$. The continuous spectrum of the electron suggested an 1 to 3 process instead of a two-body decay, so W. Pauli proposed the particle that E. Fermi later called the neutrino (ν). Since no further information was known about the fundamental process that lead to this one, Fermi proposed a general 4-fermion interaction as it is seen in eq. (2.1). An effective field theory for the electroweak interactions had started to emerge. The theory of weak interactions became richer with strangeness violating processes, as

$$K^0 \to \pi^+\pi^-, \qquad K^0 \to \pi^+\pi^-\pi^0, \tag{2.1}$$

which presumably added parity violation to the theory, since the final states have $P = +1$ and $P = -1$, respectively. Lee and Yang proposed then the weak interaction as a new fundamental one [16]. Later, experimental evidence of this statement was given [17], the observation that weak interaction did not just violate parity but did it maximally, gave rise to the V-A theory. Such a framework proposed that all weak interactions could be derived from a current-current $(j \times j)$ interaction of the form:

$$\mathcal{M} = \left\langle \frac{4G_F}{\sqrt{2}} j_L^\mu j_{\mu L} \right\rangle, \tag{2.2}$$

where the fermion currents were given by νe and u, d left-handed pieces

$$j_L^\mu = \bar{\nu}_L \gamma^\mu e_L + \bar{u}_L \gamma^\mu d_L + \text{h.c.}$$

Later (as mentioned at the beginning of this section), a deeper understanding of the fundamental interaction was sought, and with it, a more formal description of them: The Standard Electroweak Theory. It is the intention of this section to stress that even though a fundamental description is the ideal procedure to study the phenomenology of any interaction, an EFT is an useful tool which can reproduce the experimental data, but can be used too to predict yet unobserved phenomena.

2.1.2 The Gauge Group $SU(2)_L \otimes U(1)_Y$

The Standard Model is based on the gauge group $G = SU(3) \times SU(2) \times U(1)$. The EW sector (SU(2) $\times U(1)$), has different representations for left and right chiralities

of particles. The description of one family of quarks can be reproduced to study the three of them, and the lepton sector as well. So, in general, the representations of fermions in the theory are:

$$\phi_1(x) = \begin{pmatrix} u \\ d \end{pmatrix}_L, \qquad \phi_2(x) = u_R, \qquad \phi_3(x) = d_R, \tag{2.3}$$

which means that the left-hand particles do interact under the $SU(2)$ sector and the right-handed particles do not; also, their representation under $U(1)$ is a singlet, characterized by their weak hypercharge. With these representations, the most general Lagrangian can be built, so that it is invariant under global transformations of the EW group:

$$\mathcal{L} = \sum_{j=1}^{3} i\bar{\phi}_j(x)\gamma^\mu \partial_\mu \phi_j(x). \tag{2.4}$$

For the interactions to happen, the global symmetry needs to be promoted to a local one, according to the gauge principle. For this purpose, the theory requires one boson per each generator of the theory, so that the covariant derivatives have the correct behavior under local transformations:

$$D_\mu \phi_1(x) = [\partial_\mu + ig\frac{\sigma_i}{2}W_\mu^i(x) + ig'y_1 B_\mu(x)]\phi_1(x),$$
$$D_\mu \phi_2(x) = [\partial_\mu + ig'y_2 B_\mu(x)]\phi_2(x),$$
$$D_\mu \phi_3(x) = [\partial_\mu + ig'y_3 B_\mu(x)]\phi_3(x). \tag{2.5}$$

The gauging of the symmetry (making it local) gave rise to the interactions, as we intended. An important feature of this group is that it is non-abelian (their generators do not commute), so 3- and 4-boson interactions are predicted by the theory. Another important feature is the fact that it is not W^0 (or W^3) related to Z^0, nor B to γ, but a combination of them: the weak eigenstates B and W^3 mix to yield the physical (mass eigenstates) γ and Z^0 states.

2.1.3 Form Factors in EW theory

Form factors can be found within the EW theory, as they describe what we cannot say from tree level interactions. For example, when considering higher order effects in the interaction of a fermion with light: The tree level contribution is easily calculated from the Feynman rules of QED. The whole interaction: tree level, one loop and higher order corrections, can be considered into a single effective vertex, which
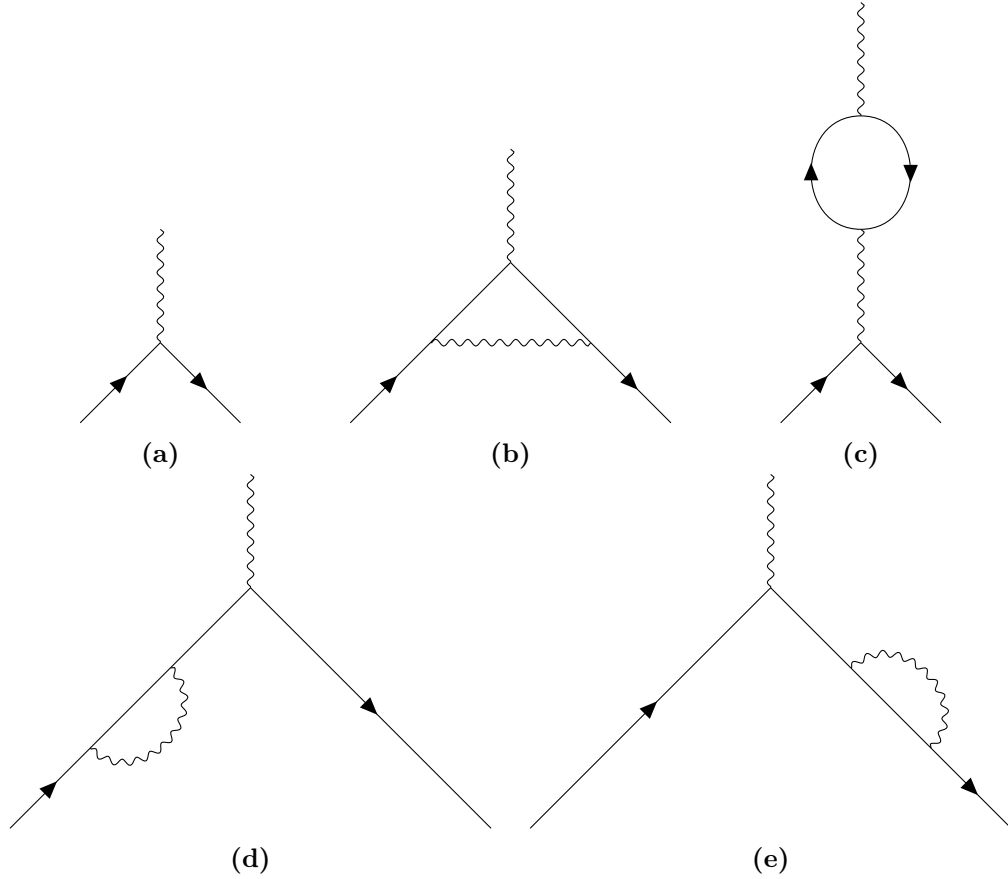
Figure 2.3. Feynman diagrams for fermion interaction with light: **(a)** is the tree level interaction, **(b)-(e)** are the one-loop corrections to this process.

Lorentz structure can be predicted based on the symmetries of the theory.
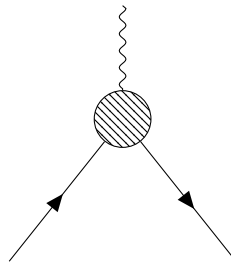
Figure 2.4. Effective interaction of a fermion with a photon.

From QED, it is known that the general structure of the amplitude is:

$$\bar{u}_2 \Gamma^\mu(p1, p2) u_1, \tag{2.6}$$

where u_1 is the incoming fermion's spinor, and $\bar{u}_2$ is the outcoming. The link between them is the most general Lorentz structure that can be constructed using $(p1, p2)$.

Since γ is a vector boson, the structure has to be a Lorentz vector. Gordon's decomposition indicates that it is enough to consider the combination $p_{1(2)}^{\mu}$ with γ's momentum, q^{μ}[18]. Since QED is reflection invariant, just 3 structures can be constructed, so the most general amplitude compatible with the symmetries of the theory is:

$$\bar{u}_2 \Gamma^{\mu}(p1, p2)u_1 = \bar{u}_2 \left[\gamma^{\mu} F_1(q^2) + \frac{i\sigma^{\mu\nu}}{2m} q_{\nu} F_2(q^2) + q^{\mu} F_3(q^2) \right] u_1, \qquad (2.7)$$

where the $F_{1,2,3}$ are called form factors. They can be computed in some cases, but in those where we cannot calculate them from the fundamental theory, the behavior, or the relevance of the different compatible structures at different energies can still be studied, as it happens in QCD.

The first form factor is the one related with charge conservation, the second one is related with light interaction with fermions (giving rise to the magnetic dipole moment, of maximum interest in this thesis) and both can be calculated from perturbation theory [1].

2.2 Higgs Mechanism

The Higgs mechanism gives mass trough weak interactions to elementary particles, it is the interaction with the Higgs' vacuum which gives a non-zero mass, while keeping the theory gauge-invariant[18]:
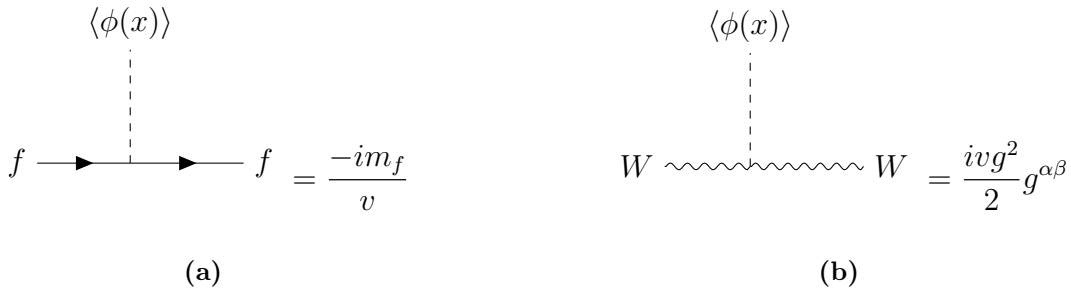
Figure 2.5. Feynman diagrams for mass terms of fermions and bosons: **(a)** is the interaction diagram and term for fermions and antifermions and **(b)** is the one for weak bosons, where $\langle \phi(x) \rangle \propto v$ is the v.e.v. of the Higgs boson (~ 246 GeV), and g is the weak coupling.

Since part of the Z and W belong to the mass-generating mechanisms (their longitudinal polarizations), their masses are related by a mixing parameter, weak-

---

[1]The third structure trivially vanishes for a real photon.

mixing or Weinberg's (although introduced by Glashow) angle (θ_W):

$$M_W^2 = \frac{1}{4}v^2 g^2, \qquad M_Z^2 = \frac{M_W^2}{cos\theta_W}. \tag{2.8}$$

This mechanism is important for EW theory's consistency and its success was one of the main theoretical particle physics achievements [19].

2.2.1 Spontaneous Symmetry Breaking

The Higgs mechanism is based on the spontaneous symmetry breaking (SSB) of a local continuous symmetry. The SSB is realized when the ground state of a dynamical system is degenerated. The degeneration is what allows to perform the expansion of the system's solutions around any choice of the ground state. The new dynamical field does not have the original symmetry. However, the original symmetry still holds since the physics is invariant under the choice of ground state [20].

As an illustrative example, we will consider a massless complex scalar field. The Lagrangian of this dynamical field is:

$$\mathcal{L}(x) = \partial^\mu \phi(x)^* \partial_\mu \phi(x) - \mu^2 \left| \phi(x) \right|^2 - \lambda \left| \phi(x) \right|^4, \qquad \phi(x) = \phi_1(x) + i\phi_2(x). \tag{2.9}$$

This Lagrangian has a $U(1)$ symmetry, since it remains unchanged as $\phi(x) \to e^{i\alpha}\phi(x)$. The potential of this Lagrangian is:

$$\mathcal{V}(x) = \mu^2 \left| \phi(x) \right|^2 + \lambda \left| \phi(x) \right|^4, \tag{2.10}$$

and for it to be bounded from below, $\lambda > 0$ is enough. For it to fulfill the requirement of degeneracy, we need $\mu^2 < 0$. For this case, the global minima full set is parametrized by:

$$\phi(x) = \phi_0 = \left(\frac{-\mu^2}{2\lambda} \right)^{1/2} e^{i\theta} = \frac{1}{\sqrt{2}}v e^{i\theta}, \qquad 0 \le \theta < 2\phi. \tag{2.11}$$

SSB is realized when an specific value of θ is chosen. If we choose ϕ_0 to be real, we can expand the excitations of the dynamical field as $\sigma(x)$ and $\eta(x)$ so that $\phi(x) = \frac{1}{\sqrt{2}}(v + \sigma(x) + i\eta(x))$. The new quadratic terms of the Lagrangian in this parametrization are:

$$\mathcal{L}_0(x) = \frac{1}{2}\partial^\mu \sigma(x) \partial_\mu \sigma(x) - \frac{1}{2}(2\lambda v^2)\sigma^2(x) + \frac{1}{2}\partial^\mu \eta(x) \partial_\mu \eta(x), \tag{2.12}$$

the cubic and quartic terms give interactions, which are not invariant under $\phi(x) \to e^{i\alpha}\phi(x)$. The theory is then said to be spontaneously broken. The field $\sigma(x)$ acquired a non-zero mass and the field $\eta(x)$ is a massless field, about which we continue discussing in the next section.

2.2.2   The Goldstone Theorem

The U(1) globally invariant case is a rather simple example of Goldstone's theorem: "When SSB is realized for a theory which has a global continuous symmetry with N generators, and n of them are broken in the process, n massless spin-0 bosons emerge". These massless spin-0 bosons are the so called *Nambu-Goldstone bosons*. A more general construction of the theorem can be done. So let us start from a theory which is invariant under transformations of a continuous group G with N generators T_k:

$$g \in G: \ \vec{\boldsymbol{\Phi}}(x) \mapsto e^{-i\sum_{k=1}^{N} a_k T_k} \vec{\boldsymbol{\Phi}}(x) \approx \left(1 - i\sum_{k=1}^{N} a_k T_k\right) \vec{\boldsymbol{\Phi}}(x). \qquad (2.13)$$

If we now consider that SSB occurs, such that the v.e.v of $\vec{\boldsymbol{\Phi}}(x)$ remains invariant under the subgroup H of G. Then, an expansion of $\mathcal{V}(x)$ is performed around the choice of vacuum $\vec{\boldsymbol{\Phi}}_{min}$,

$$\mathcal{V}(\vec{\tilde{\boldsymbol{\Phi}}}) = \vec{\boldsymbol{\Phi}}_{min} + \frac{\partial\left(\vec{\boldsymbol{\Phi}}_{min}\right)}{\partial\boldsymbol{\Phi}_i}\chi_i + \frac{1}{2}\frac{\partial^2\left(\vec{\boldsymbol{\Phi}}_{min}\right)}{\partial\boldsymbol{\Phi}_i\partial\boldsymbol{\Phi}_j}\chi_i\chi_j + ..., \qquad (2.14)$$

where χ_i are the degrees of freedom after the expansion. We can notice that the second term vanishes form the minimum condition and that the matrix term with second derivatives (excluding the $\frac{1}{2}$ factor) is the mass matrix element M_{ij}^2. If we evaluate it for $\vec{\boldsymbol{\Phi}}_{min}$ and use the last expression in (2.14) to substitute it in (2.15), and differentiate with respect to $\boldsymbol{\Phi}_j$, we find the vector equation:

$$M^2 T_k \vec{\boldsymbol{\Phi}}_{min} = \vec{0}. \qquad (2.15)$$

From here, Goldstone's theorem can be read: for the $N - n$ unbroken generators, $T_{unbroken,k}$, eq. (2.16) is automatically satisfied. However, for the n broken ones, $T_{broken,k}$, each of the vectors $T_{broken,k}\vec{\boldsymbol{\Phi}}_{min}$ is an eigenvector of M^2 with zero eigenvalue. This is Goldstone's theorem: for each broken generator, there is a zero eigenvalue of the mass matrix.

2.2.3 Explicit Symmetry Breaking

When the symmetry is not exact, symmetry breaking appears as small terms in the Lagrangian which set the scale of the symmetry breaking. The Nambu-Goldstone bosons acquire a mass term proportional to the scale of the symmetry breaking and are called Pseudo-Goldstone bosons, or PGb for short. Let us take a simpler discrete case to illustrate the point, a reflection invariant $(\vec{\phi}(x) \rightarrow -\vec{\phi}(x))$ three component real scalar field, with an explicit symmetry breaking with scale a:

$$\mathcal{L}'(x) = \partial^\mu \vec{\phi}(x) \cdot \partial_\mu \vec{\phi}(x) - m^2 \left|\vec{\phi}(x)\right|^2 - \lambda \left|\vec{\phi}(x)\right|^4 - a\phi_3(x), \qquad (2.16)$$

this Lagrangian is clearly non-invariant under a reflection transformation. The vacuum of the theory is modified by the $a\phi_3(x)$ term:

$$\langle\phi_3\rangle_\pm = \pm\sqrt{-\frac{m^2}{\lambda} + \frac{a}{2m^2}}. \qquad (2.17)$$

If we perform an expansion around $\langle\phi_3\rangle_+$, we obtain the masses:

$$m^2_{\phi_1} = m^2_{\phi_1} = a\sqrt{-\frac{\lambda}{m^2}}$$
$$m^2_{\phi_3} = -2m^2 + 3a\sqrt{-\frac{\lambda}{m^2}}, \qquad (2.18)$$

in the SSB case, $m^2_{\phi_{1(2)}}$ would be zero since 2 generators got broken. However, the explicit symmetry breaking, induced a mass term proportional to the symmetry breaking scale a [20].

2.3 Quantum Chromodynamics

Quantum Chromodynamics is the fundamental theory for strong interactions. In the mid 60's, it was both theoretically and experimentally hard to work on the topic, since all the observed particles are "colorless", they are singlets under the gauge group. So, why it is necessary to talk about a force for which all asymptotic states are invisible to it? It is because the constituents of composite particles as protons and neutrons are not blind to this force, and so, they do interact strongly. Considering the fact that they interact but are confined inside the nucleons (and some other particles too), very high-energy processes should be studied in order to see the effects of this force. An example of this need is the experimental ratio be-

tween $e^-e^+ \rightarrow \mu^-\mu^+$ to $e^-e^+ \rightarrow$ hadrons, which is sensitive to N_C and verifies that $N_C = 3$. Also, spin $\frac{1}{2}$ particles in the fundamental representation and the conjugate representation can form bounded colorless integer spin particles (bosons) and three spin $\frac{1}{2}$ particles in the fundamental representation can form bounded colorless semi-integer spin particles (baryons) [21].

This success was both experimental and theoretical, and came in several pieces. First the Feynman's parton model proposed that nucleons were constituted by smaller spin $\frac{1}{2}$ point-like particles which carry part of the nucleon's momenta (evidence of this statement was found in Deep Inelastic Scattering experiments) [13], then the quark model appeared, which correctly predicted magnetic moments of nucleons; however, it predicted the existence of both quarks and gluons which were not detected directly [21]. Indirect evidence for quarks and gluons eventually appeared and the theory was "complete", except for the fact that elementary particles of the theory are not seen free (confinement) and that at very high energy, they behave as free particles (asymptotic freedom), these two facts were major issues because the fundamental theory was of no practical use as seen from QFT [22], since perturbation theory could not be used for calculations in some energy regimes.

2.3.1 QCD Lagrangian

Even though perturbation theory cannot be used for some calculations, the QCD Lagrangian can be used to construct an EFT based on the symmetries of the underlying theory and the degrees of freedom of the effectively interacting particles (mesons and baryons), which can instead be used in these troublesome energy regimes. The $SU_C(3)$ locally invariant Lagrangian is (neglecting gauge-fixing and ghost terms):

$$\mathcal{L}_{QCD} = -\frac{1}{4}G^i_{\mu\nu}G^{\mu\nu i} + \sum_r \bar{q}^{\alpha}_r i \not{D}^{\beta}_{\alpha} q_{r\beta} - \sum_r m_r \bar{q}^{\alpha}_r q_{r\alpha} + \frac{\theta_{QCD}}{32\pi^2} g_s^2 G^i_{\mu\nu}\tilde{G}^{\mu\nu i}, \quad (2.19)$$

where the r index runs over the six quark flavors, α runs over three colors and i runs over the eight gauge bosons, the gluons; g_s is the strong interactions coupling and the field strength tensor is given by:

$$G^i_{\mu\nu} = \partial_\mu G^i_\nu - \partial_\nu G^i_\mu - g_s f_{ijk} G^j_\mu G^k_\nu, \quad (2.20)$$

where the quark gauge covariant derivative is:

$$D_\alpha^{\mu\beta} = \partial^\mu \delta_\alpha^\beta + \frac{ig_s}{\sqrt{2}} G_\alpha^{\mu\beta}, \tag{2.21}$$

with

$$G_\alpha^\beta = \sum_{i=1}^8 G^i \frac{\lambda_\alpha^{i\beta}}{\sqrt{2}}, \tag{2.22}$$

and λ^i are the eight hermitian generators of $SU(3)_C$.

2.3.2   Beta Functions

An important feature which enables $SU(3)_C$ to match the phenomenology (confinement and asymptotic freedom) is the Beta Function of QCD. The running of the coupling of any interaction is given by its beta function

$$\frac{dg^2}{d\ln Q^2} = 4\pi\beta g^2 = bg^4 + O(g^6) + ..., \tag{2.23}$$

where g is the coupling of the theory and Q^2 is the scale of the experiment. The b coefficient is given by

$$b = -\frac{1}{(4\pi^2)} \left[\frac{11}{3} C_2(G) - \frac{4}{3} T_F - \frac{1}{3} T_{\phi_c} - \frac{1}{6} T_{\phi_h} \right], \tag{2.24}$$

where $C_2(G)$ is the quadratic Casimir of the group, for $SU(N)$ is just N except for $N = 1$ where it is zero. T_F, T_{ϕ_c}, and T_{ϕ_h} are the fermion, complex scalar and hermitian scalar Dynkin indices. It turns out that for $SU(3)_C$

$$b = \frac{2n_q - 33}{48\pi^2}, \tag{2.25}$$

where n_q is the number of active quark fields (they become active as the energy is enough to produce them), so at any value of n_q, b is negative, resulting in asymptotic freedom

$$\frac{1}{\alpha_s(Q^2)} = \frac{1}{\alpha_s(M^2)} + \frac{33 - 2n_q}{12\pi} \ln \frac{Q^2}{M^2}. \tag{2.26}$$

This behavior of the coupling $\alpha_s(Q^2)$ means that at higher energy scales, the particles decouple and asymptotic freedom occurs. The counter effect of this is the fact that at lower energies, the theory becomes non-perturbative as the interaction becomes stronger and $\alpha_s \sim O(1)$ [13].

2.3.3 Form factors in QCD

In Figure 2.1, it is represented, diagrammatically, the fact the fundamental particles of QCD are not free interacting particles. Instead, composite objects are interacting and consequently there is information that cannot be obtained from the underlying theory. As in eq. (2.8), form factors can be obtained from the symmetries of the theory. In contrast with EW theory, which can be studied perturbatively, the form factors cannot be computed from Feynman diagrams. Instead, effective field theories can be implemented to study their behavior. A relevant form factor for this work is the one related with pseudoscalar meson's transition into two photons (the so-called meson transition form factor).
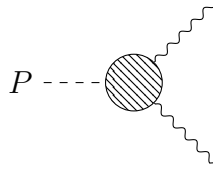
Figure 2.6. Pseudoscalar transition form factor $P \to \gamma\gamma$.

Electromagnetic and strong interactions occur in this process, since the pseudoscalar particles (π^0, η, η') are not fundamental entities, its interaction with light cannot be studied from QCD's fundamental Lagrangian, so EFT's can be worked out in order to obtain the P-TFF compatible with fundamental theory symmetries and predictions.

3. Chiral Perturbation Theory (χPT)

As mentioned in the previous chapter, QCD is the fundamental theory for strong interactions, however, perturbation theory fails to work at low and intermediate energies ($E \leq 2$ GeV). A construction for the study of QCD phenomenology can be performed, in a different way that was worked for EW theory with the Fermi theory (motivated by the fact that the EW is a weakly-coupled case and that of low-energy QCD is strongly-coupled). For low energy ($E \leq 1$ GeV), Chiral Perturbation Theory (χPT) succeeds in the description of pseudoscalar mesons (π, K, η) phenomena, as $\pi^{\pm}$ decay, $\pi\pi$ scattering, $\pi\gamma$ scattering, and the different processes involving other pseudoscalar mesons as well.

3.1 Effective field theories

An EFT is a valid approximation for energies that are small compared to some scale Λ of the underlying theory. An EFT can be systematically constructed based on Weinberg's theorem [16]: "*if one writes down the most general possible Lagrangian, including all terms consistent with assumed symmetry principles, and then calculates matrix elements with this Lagrangian to any given order of perturbation theory, the result will simply be the most general possible S-matrix consistent with analyticity, perturbative unitarity, cluster decomposition and the assumed symmetry principles*". Let us start with an example. Consider a system of two scalar particles ϕ and Φ with masses m and M, respectively. They interact with each other as given by the following Lagrangian:

$$\mathcal{L}_{fund} = \frac{1}{2} \left(\partial_{\mu}\phi\partial^{\mu}\phi + \partial_{\mu}\Phi\partial^{\mu}\Phi \right) - \frac{1}{2} \left(m^2\phi^2 + M^2\Phi^2 \right) - \frac{\lambda}{2}\Phi\phi^2, \qquad (3.1)$$

the Feynman diagram regarding the interaction is shown in Figure 3.1.
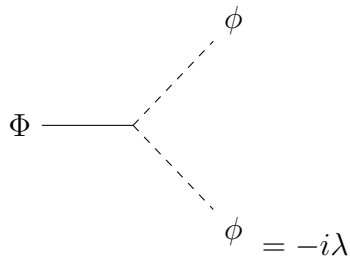
Figure 3.1. Interaction of scalar fields Φ (solid line) and ϕ (dashed line) and corresponding Feynman rule.

The elastic scattering $\phi(p_1)\phi(p_2) \rightarrow \phi(p_3)\phi(p_4)$ is mediated by the heavier scalar Φ through the interaction in eq. (3.1) in the s, t, u channels, as shown in Figure 3.2.
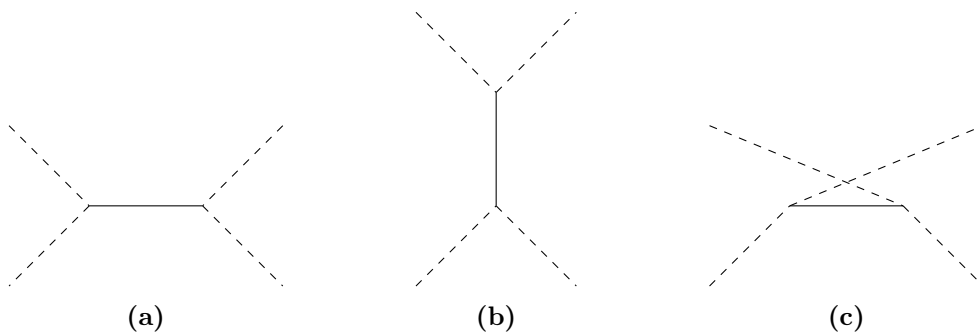
Figure 3.2. Feynman diagrams for s, t and u respectively for the elastic scattering of two scalars ϕ mediated by the scalar Φ.

The amplitude for this process is

$$\mathcal{M}_{fund} = \lambda^2 \left(\frac{i}{s - M^2 + i0^+} + \frac{i}{t - M^2 + i0^+} + \frac{i}{u - M^2 + i0^+} \right). \qquad (3.2)$$

At low energies with respect to M, $\{s, |t|, |u|\} \ll M^2$, an expansion on $\frac{s,t,u}{M^2}$ can be performed and the leading order contribution is

$$\mathcal{M}_{fund} = \frac{3i\lambda^2}{M^2} + O\left(\frac{\{s, |t|, |u|\}}{M^2} \right). \qquad (3.3)$$

If one works at the scale where any Mandelstam variable is $\ll M^2$, Φ is frozen out. In this way, the equations of motion are reproduced by the effective Lagrangian

$$\mathcal{L}_{eff} = \frac{1}{2} \left(\partial^\mu \phi \partial_\mu \phi - m^2 \phi^2 \right) + \frac{\lambda^2}{8M^2} \phi^4. \qquad (3.4)$$

The effective coupling will give out a contact term of 4 ϕ's as seen in the following figure.
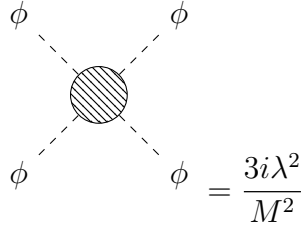
Figure 3.3. Contact term of $\mathcal{L}_{eff}$ for 4 ϕ's interaction.

This gives the following amplitude to the elastic scattering of two ϕ's

$$\mathcal{M}_{eff} = \frac{3i\lambda^2}{M^2}. \tag{3.5}$$

This reproduces exactly the leading order contribution $\mathcal{L}_{fund}$ in the expansion for $\frac{\{s,|t|,|u|\}}{M^2} << 1$.

An example of an effective field theory for a simple theory points out two important ideas which can help us understand how to build an EFT for any theory. The part of the theorem that mentions "including all terms" requires infinite terms, but this is of no practical use. To overcome this issue, we have to stop at some point, considering the level of accuracy we are aiming to. In our example, we could have continued to expand the equations of motion to the next order in $\frac{p^2}{M^2}$ terms and included these corrections in the effective Lagrangian. This would have matched the next to leading order (NLO) terms of eq. (3.3) and so would have done if we included the next to next to leading order (NNLO) and so on, but how precise we need to go will tell us how many orders should we consider. Since the EFT works in a limited energy regime, $\frac{p^2}{\Lambda^2}$ is a favorable expansion parameter for the terms in the effective Lagrangian, as it was also seen in our example.

In this sense an EFT for QCD can be constructed based on the Lagrangian in eq. (2.20), as it gives us the symmetry principles to start working with. Also, the degrees of freedom observed in nature are hadrons, so they must be used to construct the EFT, instead of the unobserved quarks and gluons at different energy regimes.

QCD can be divided into three scales: high energy QCD ($E > 2$ GeV), low energy QCD ($E \leq 1$ GeV) and the resonant region which is in the middle of both.

Because of the limits in the energy scales, quarks can be split into the 3 light ones (u, d, s) and the heavy ones (c, b, t), and because of the masses of the heavy ones, an effective field theory only considering the light quarks can be worked out and be useful. First, in this chapter, the building blocks of the procedure will be worked out in the low energy limit (χPT) and then, in the next chapter, the intermediate region will be constructed $(R\chi T)$ from this one [20].

3.2 Chiral Symmetry in QCD

In order to start the construction of an EFT for QCD at low energies, the symmetries must be the first point to look at. As mentioned in the previous chapter, for the non-perturbative regime, it is enough to consider the 3 lightest quarks (u, d, s). The QCD Lagrangian for just these free quarks is:

$$\mathcal{L}_{free\,quarks} = \sum_{A=1}^{3} \sum_{f=u,d,s} \bar{q}_{fA} \left(\gamma^{\mu} i \partial_{\mu} - m_f\right) q_{fA}, \tag{3.6}$$

where f is the flavor index and A are the 3 colors. The color sum can be written in the form of a color triplet

$$q_f = \begin{pmatrix} q_{f,1} \\ q_{f,2} \\ q_{f,3} \end{pmatrix}, \tag{3.7}$$

and the local symmetry can be achieved by adding the gluons into the picture, in the adjoint representation of color SU(3). However, this symmetry is not the one we are using for the construction of the EFT.

3.2.1 Chiral Limit

There is an accidental symmetry in here by taking the limit where these quarks are massless (this can be approximately realized if the characteristic energy of the process is much larger than these masses), this is the so called *Chiral Limit*. The Lagrangian then takes the form

$$\mathcal{L}_{Chiral} = \sum_{f=u,d,s} \bar{q}_f \gamma^{\mu} i \partial_{\mu} q_f, \tag{3.8}$$

then the Lagrangian can be split into left and right chiral components of q: $q_{R(L)} = \frac{1}{2}(1 \pm \gamma_5)q$.

$$\mathcal{L}_{Chiral} = \sum_{f=u,d,s} \bar{q}_{Lf}\gamma^\mu i\partial_\mu q_{Lf} + \bar{q}_{Rf}\gamma^\mu i\partial_\mu q_{Rf}. \qquad (3.9)$$

This Lagrangian is invariant under two independent global transformations:

$$\begin{pmatrix} u_L \\ d_L \\ s_L \end{pmatrix} \to U_L \begin{pmatrix} u_L \\ d_L \\ s_L \end{pmatrix} = \exp\left(-i\sum_{a=1}^{8}\Theta_{La}\frac{\lambda_a}{2}\right)e^{-i\Theta_L}\begin{pmatrix} u_L \\ d_L \\ s_L \end{pmatrix},$$

$$\begin{pmatrix} u_R \\ d_R \\ s_R \end{pmatrix}, \to U_R \begin{pmatrix} u_R \\ d_R \\ s_R \end{pmatrix} = \exp\left(-i\sum_{a=1}^{8}\Theta_{Ra}\frac{\lambda_a}{2}\right)e^{-i\Theta_R}\begin{pmatrix} u_R \\ d_R \\ s_R \end{pmatrix},$$

$$\qquad (3.10)$$

where $U_{L(R)}$ are independent 3×3 complex rotations times a global phase. So, the chiral Lagrangian (3.8) is invariant under a global $SU(3)_L \times SU(3)_R \times U(1)_L \times U(1)_R$ which can be rewritten since completeness allows us to do a $(L, R) \to (V, A)$ basis change. This is convenient, since (V, A) have a definite behavior under parity transformation, which is a good label for the hadron multiplets. Chiral currents related with these symmetries can be written, according to Nöether's Theorem[20]

$$V_a^\mu = \bar{q}\gamma^\mu\frac{\lambda_a}{2}q,$$
$$A_a^\mu = \bar{q}\gamma^\mu\gamma_5\frac{\lambda_a}{2}q,$$
$$V^\mu = \bar{q}\gamma^\mu q,$$
$$A^\mu = \bar{q}\gamma^\mu\gamma_5 q, \qquad (3.11)$$

making 18 conserved currents. However, as it is seen in nature, there is an observed asymmetry between particles with the same spin and opposite parity. This fact of nature gives us the hint that somewhere there, a symmetry breaking must occur (otherwise these multiplets should be degenerate according to the symmetries discussed above).

3.2.2 Chiral symmetry breaking

When the masses of light quarks are taken into account in the QCD Lagrangian, chiral symmetry is explicitly broken. The divergence of (almost all) chiral currents

(3.11) becomes non-zero

$$\partial_\mu V_a^\mu = i\bar{q}\left[\mathcal{M}, \frac{\lambda_a}{2}\right],$$

$$\partial_\mu A_a^\mu = i\bar{q}\gamma_5\left\{\mathcal{M}, \frac{\lambda_a}{2}\right\},$$

$$\partial V^\mu = 0,$$

$$\partial_\mu A^\mu = 2i\bar{q}\gamma_5\mathcal{M}q + \frac{3g_s^2}{32\pi^2}\varepsilon_{\mu\nu\rho\sigma}G_a^{\mu\nu}G_a^{\rho\sigma}, \tag{3.12}$$

where the mass matrix is $\mathcal{M} = \text{diag}\{m_u, m_d, m_s\}$ and the second term of $\partial_\mu A_\mu$ comes from the quantum corrections (it is related to the extremely approximate CP symmetry of the strong interactions, which must be discussed in presence of the electroweak sector of the SM and is not yet understood). It is important to make some remarks regarding the inclusion of non-zero quark masses:

1. For any values of quark masses, the individual flavor currents $\bar{f}\gamma^\mu f$ are conserved in the strong interactions, so strong coupling is flavor independent.

2. All 18 currents, except the vector singlet current (so baryon number is exactly conserved, but for anomalous effects), get a non-vanishing divergence for different quark masses.

3. For equal quark masses, the 9 vector currents (octet + singlet) are conserved.

4. Considering a more realistic case, $m_u = m_d \neq m_s$, the $SU(3)$ flavor symmetry is reduced to $SU(2)$ isospin symmetry.

5. $m_u - m_d$ (compared to the typical energy scale of a given process) is then a scale of isospin symmetry breaking.

This information will become important when discussing the symmetry breaking in QCD at low energies.

3.3 Chiral Perturbation Theory for Mesons

Having discussed the main features of chiral symmetry and its explicit breaking, due to quark masses, the elements for constructing an EFT for mesons made of the light quarks is set. The fact that parity is a good symmetry of the QCD Lagrangian but not of the hadron spectrum will be explained via spontaneous symmetry breaking.

3.3.1 Goldstone Theorem Realization in QCD

Spontaneous symmetry breaking in QCD is feasible due to the known experimental input discussed before. Considering the chiral limit, a sufficient but not necessary condition for it to happen is $\langle \bar{q}q \rangle \neq 0$, also known as *the scalar singlet quark condensate*. This nomenclature comes from the fact that $\bar{q}q$ transforms as a scalar under the Lorentz group and as a singlet under $SU(3)_V$. The "condensation" is a non-perturbative phenomenon of the QCD ground state that is driven by the formation of quark-antiquark pairs. The definition of scalar and pseudoscalar densities will be of practical use:

$$
\begin{aligned}
S_a(y) &= \bar{q}(y)\lambda_a q(y), \\
P_a(y) &= i\bar{q}(y)\gamma_5\lambda_a q(y),
\end{aligned}
\tag{3.13}
$$

with $a = 0, ..., 8$ being $\lambda_0 = \sqrt{\frac{2}{3}}I_3$, and the other 8 are the usual Gell-Mann matrices. In the chiral limit, $\langle S_a \rangle = 0$, which for the diagonal matrices gives the relations

$$
\begin{aligned}
\langle \bar{\lambda}_1 \rangle &= \sqrt{\frac{2}{3}}\langle \bar{u}u + \bar{d}d + \bar{s}s \rangle = 0, \\
\langle \bar{\lambda}_3 \rangle &= \langle \bar{u}u - \bar{d}d \rangle = 0, \\
\langle \bar{\lambda}_8 \rangle &= \sqrt{\frac{1}{3}}\langle \bar{u}u + \bar{d}d - 2\bar{s}s \rangle = 0,
\end{aligned}
\tag{3.14}
$$

$$
\tag{3.15}
$$

leading to the fact that all $\langle \bar{f}f \rangle$ are equal. If we then take a non-zero value of the singlet quark condensate we get:

$$
\langle \bar{q}q \rangle = 3\langle \bar{f}f \rangle.
\tag{3.16}
$$

This results in the fact that $P_a(y)$ has a non-vanishing matrix element between the vacuum and the massless one-particle state $|\phi_b\rangle$, meaning that chiral symmetry has been spontaneously broken, resulting in $SU_L(3) \times SU_R(3) \to SU_V(3)$, giving rise to 8 pseudoscalar Goldstone bosons. This fits perfectly with the explanation we are aiming at, yielding the construction of the pseudoscalar meson octet, which will have different nature than its parity partner. The explicit symmetry breaking by quark masses will give rise instead -for these lightest pseudoscalars- to pseudo-Goldstone bosons.

3.3.2 Effective Lagrangian for low-energy QCD: χPT

The facts of nature lead to the search for a mechanism which breaks spontaneously the chiral symmetry. This gives us an useful mechanism to construct a theory with 8 pseudoscalar Goldstone bosons. Here, the lightest octet of pseudoscalar mesons (π, K, η) can be identified with each one of the Goldstone bosons. So an effective theory to study interactions between them can be constructed.

3.3.2.1 Transformation properties of the Goldstone Bosons

Before constructing the effective Lagrangian for these Goldstone bosons, it is necessary to understand how do they transform under the action of the symmetry group and which object is the ideal one for it. The Goldstone bosons can be arranged in a n-dimensional vector $\boldsymbol{\Phi} = (\phi_1, ...\phi_n)$, which is a map from Minkowski space into a vector space:

$$M_1 = \left\{ \boldsymbol{\Phi} : M^4 \to \mathcal{R}^n | \phi_i : M^4 \to \mathcal{R} \right\}. \tag{3.17}$$

For the purpose of the construction, we will discuss some properties of all the left co-sets called the quotient G/H, defined as

$$G/H = \{gH | g \in G\}, \tag{3.18}$$

where at the same time gH is defined as:

$$gH = \{gh | h \in H\}, \tag{3.19}$$

with G (H) the symmetry group of a dynamical Lagrangian system (the vacuum). An important property is that co-sets either completely overlap, or are completely disjoint. This allows us to do an isomorphic mapping between the quotient G/H and the Goldstone bosons fields. This mapping, which we call φ, has an important property: any given element $g \in G$ can map a vector Φ into another Φ'. Given this, it can be applied to our chiral QCD case. The symmetry group of chiral QCD is $G = SU(3)_L \times SU(3)_R$ and of its vacuum is $H = SU(3)_V$. Let $\tilde{g} = (\tilde{L}, \tilde{R}) \in G$. A representative element of the left co-set can be characterized as $\tilde{g}H = (1, \tilde{R}\tilde{L}^\dagger)H$ in the convention where it has the identity matrix in the first argument. Under the action of an element g, a left co-set element $\tilde{g}$ transforms as

$$g\tilde{g}H = (L, R\tilde{R}\tilde{L}^\dagger)H = (1, R\tilde{R}\tilde{L}^\dagger L^\dagger)(L, L)H = (1, R(\tilde{R}\tilde{L}^\dagger)L^\dagger)H, \tag{3.20}$$

where in the last step we have used the fact that (L, L) belongs to $SU(3)_V$ and for group properties, it is mapped into H itself. The representative matrix $\tilde{g}$ is then transformed as

$$U(x) \rightarrow RU(x)L^{\dagger}, \tag{3.21}$$

under the action of the group element g. Then, if we want to construct a basis for an $SU(3)$ element, we must get a set of hermitian traceless 3×3 matrices. This can be done by using the exponential parametrization and the fact that there is an isomorphism between the elements of the group G and the elements of the vector space spanned by the Goldstone bosons. So we can write an $SU(3)$ element as

$$U(x) = \exp\left(i\frac{\Phi(x) \cdot \lambda}{F_0}\right), \tag{3.22}$$

where

$$\phi = \Phi \cdot \lambda = \begin{pmatrix} \pi^0 + \frac{1}{\sqrt{2}}\eta_8 & \sqrt{2}\pi^+ & \sqrt{2}K^+ \\ \sqrt{2}\pi^- & -\pi^0 + \frac{1}{\sqrt{2}}\eta_8 & \sqrt{2}K^0 \\ \sqrt{2}K^- & \bar{K}^0 & -\frac{2}{\sqrt{3}}\eta_8 \end{pmatrix}, \tag{3.23}$$

and the constant F_0 is a scale introduced to make the argument of the exponential function dimensionless, and will be set by experimental input. We can (and will) choose $R(x) = L^{\dagger}(x) = u(x)$ so that $u^2(x) = U(x)$. These elements transform under the action of the group as in eq. (3.21), under the action of g. This allows us to construct not just the building blocks of the EFT but also to look for the independent terms allowed by the theory. Since the construction is made in (even) powers of $\frac{p}{\Lambda}$, which for this case is $\Lambda = 4\pi F_{\pi} \approx 1.170$ GeV [20], it will converge rather well at low energies. It is an useful remark that $\partial_{\mu}U(x)$ terms are of order $\frac{p}{F_0}$ and $U(x)$ is of order p^0.

3.3.2.2 χPT at order p^2

The independent terms must be constructed order by order using eq. (3.22) and its derivative, knowing that it transforms as eq. (3.21) and considering the chiral counting. From properties of λ matrices, and the transformation under G, it is evident that traces must be taken for terms to be globally invariant under G. It is also found that the odd terms in U cancel. Knowing this, the first order is p^2. And the only independent term is:

$$\mathcal{L}_{eff} = \frac{F_0^2}{4}Tr\left[\partial_{\mu}U\partial^{\mu}U^{\dagger}\right], \tag{3.24}$$

29

where a convenient normalization has been chosen. However, the particles in the pseudoscalar octet of mesons are not massless, so an explicit symmetry breaking term must be added for the particles to become pseudo-Goldstone bosons (pGb). This term is:

$$\mathcal{L}_{s.b.} = \frac{F_0^2 B_0}{2} Tr \left[\mathcal{M} U^\dagger + U \mathcal{M}^\dagger \right] , \tag{3.25}$$

with $\mathcal{M} = \text{diag} \{m_u, m_d, m_s\}$ being the mass matrix of quarks. Given this, external sources may be added with the correct structure in order to reproduce electromagnetic and weak interactions of the pGbs.

3.3.2.3 Interaction with external sources

External sources can be included in the effective field theory since Ward identities are obtained from a locally invariant generating functional involving a coupling to external fields [20]. This can address the aim to include EW interactions into the EFT theory. From the structure of the conserved currents, external fields can couple in the 4 same structures: v, a, s, p or l, r, s, p. It will be useful to employ it in the last form, since electromagnetic interactions are non-chiral and electroweak interactions are just left-handed. When promoting the theory to be locally invariant, the derivatives must be generalized to covariant derivatives. Since U transforms as (3.21) now locally, the covariant derivative is rather different than usual

$$D_\mu U = \partial_\mu U - i r_\mu U + i U l_\mu, \tag{3.26}$$

with r_μ and l_μ transforming so that

$$D_\mu U \to V_R (D_\mu U) V_L^\dagger. \tag{3.27}$$

Since the effective Lagrangian will ultimately contain arbitrarily high powers of derivatives we also need field-strength tensors:

$$f_{R(L)\mu\nu} = \partial_\mu r(l)_\nu - \partial_\nu r(l)_\mu - i[r(l)_\mu, r(l)_\nu]. \tag{3.28}$$

By the convention of Gasser and Leutwyler [23]

$$\mathcal{L}_{s.b.} = \frac{F_0^2}{4} Tr \left(\chi U^\dagger + U \chi^\dagger \right), \quad \chi = 2B_0(s + ip), \tag{3.29}$$

where s and p are the scalar and pseudoscalar external sources. The mass matrix can be included in s. The final order p^2 Lagrangian locally invariant under $SU(3)_V \times SU(3)_A$ is:

$$\mathcal{L}_2 = \frac{F_0^2}{4} Tr \left[D_\mu U (D^\mu U)^\dagger \right] + \frac{F_0^2}{4} Tr \left[\chi U^\dagger + U \chi^\dagger \right] . \tag{3.30}$$

3.3.3 Application of the lowest order EFT

Some exercises can be performed in order to check consistency with observations and to set those non-restricted by symmetry constraints.

3.3.4 Pseudo-Goldstone Boson Masses

As an exercise, an expansion on quadratic terms of the pGb can be performed in order to find the masses that theory predicts:

$$\mathcal{L}_{s.b.} = -\frac{B_0}{2} Tr \left[\mathcal{M} \phi^2 \right] , \tag{3.31}$$

by taking the isospin limit $m_u = m_d = m$ it results in the following masses:

$$m_\pi^2 = 2m B_0,$$
$$m_K^2 = B_0(m + m_s),$$
$$m_\eta^2 = \frac{2}{3} B_0(m + 2m_s). \tag{3.32}$$

This result is compatible with observed pseudoscalar masses so it sets the value of B_0 ($F_0^2 B_0 \sim (275\,\mathrm{MeV})^2$). Higher order corrections (including those of electromagnetic origin) account for the mass differences between neutral and charged particles.

3.3.4.1 π^+ Decay

π^+ decay can be studied in its main channel $\pi^+ \to \mu^+ \nu_\mu$.
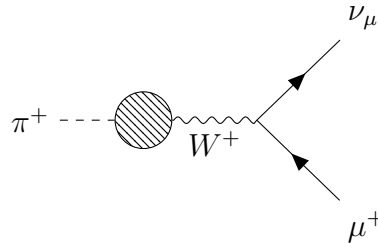
Figure 3.4. $\pi^+ \to \mu^+ \nu_\mu$ decay. In χPT the W boson propagator shrinks to a point.

As it is shown in Figure 4.1 this process happens by a weak interaction. It can be described within χPT by taking a left external field

$$l_\mu = -\frac{g}{\sqrt{2}}(W_\mu^+ T_+ + W_\mu^- T_-), \quad s = p = r_\mu = 0, \tag{3.33}$$

where

$$T_+ = T_+^\dagger = \begin{pmatrix} 0 & V_{ud} & V_{us} \\ 0 & 0 & 0 \\ 0 & 0 & 0 \end{pmatrix}, \tag{3.34}$$

the transition $\pi^+ \to W^+$ will come from the left term in the covariant derivative and the $\partial_\mu \pi$ part from (3.26). By taking the trace in the relevant operators, the decay rate can be computed:

$$\Gamma = \frac{1}{4\pi} G_F^2 V_{ud}^2 F_0^2 m_\mu^2 m_\pi \left(1 - \frac{m_\mu^2}{m_\pi^2}\right)^2. \tag{3.35}$$

Since all the other constants have already being computed from diverse observables, F_0 can be obtained from measuring π^+ decay ($F_0 \sim 90$ MeV).

3.3.4.2 Pion scattering

The process $\pi\pi \to \pi\pi$ can be computed from the effective theory.
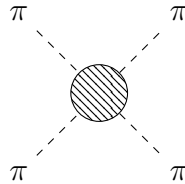
Figure 3.5. 4 π scattering in χPT.

Expanding the Lagrangian (3.30), no cubic terms in the pGb's is obtained, so the first interaction to be studied is the interaction between 4 pions

$$\mathcal{L}_2^{4\phi} = \frac{1}{6F}(\phi_i \partial^\mu \phi_i \partial_\mu \phi_j \phi_j - \phi_i \phi_i \partial^\mu \phi_j \partial_\mu \phi_j) + \frac{m_\pi^2}{24F^2} \phi_i \phi_i \phi_j \phi_j, \tag{3.36}$$

where i, j are cartesian indexes, and shall not be confused with flavor indexes. We

get the amplitude for this process

$$\mathcal{M} = i\left[\delta_{ab}\delta_{cd}\frac{s - m_\pi^2}{F^2} + \delta_{ac}\delta_{bd}\frac{t - m_\pi^2}{F^2} + \delta_{ad}\delta_{bc}\frac{u - m_\pi^2}{F^2}\right]$$
$$- \frac{i}{3F^2}(\delta_{ab}\delta_{cd} + \delta_{ac}\delta_{bd} + \delta_{ad}\delta_{bc})(\Lambda_a + \Lambda_b + \Lambda_c + \Lambda_d) \tag{3.37}$$

where $\Lambda_i = p_i^2 - m_\pi^2$ and vanishes for on shell contributions. s, t, u are the known Mandelstam variables ($s + t + u = 4m_\pi^2$). Dispersion with light is also an achievable process to study within the EFT for pGb.

3.3.5 Higher order χPT

If more precision is required, more orders of p^2 should be added, this can go on as higher as it is necessary. At some point, it gets messy. However, there are features that are not found at leading order.

3.3.5.1 Order p^4 Lagrangian

Based on the transformation of the different objects available, the most general Lagrangian compatible with assumed symmetries can be obtained at $\mathcal{O}(p^4)$

$$\begin{aligned}
\mathcal{L}_4 =& L_1\left\{Tr[D_\mu U(D^\mu U)^\dagger]\right\}^2 + L_2 Tr[D_\mu U(D_\nu U)^\dagger]Tr[D^\mu U(D^\nu U)^\dagger] \\
&+ L_3 Tr[D_\mu U(D^\mu U)^\dagger D_\nu U(D^\nu U)^\dagger] + L_4 Tr[D_\mu U(D^\mu U)^\dagger]Tr(\chi U^\dagger + U\chi^\dagger) \\
&+ L_5 Tr[D_\mu U(D^\mu U)^\dagger(\chi U^\dagger + U\chi^\dagger)] + L_6\left[Tr(\chi U^\dagger + U\chi^\dagger)\right]^2 \\
&+ L_7\left[Tr(\chi U^\dagger - U\chi^\dagger)\right]^2 + L_8 Tr(U\chi^\dagger U\chi^\dagger + \chi U^\dagger \chi U^\dagger) \\
&- iL_9 Tr[f_{R\mu\nu}D^\mu U(D^\nu U)^\dagger + f_{L\mu\nu}(D^\mu U)^\dagger D^\nu U] + L_{10} Tr(U f_{L\mu\nu} U^\dagger f_R^{\mu\nu}) \\
&+ H_1 Tr(f_{R\mu\nu}f_L^{\mu\nu}) + H_2 Tr(\chi\chi^\dagger).
\end{aligned} \tag{3.38}$$

The last two terms are purely external fields so they are not relevant for pGb interactions with external fields (but are needed for renormalization). It is a good point now, to mention that renormalizability is not achieved in χPT in the usual form. χPT is renormalizable order by order, since divergent diagrams from $\mathcal{L}_2$ are of order p^4 and so on. This means that the constants L_i from (3.38) need to be renormalized. This is not relevant for our discussion but it is important to be aware of it.

3.3.5.2 Pseudo-Goldstone Bosons masses at order p^4

With eq. (3.38), corrections for pGb masses can be performed. The mass corrections $m_P^2 - m_{P\mathcal{L}^2}^2$ are:

$$m_{\pi^0 \mathcal{L}_4}^2 = \frac{64B_0^2}{F_0^2} \left[(2m + m_s)mL_6 + m^2 L_8\right],$$

$$m_{\pi^\pm \mathcal{L}_4}^2 = \frac{32B_0^2}{F_0^2} \left[m^2 L_8\right],$$

$$m_{K^0 \mathcal{L}_4}^2 = m_{K^\pm \mathcal{L}_4}^2 = \frac{32B_0^2}{F_0^2} \left[mm_s L_8\right],$$

$$m_{\eta \mathcal{L}_4}^2 = \frac{64B_0^2}{F_0^2} \left[(m + 2m_s)(2m + m_s)L_6 + 2m_s^2 L_7 + (m^2 + 2m_s^2)L_8)\right]. \qquad (3.39)$$

In this case no direct comparison between masses can be performed as easily as in (3.30). However, a difference between the charged and neutral pions can be addressed as they depend on different constants. Order p^6 Lagrangian is calculated in [24], and depending on the precision of the problem, it can be useful.

3.3.6 Chiral Anomaly: The Wess-Zumino-Witten Effective Action

Intrinsic parity is an accidental symmetry in the construction of χPT, this forbids odd-intrinsic-parity process as $K^+ K^- \to \pi^+ \pi^- \pi^0$ and $\pi^0 \to \gamma\gamma$. However, these occur in nature and are detected in different hadronic experiments, which points to the fact that anomalous contributions are needed to understand them [1]. This lead to the development of the Wess-Zumino-Witten action[25][26]

$$S_{WZW}[[U, l, r] = -\frac{iN_C}{240\pi^2} \int d\sigma^{ijklm} Tr \left[\Sigma_i^L \Sigma_j^L \Sigma_k^L \Sigma_l^L \Sigma_m^L\right]$$
$$- \frac{iN_C}{48\pi^2} \int dx^4 \varepsilon_{\mu\nu\rho\sigma} \left(W(U, l, r)^{\mu\nu\rho\sigma} - W(1, l, r)^{\mu\nu\rho\sigma}\right), \qquad (3.40)$$

---

[1]A complementary point of view comes from the fact that the QCD Lagrangian has the chiral anomaly, which must be implemented in its effective realization at low energies, given by χPT.

where $W(U, l, r)$ is defined as

$$
\begin{aligned}
W(U, l, r)^{\mu\nu\rho\sigma} = Tr \Big[& U l^\mu l^\nu l^\rho U^\dagger r^\sigma + \frac{1}{4} U l^\mu U^\dagger r^\nu U l^\rho U^\dagger r^\sigma \\
& + i U \partial^\mu l^\nu l^\rho U^\dagger r^\sigma + i \partial^\mu r^\nu U l^\rho U^\dagger r^\sigma - i \Sigma^{L\mu} l^\nu U^\dagger r^\rho U l^\sigma \\
& \Sigma^{L\mu} U^\dagger \partial^\nu r^\rho U l^\sigma - \Sigma^{L\mu} \Sigma^{L\nu} U^\dagger r^\rho U l^\sigma + \Sigma^{L\mu} l^\nu \partial^\rho l^\sigma + \Sigma^{L\mu} \partial^\nu l^\rho l^\sigma \\
& - i \Sigma^{L\mu} l^\nu l^\rho l^\sigma + \frac{1}{2} \Sigma^{L\mu} l^\nu \Sigma^{L\rho} l^\sigma - i \Sigma^{L\mu} \Sigma^{L\nu} \Sigma^{L\rho} l^\sigma \Big] - (L \leftrightarrow R),
\end{aligned}
\tag{3.41}
$$

and $\Sigma_\mu^{L(R)}$ are

$$
\Sigma_\mu^L = U^\dagger \partial_\mu U, \qquad \Sigma_\mu^R = U \partial_\mu U^\dagger, \tag{3.42}
$$

where $L \leftrightarrow R$ means $\Sigma_\mu^L L \leftrightarrow R \Sigma_\mu^R$, $l_\mu \leftrightarrow r_\mu$ and $U \leftrightarrow U^\dagger$. This Lagrangian is of order p^6 and cannot be produced by χPT, according to the framework that we have explained, so it must be added by hand for the theory to have intrinsic parity violating processes, induced by the chiral anomaly of QCD.

3.3.6.1 π^0-TFF at Leading Order

Among the processes described by (3.40), the most important one for this work is the pion transition form factor (π-TFF), this is, the decay of a π^0 into two photons. This process is described in an EFT since π^0 is not a fundamental particle.
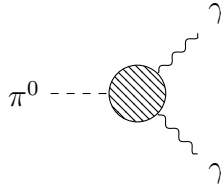
Figure 3.6. $\pi^0 \to \gamma\gamma$.

The main contribution for this process within χPT is given by the $\pi\gamma\gamma$ part of (3.40)

$$
\mathcal{L}_{\pi\gamma\gamma} = -\varepsilon_{\mu\nu\rho\sigma} \frac{e^2 N_C F^{\mu\nu} F^{\rho\sigma} \pi^0}{96\pi^2 F}, \tag{3.43}
$$

which translates into the amplitude

$$
\mathcal{M} = -i e^2 \varepsilon_{\mu\nu\rho\sigma} q_1^\mu q_2^\mu \epsilon_1^{*\rho} \epsilon_2^{*\sigma} \left(\frac{2}{3F} \right) \left(\frac{N_C}{8\pi^2} \right). \tag{3.44}
$$

More contributions will come from higher order terms within the anomalous sector of χPT, and also from the inclusion of vector meson resonances into the calculation.

4. Resonance Chiral Theory (RχT)

At higher energies $(E \geq M_\rho)$, the hadronic spectrum becomes richer and χPT ceases to describe strong interactions fully. Even including arbitrary higher orders in χPT will not solve the problem, since resonances become dynamic degrees of freedom. Consequently, they must be included in the action. Because of this, an extension of our EFT must be constructed [7]. After the pseudoscalar mesons octet, the second multiplet that becomes active (dynamical fields) is the vector meson multiplet (ρ's, ω, K^*'s and the ϕ). Thus, it will be incorporated in the antisymmetric tensor formulation [27]: by respecting Weinberg's theorem, every term compatible with the assumed symmetries must be included. The aim of RχT is to match both the chiral limit (to yield χPT) and to reproduce the constraints imposed by high-energy QCD. In doing so, we assume that, bridging between both known regimes, RχT captures the most essential features of the resonance region, guided by symmetry principles (unitary symmetry and the large number of colors limit of QCD). Ultimately, its phenomenological successes indicate this is a sensible approach.

4.1   RχT Lagrangian

The Lagrangian is constructed as mentioned before, it must respect QCD symmetries. The vector meson multiplet in the large-N_C limit is [28] [1]

$$V_{\mu\nu} = \begin{pmatrix} (\rho^0 + \omega^0)/\sqrt{2} & \rho^+ & K^{*+} \\ \rho^- & (-\rho^0 + \omega^0)/\sqrt{2} & K^{*0} \\ K^{*-} & \bar{K}^{*0} & \phi \end{pmatrix}_{\mu\nu} . \tag{4.1}$$

---

[1]Ideal meson mixing between the $\omega_{8,1}$ flavor states to yield the physical ω, ϕ particles is used throughout. With $N_C \to \infty$ the $SU(3)_V$ octets and singlets converge into nonets.

The rest of the building blocks of this formalism are [7]:

$$u = \exp\left(i\frac{\Phi}{\sqrt{2}F}\right), \quad \Phi = \sum_{a=0}^{8}\frac{\lambda_a \phi^a}{\sqrt{2}},$$

$$u_\mu = i\left[u^\dagger(\partial_\mu - ir_\mu)u - u(\partial_\mu - il_\mu)u^\dagger\right],$$

$$\Gamma_\mu = \frac{1}{2}\left[u^\dagger(\partial_\mu - ir_\mu)u + u(\partial_\mu - il_\mu)u^\dagger\right],$$

$$\nabla_\mu \cdot = \partial_\mu + [\Gamma_\mu, \cdot], \quad f_\pm^{\mu\nu} = uf_L^{\mu\nu}u^\dagger \pm u^\dagger f_R^{\mu\nu}u, \tag{4.2}$$

$$\chi_\pm = u^\dagger \chi u^\dagger \pm u\chi^\dagger u, \; \chi = 2B_0(s + ip). \tag{4.3}$$

Given the building blocks, the EFT can be constructed, respecting chiral symmetry for the pseudo-Goldstone bosons and unitary symmetry for the resonance states. It is important to clarify that the χPT expansion parameter, $(p^2 \sim m^2)/(4\pi F)^2$, no longer holds in the resonance region. Instead, an expansion in the inverse of the number of colors of the QCD gauge group $(1/N_C)$ will be used. We will work at leading order in this expansion. In this way, multi-trace operators are typically suppressed (this is non-trivial once the η' is considered, but we will not dwell into this here), as well as meson loops [2]. With $N_C \to \infty$, there is a tower with an infinite number of mesons per set of quantum numbers. In previous works, this spectrum was cut to the lightest resonance multiplets (this effectively modifies the parameters of the lowest-lying resonances as a result of integrating all other states out). Here, we go beyond this simplification for the most important contributions, coming from vector (and for consistency pseudoscalar) mesons.

Still, proceeding as outlined above, the number of operators at leading order, would still be infinite. The key observation that limits them (and keeps the predictability of the theory) comes from the fact that it must match QCD asymptotic behavior, as well as from restricting to operators that actually contribute to our processes of interest. Indeed, an operator in RχT is made from a χPT tensor and a(some) resonance(s) operator(s). If we increase the order of the chiral tensor (in the chiral counting), the leading asymptotic contribution (coming from the operator of highest order in the chiral expansion) will have to vanish, according to QCD constraints. On the other hand, if we increase the number of resonance fields, it will not contribute to our process of interest, since a vector(axial) resonance will yield

---

[2]In general, resonance widths are the dominant next-to-leading order effect in this expansion, and need to be included to make contact with phenomenology. This is not the case here, as the pseudo-Goldstone's transition form factors (the non-perturbative ingredient needed for our computations) probe the spacelike ($q^2 < 0$ in our metric) region.

-at least- two(three) pseudo-Goldstone bosons. This reasoning shows the way in which QCD short-distance constraints, together with the process we are studying, specify a given number (which we can, in fact, handle) of operators for our RχT calculations.

4.1.1 Even Intrinsic Parity Sector

The behavior of the vector resonance multiplet under the chiral group will give us the most general Lagrangian which -upon resonance integration- contributes to the $\mathcal{O}(p^4)$ chiral low-energy constants [3]:

$$\mathcal{L}_V^{kin} = -\frac{1}{2}\langle \nabla_\lambda V^{\lambda\nu}\nabla^\rho V_{\rho\nu}\rangle + \frac{1}{4}M_V^2\langle V_{\mu\nu}V^{\mu\nu}\rangle,$$

$$\mathcal{L}_V^{even} = \frac{F_V}{2\sqrt{2}}\langle V_{\mu\nu}f_+^{\mu\nu}\rangle + \frac{\lambda_V}{\sqrt{2}}\langle V_{\mu\nu}\{f_+^{\mu\nu},\chi_+\}\rangle + i\frac{G_V}{\sqrt{2}}\langle V_{\mu\nu}u^\mu u^\nu\rangle, \tag{4.4}$$

where $\langle\rangle$ is an abbreviation for the trace operator. In the even parity sector, there are also the relevant $\mathcal{O}(p^6)$ operators [24], with their contribution included as [4]:

$$\mathcal{L}_6^{even} = \sum_{i=7,8,22} C_i^W O_i^W. \tag{4.5}$$

The O_i^W terms are:

$$O_7^W = i\epsilon_{\mu\nu\rho\sigma}\langle \chi_- f_+^{\mu\nu}f_+^{\rho\sigma}\rangle,$$

$$O_8^W = i\epsilon_{\mu\nu\rho\sigma}\langle \chi_-\rangle\langle f_+^{\mu\nu}f_+^{\rho\sigma}\rangle,$$

$$O_{22}^W = \epsilon_{\mu\nu\rho\sigma}\langle u^\mu\{\nabla_\lambda f_+^{\lambda\nu},f_+^{\rho\sigma}\}\rangle. \tag{4.6}$$

All above terms in the resonance Lagrangian include the kinetic part of the new particles in RχT and their interactions with both external fields and pGbs.

---

[3]Terms including axial/scalar resonances do not contribute to the pGb TFF and are thus omitted here; pseudoscalar resonances only contribute through the anomalous sector, where they are introduced.

[4]The operator with coefficient λ starts contributing to the $\mathcal{O}(p^6)$ chiral couplings. It gives rise to coupling constants splittings within the resonance multiplet via a shift in F_V. That is why we preferred to introduced it above.

i	$\mathcal{O}^i_{\mathbf{VJP}}$
1	$\{V^{\mu\nu}, f_+^{\rho\alpha}\}\nabla_\alpha u^\sigma$
2	$\{V^{\mu\alpha}, f_+^{\rho\sigma}\}\nabla_\alpha u^\nu$
3	$i\{V^{\mu\nu}, f_+^{\rho\sigma}\}\chi_-$
4	$iV^{\mu\nu}[f_-^{\rho\sigma}, \chi_+]$
5	$\{\nabla_\alpha V^{\mu\nu}, f_+^{\rho\alpha}\}u^\sigma$
6	$\{\nabla_\alpha V^{\mu\alpha}, f_+^{\rho\sigma}\}u^\nu$
7	$\{\nabla^\sigma V^{\mu\nu}, f_+^{\rho\alpha}\}u_\alpha$

Table 4.1. Odd-intrinsic parity sector in $R\chi T$ with 1 vector resonance, a pGb and a vector current. An $\epsilon_{\mu\nu\rho\sigma}$ is omitted in all cases.

4.2 Odd intrinsic parity sector

The odd intrinsic parity sector can be split into two different contributions: with one or two resonances involved [29].

4.2.1 1 resonance contributions

For 1 resonance, all the independent contributions will have a coupling constant $\frac{c_i}{M_V}$:

$$\mathcal{L}_V^{odd} = \sum_{i=1}^{7} \frac{c_i}{M_V} O_{VJP}^i, \qquad (4.7)$$

where O_{VJP}^i are listed in Table 4.1. The sub-index VJP means that there is one vector resonance, one external spin-one current and a pseudoscalar meson in each independent term.

4.2.2 2 resonance contributions

In the 2 resonance case, the methodology is the same, all terms that are compatible with the symmetries are included in the odd intrinsic parity Lagrangian, this consists in an even-intrinsic parity term which contributes to mass term corrections and 4 odd parity terms, which contribute to interactions.

$$\mathcal{L}_{VV}^{even} = -e_m^V \langle V_{\mu\nu} V^{\mu\nu} \chi_+ \rangle,$$

$$\mathcal{L}_{VV}^{odd} = \sum_{i=1}^{4} d_i O_{VVP}^i, \qquad (4.8)$$

where the O_{VVP} terms are listed in Table 4.2. The index VVP means that there are

i	**VVP**
1	$\{V^{\mu\nu}, V^{\rho\alpha}\}\nabla_\alpha u^\sigma$
2	$i\{V^{\mu\nu}, V^{\rho\sigma}\}\chi_-$
3	$\{\nabla_\alpha V^{\mu\nu}, V^{\rho\alpha}\}u^\sigma$
4	$\{\nabla^\sigma V^{\mu\nu}, V^{\rho\alpha}\}u_\alpha$

Table 4.2. Odd-intrinsic parity sector in $R\chi T$ with 2 vector resonances and a pseudoscalar. An $\epsilon_{\mu\nu\rho\sigma}$ is omitted in all cases.

two vector meson resonances and a pseudoscalar in the interactions. An important remark is the fact that even though the label includes 1 pseudoscalar, the number of pseudoscalar mesons can rise since the expansion is infinite. However, for the purpose of this work, there is no need of more [5].

4.3   RχT application: $\omega \to \pi^0\gamma$

As usual, an application of the previously developed formalism is useful to prove its outreach. In this case, the calculation for $\omega \to \pi\gamma$ is a convenient exercise, as it has experimental information available for comparison. Because of the scale of the process, the λ_V term in (4.4) will be omitted as it breaks explicitly chiral symmetry and these corrections are negligible in this instance. It is important to remark
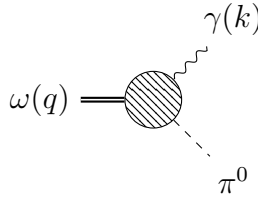
Figure 4.1. $\omega \to \pi^0\gamma$.

that, for electromagnetic interactions, the external fields are written in terms of the electromagnetic field-strength tensor:

$$F_L^{\mu\nu} = F_R^{\mu\nu} = eQF^{\mu\nu}, \tag{4.9}$$

where e is the electron's charge, $Q = \text{diag}\{\frac{2}{3}, -\frac{1}{3}, -\frac{1}{3}\}$ and, as mentioned above, $F^{\mu\nu}$ is the known electromagnetic field-strength tensor.

---

[5]However, the VVP and VJP operators listed here are a basis for processes with only one pseudoscalar. In the general case the minimal set of operators is given in ref. [31]. The translation between both bases is worked out in ref. [24].

i	$\mathcal{L}^{c_i}$
1	$-i\varepsilon_{\mu\nu\rho\sigma}\frac{c_1 2\sqrt{2}e}{F_0 M_V}\partial^\sigma\partial_\alpha\pi^0 F^{\rho\alpha}\omega^{\mu\nu}$
2	$-i\varepsilon_{\mu\nu\rho\sigma}\frac{c_2 2\sqrt{2}e}{F_0 M_V}\partial^\nu\partial_\alpha\pi^0 F^{\rho\sigma}\omega^{\mu\alpha}$
3	$i\varepsilon_{\mu\nu\rho\sigma}\frac{c_3 4\sqrt{2}e m_\pi^2}{F_0 M_V}\pi^0 F^{\rho\sigma}\omega^{\mu\nu}$
4	0
5	$-i\varepsilon_{\mu\nu\rho\sigma}\frac{c_5 2\sqrt{2}e}{F_0 M_V}\partial^\sigma\pi^0 F^{\rho\alpha}\partial_\alpha\omega^{\mu\nu}$
6	$-i\varepsilon_{\mu\nu\rho\sigma}\frac{c_6 2\sqrt{2}e}{F_0 M_V}\partial^\nu\pi^0 F^{\rho\sigma}\partial_\alpha\omega^{\mu\alpha}$
7	$-i\varepsilon_{\mu\nu\rho\sigma}\frac{c_7 2\sqrt{2}e}{F_0 M_V}\partial_\alpha\pi^0 F^{\rho\alpha}\partial^\sigma\omega^{\mu\nu}$

Table 4.3. Lagrangian terms contributing to the process $\omega \to \pi\gamma$ at tree level in RχT.

4.3.1 Relevant Lagrangian terms

Since the Lagrangian can be expanded indefinitely (because of the exponential function in (3.22)), the Lagrangian must be truncated at the quantity of pseudoscalar mesons for this process, in this case, 1. The only contributions for this process will come from the odd intrinsic parity sector. The Lagrangian will be split by contributions' type, since it is easier to calculate the amplitudes in this way.

4.3.2 O_{VJP} contributions to $\omega \to \pi^0\gamma$

This contribution will also be labeled as $\mathcal{L}_{\omega\pi\gamma}^{direct}$, since there is a coupling $\rho \to \gamma$ that can mediate the process too, as we will see next. The relevant terms in the Lagrangian are obtained through computational methods as there are a large amount of terms appearing, even in the 1 pseudoscalar reduction. The contributions are collected in Table 4.3.

All these contributions define the vertex of Figure 4.2 in our EFT.
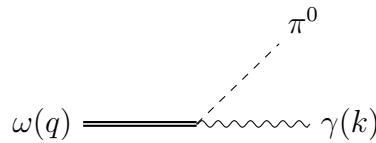
Figure 4.2. Direct $\omega \to \pi^0\gamma$ vertex in RχT.

i	$\mathcal{L}^{d_i}$
$\rho \to \gamma$	$\frac{ie F_V}{2}$
1	$-i\varepsilon_{\mu\nu\rho\sigma}\frac{2d_1}{F_0}\partial^\sigma\partial_\alpha\pi^0(\rho^{\mu\nu}\omega^{\rho\alpha} + \omega^{\mu\nu}\rho^{\rho\alpha})$
2	$i\varepsilon_{\mu\nu\rho\sigma}\frac{8m_\pi^2 d_2}{F_0}\pi^0\rho^{\mu\nu}\omega^{\rho\sigma}$
3	$-i\varepsilon_{\mu\nu\rho\sigma}\frac{2d_3}{F_0}\partial^\sigma\pi^0(\partial_\alpha\rho^{\mu\nu}\omega^{\rho\alpha} + \partial_\alpha\omega^{\mu\nu}\rho^{\rho\alpha})$
4	$-i\varepsilon_{\mu\nu\rho\sigma}\frac{2d_4}{F_0}\partial_\alpha\pi^0(\partial^\sigma\rho^{\mu\nu}\omega^{\rho\alpha} + \partial^\sigma\omega^{\mu\nu}\rho^{\rho\alpha})$

Table 4.4. Lagrangian term contributions to the process $\omega \to \pi\gamma$ mediated by a resonant ρ in RχT.

4.3.3 O_{VVP} contributions to $\omega \to \pi^0\gamma$

This other contribution will be labeled $\mathcal{L}^\rho_{\omega\pi\gamma}$ since (4.8) has a contribution $\omega \to \pi\rho$ and ρ has a transition term for $\rho \to \gamma$ coming from the F_V term in $\mathcal{L}^{even}_V$ in eq. (4.4) that will contribute. The relevant terms are gathered in Table 4.4.

All these terms define the $\omega \to \pi\rho$ and $\rho \to \gamma$ vertices in Figure 4.3.
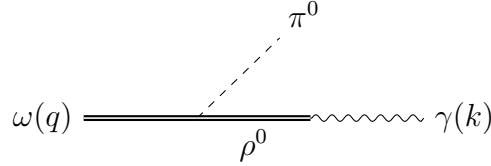
Figure 4.3. $\omega \to \pi^0\gamma$ process mediated by a ρ in RχT.

All amplitudes related to this process can be computed by using the antisymmetric tensor formulation for the vector meson resonances and the known Feynman rules for the rest of particles, shown in Table 4.5.

Process	Feynman Rule
$\langle 0 \vert V_{\mu\nu} \vert V, q\rangle$	$\frac{i}{M_V}(q_\mu\varepsilon_\nu(q) - q_\nu\varepsilon_\mu(q))$
$\langle 0 \vert F_{\mu\nu} \vert A, k\rangle$	$-i(k_\mu\varepsilon_\nu(k) - k_\nu\varepsilon_\mu(k))$
$\langle 0 \vert T\{V_{\mu\nu}(x), V_{\rho\sigma}(y)\} \vert 0\rangle$	$\frac{i}{M_V^2}\int\frac{d^4k e^{-ik(x-y)}}{(2\pi)^4(M_V^2-k^2-i\epsilon)}[g_{\mu\rho}g_{\nu\sigma}(M_V^2-k^2)$
	$+g_{\mu\rho}k_\nu k_\sigma - g_{\mu\sigma}k_\nu k_\rho + (\mu \leftrightarrow \nu)]$

Table 4.5. Feynman rules for electromagnetic fields and vector mesons in the antisymmetric tensor formulation.

Using these Feynman rules, and the convention that derivatives acting on incoming particles extract a factor $\partial_\mu A \to -ip_\mu A$ and outgoing particles take the

opposite sign, we get the following amplitudes

$$\mathcal{M}^{direct}_{\omega\pi\gamma} = i\varepsilon_{\mu\nu\rho\sigma}\varepsilon^{*\mu}_{\omega}\varepsilon^{*\nu}_{\gamma}q^{\rho}k^{\sigma}\frac{2\sqrt{2}e}{M_{\omega}M_{V}F}\left[-c_{1256}M^2_{\omega} + c_{1235}m^2_{\pi}\right],$$

$$\mathcal{M}^{\rho}_{\omega\pi\gamma} = -i\varepsilon_{\mu\nu\rho\sigma}\varepsilon^{*\mu}_{\omega}\varepsilon^{*\nu}_{\gamma}q^{\rho}k^{\sigma}\frac{4e}{M_{\omega}M^2_{V}}\frac{F_{V}}{F}\left[d_3 M^2_{\omega} + d_{123}m^2_{\pi}\right],$$

(4.10)

where the multi-index terms come from combinations of the coupling constants of (4.3)-(4.8) after applying Feynman rules of Table 4.5 and are defined as:

$$c_{1256} = c_1 - c_2 - c_5 + 2c_6,$$

$$c_{1235} = c_1 + c_2 + 8c_3 - c_5,$$

$$d_{123} = d_1 + 8d_2 - d_3.$$

(4.11)

High-energy limits on QCD behavior will impose constraints on the coupling constants of the EFT [24] since the theory is constructed to reproduce both χPT and perturbative QCD. This will be discussed in further detail in chapters 6 and 7 and here the result will be just quoted and briefly discussed. The obtained amplitude after applying these constraints is:

$$\mathcal{M}_{\omega\to\pi\gamma} = i\epsilon_{\alpha\beta\rho\sigma}\epsilon^{\alpha}_{\omega}\epsilon^{\beta}_{\gamma}q^{\rho}k^{\sigma}\frac{e}{F_V}\left(\frac{N_c}{8\pi^2}\frac{M_{\omega}}{F} - \frac{F}{2}\frac{M_{\omega}}{M^2_V}\frac{m^2_{\pi}}{M^2_{\omega}}\right).$$

(4.12)

Before these constrictions were obtained, the relations between couplings in ref. [29] were used. With these, an error of $\sim 30\%$ was obtained, compared with experimental data in [30]. With the consistent constraints in ref. [24], the error is reduced to $[7,9]\%$.

4.4   RχT extensions

A consistent set of short-distance distance constraints [24] requires the inclusion of the lightest pseudoscalar resonance nonet. This multiplet P' must be included for the sake of consistency between different observables and the constraints they impose. This multiplet is $P' = \sum^8_{a=0}\frac{\lambda_a P'^a}{\sqrt{2}}$, and assuming ideal mixing, its diagonal elements are $(P'_{11}, P'_{22}, P'_{33}) = \frac{1}{\sqrt{2}}(\pi_{1300} + \eta_{1295}, -\pi_{1300} + \eta_{1295}, \sqrt{2}\eta'_{1405})$, where the sub-indexes refer to the mass of the resonances in MeV. The kinematic and interaction terms

are [31]:

$$\mathcal{L}_{P'}^{even} = \frac{1}{2}\langle\nabla_\mu P'\nabla^\mu P'\rangle + id_m\langle P'\chi_-\rangle,$$
$$\mathcal{L}_{P'}^{odd} = \varepsilon_{\mu\nu\rho\sigma}\langle\kappa_5^P\left\{f_+^{\mu\nu}, f_+^{\rho\sigma}\right\}P' + \kappa_3^{PV}\left\{V^{\mu\nu}, f_+^{\rho\sigma}\right\}P' + \kappa^{PVV}V^{\mu\nu}V^{\rho\sigma}P'\rangle. \qquad (4.13)$$

A discussion on correct asymptotic behavior for $\langle VVP\rangle$ correlators is done in ref. [32] and it demonstrates that for the complete set of high energy conditions for $\langle VVP\rangle$ to be fulfilled, two vector meson and two pseudoscalar resonances (not to be confused with pGb) must be included. However, it is mentioned that no change in the pseudoscalar transition form factor functional form occurs as the second multiplet of pseudoscalar resonances is included. So, motivations for including more resonances exist; however, the problem of working them out limits the richness of the hadronic spectrum, so as to be useful and pragmatic. The inclusion of heavier particles is systematic but no computationally trivial, making this last note important.

5. The a_μ Anomaly

The interaction between magnetic field and angular momenta is a well known phenomenon in classical electrodynamics, a particle with a non-zero angular momentum interacts with a magnetic field [33]. In quantum theory the same happens when a non-zero spin particle interacts with a magnetic field [34]. However, a factor g between the classical prediction and the quantum case appears.

This quantum observable can be calculated for leptons with extreme precision within the electromagnetic quantum theory introduced in chapter 1, QED. Experimental information is unavailable for τ since it lives much shorter that the lighter leptons e, μ. For both e and μ there is a tension between experiment and The Standard Model's prediction (with opposite signs, however). This difference can be caused by new physics, which is generically suppressed by the factor $\frac{m_l^2}{\Lambda_{NP}^2}$, so μ will in principle be more sensitive to new physics [1].

5.1   Classical description of the gyromagnetic ratio

For the understanding of the quantum nature of the gyromagnetic ratio, a classical description can be helpful as a starting point. So let us begin with the description of the magnetic dipole moment of a loop of charge Q and mass M that rotates with an angular frequency ω.
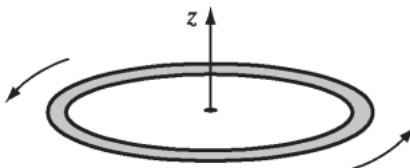
Figure 5.1. Rotating charged loop.

---

[1]Despite a_e is measured more precisely, this sensitivity to Λ_{NP} makes currently the new physics scale probed by $a_\mu \sim 20$ times higher than for the electron.

The loop has both orbital angular momentum ($\vec{L}$) and magnetic dipole moment ($\vec{m}$), these quantities are related by:

$$\vec{m} = \left(\frac{Q}{2M}\right)\vec{L}.$$ (5.1)

The factor connecting the magnetic dipole moment with the angular momentum is called the gyromagnetic ratio, which also applies for a pointlike particle. If classical theory were right, a lepton with spin $\frac{1}{2}$ would have the gyromagnetic ratio

$$\frac{|\vec{m}|}{\left|\vec{S}\right|} = \frac{e\hbar}{2m},$$ (5.2)

this is the so called *Bohr magnetron*, so that, in these units, g would be one.

5.2 μ Interaction With Light

Since μ is more sensitive than e to new physics, it is more interesting to look for a discrepancy in here. Also, the current status of the tension is greater in μ [35]. The observable in the scope of QFT is described by the following interaction.
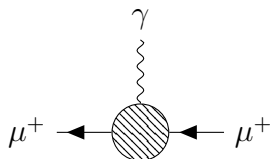
Figure 5.2. μ^+ interaction with a photon.

The blob in Figure 5.2 represents every possible contribution to this interaction. The tree level contribution in QED comes from (1.1), in the so called Gordon's decomposition [18]

$$\bar{u}_s(p')\gamma^\mu u_r(p) = \frac{1}{2m}\bar{u}_s(p')[(p'+p)^\mu + i\sigma^{\mu\nu}(p'-p)_\nu]u_r(p),$$ (5.3)

which defines the interaction of a μ with transferred momentum $p-p'$ in the interaction with a photon, which is a rotated version of (c) in Figure 1.1. The second term in (5.3) is the one which defines the electromagnetic interaction of a photon with the spin of a lepton. The spin operator is proportional to $\frac{\sigma^{\mu\nu}}{2}$, so the gyromagnetic ratio is $\frac{e}{m}$ and $g = 2$, instead of one, that would correspond to a classical angular

momentum. This is the tree level contribution, which gets slightly modified by loop corrections from all SM sectors: QED, electroweak and QCD.

5.3   1-Loop Corrections

Since the deviation from the QED classical result is the interesting observable, the *anomalous magnetic moment* of the muon is defined as:

$$a_\mu = \frac{(g-2)_\mu}{2} .$$
(5.4)

The first correction to the fundamental value of $g^{tree} = 2$ comes from the 1 loop QED contributions which are found in Figure 2.3. After renormalization, just (b) and (c) terms contribute to the vertex correction. And after explicit calculation, just the diagram in (b) contributes in the famous Schwinger's result

$$a_\mu = \frac{\alpha}{2\pi} = 0.00116.$$
(5.5)

There are second order contributions coming from the EW theory, for example
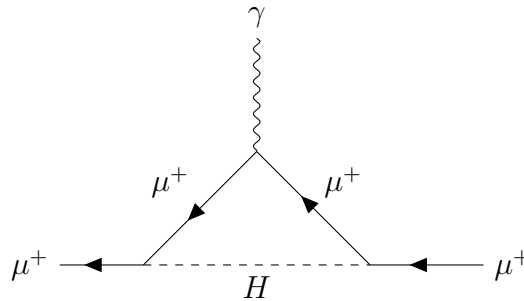
Figure 5.3. μ^+ interaction with a photon with a $\mu - H - \mu$ loop.

As this contribution, there are other 3 in the EW theory at one-loop level, involving as well Z bosons and neutrinos. Since QED and EW theories are perturbative, next to next to leading order and further corrections will increase the precision of the theoretical prediction, which will converge fast.

5.4   BNL and FNAL Experiments and the anomaly

In 2004 a dedicated experiment in Brookhaven National Lab measured a_μ [36] with unprecedented precision, finding a discrepancy between 2.2 and 2.7σ with respect to

the Standard model prediction. Both experiment and theoretical results improved and when Fermi National Lab performed a more precise measurement [37], the anomaly increased to 4.2σ, close to the required 5σ that would confirm (indirectly) the existence of new physics. These results are illustrated in Figure 5.4.
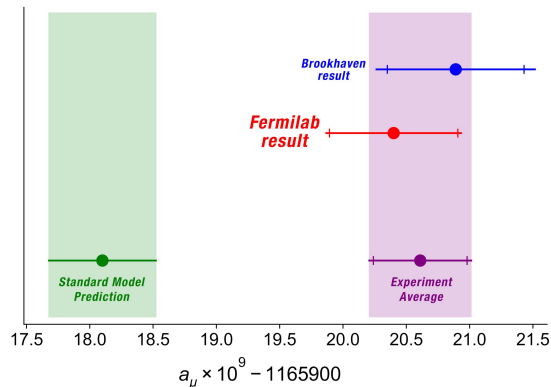
Figure 5.4. Experimental results and their deviation from The Standard Model [38].

5.4.1   Experimental Configuration

The experimental configurations are the same for both experiments (and come from the last CERN experiments), it is the precision (both systematically and statistically) which improves from BNL's to FNAL's. A picture of the last experiment is shown in Figure 5.5.
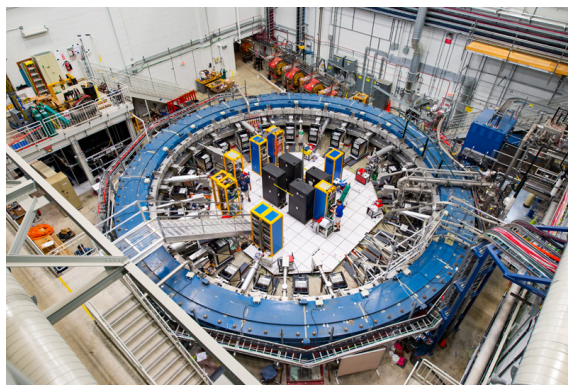
Figure 5.5. Picture of the muon g-2 experiment in FNAL [38].

The experiment consists in μ^+, which enter a solenoid of constant magnetic field right after the decay $\pi^+ \rightarrow \mu^+\nu_\mu$ (this decay occurs 99.99% of the time) and then decay via $\mu^+ \rightarrow \bar{\nu}_\mu\nu_e e^+$. The solenoid is surrounded by detectors which are

sensitive to e^+'s energy and the direction of its motion. π^+ decays are ideal, since the two-body decay has everything fixed, as it is seen in Figure 5.6.

$$\nu_\mu \xleftarrow{} \pi^+ \xrightarrow{} \mu^+$$
$$\vec{s}_{\nu_\mu} \rightarrow \qquad \leftarrow \vec{s}_{\mu^+}$$
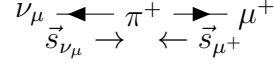
Figure 5.6. Diagram for $\pi^+ \to \mu^+ \nu_\mu$. See the main text.

The above arrow in Figure 5.6 shows the direction of the momentum of each particle and the bottom arrow is for the spin's projection in this direction (helicity). Since π^+ is a spin 0 particle, conservation of angular momentum ensures that spins are antiparallel. Also, the conservation of momentum warrants that the particles go back-to-back. Combined with the fact that νs are always left-handed, since they are massless to an excellent approximation, this translates into left-handed helicity neutrinos. This means that their spin projection is always antiparallel to its momentum. This fixes completely that the μ^+ spin projection is always antiparallel to the direction of its motion. The μ^+ starts completely polarized, but when it moves in a magnetic field B, the spin precesses with a frequency

$$\omega_0 = g_\mu \frac{Be}{2m_\mu}, \tag{5.6}$$

where g_μ is the muon gyromagnetic ratio. The μ^+ decays $\mu^+ \to \bar{\nu}_\mu \nu_e e^+$, and the maximum energy e^+ are detected, since the maximum energy is known and its direction is registered. Because the maximum energy e^+ comes in the forward direction of the antimuon's displacement, it inherits the μ^+ polarization, as they are ultrarelativistic and, because of that, have right handed helicity (the direction of the motion of e^+ is the direction of antimuon's spin before its decay). The maximum energy positron's direction is detected, at any point of the solenoid, which means that the antimuon's polarization can be measured at all points. This measurement, will be compared with the oscillation frequency of the antimuons inside the solenoid, which is [33]:

$$\omega_0 = \frac{Be}{m_\mu}. \tag{5.7}$$

With B calibrated (this needs to be done with exquisite precision and is one of the experimentalists warhorse), a direct extraction of a_μ can be performed:

$$\omega_0 - \omega_c = \frac{(g-2)_\mu}{2}(\omega_0), \tag{5.8}$$
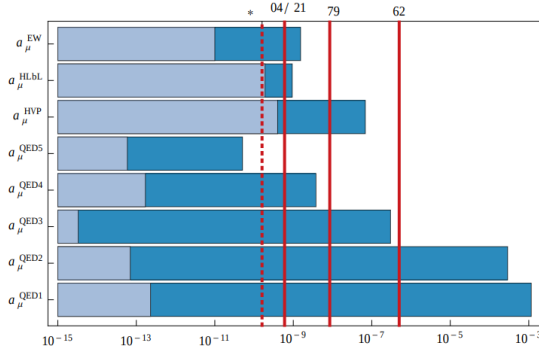
Figure 5.7. Different contributions to a_μ. The solid blue bars stand for theoretical predictions, the light blue bars are the errors for each one. The solid red lines are the experimental measurements and the dotted red lines indicate the reach of future experimental efforts [39].

Then, all the collected data can be translated into ω_0 and, with ω_c known, a_μ is obtained, in a very precise way [2].

5.5 Different contributions to a_μ

The different contributions to the muon $g - 2$ are summarized in Figure 5.7.

As it can be observed in Fig. 5.7, the main contributions come from QED calculations up to 3 loops, the 4 and 5 loops corrections are comparable with hadronic and EW contributions. However, it is observed that the hadronic uncertainties are of the same order of forthcoming a_μ measurements. For matching the experimental advances, the main effort must be done in reducing the hadronic errors.

The current status of the theoretical calculation and experimental data is [30, 8]:

$$\begin{aligned}
a_\mu^{Th'20} &= 116591810(43) \times 10^{-11}, \\
a_\mu^{Exp'21} &= 116592061(41) \times 10^{-11},
\end{aligned} \tag{5.9}$$

so that the current tension between experiment and theory is [8]:

$$\Delta a_\mu = a_\mu^{exp} - a_\mu^{th} = -251(59), \tag{5.10}$$

amounting to 4.2 standard deviations.

---

[2]In practice, not only maximum energy positrons are used. For the others, the knowledge of muon decay properties, according to Michel's distribution, is employed.

5.5.1 QED contributions

The diverse QED contributions were calculated at different moments in history. The first computation was made by Julian Schwinger in 1951 [40] and it consisted in 1 diagram. The 2-loop calculation was performed by A. Petermann and C.M. Sommerfeld in 1956 [41, 42] and it included 7 diagrams. 3-loop calculation was done by S. Laporta and E. Remiddi [43] and it comprised 72 diagrams. 4-loop calculation was accomplished by S. Laporta [44] and it consisted in 891 diagrams. Finally, the 5-loop calculation was performed numerically with 3% error by the T. Kinoshita's group [45] and it consisted in 12672 diagrams. The current value for the total QED contribution is:

$$a_\mu^{QED} = 116584718.931(104) \times 10^{-11}. \tag{5.11}$$

5.5.2 EW contributions

The EW contributions were updated in 2013 by D. Gnendiger, D. Stöckinger and H. Stöckinger-Kim up to two loops, accounting for the Higgs mass measurement [46], the current EW total contribution is:

$$a_\mu^{EW} = 153.6(1.0) \times 10^{-11}. \tag{5.12}$$

5.5.3 QCD contributions

As it was seen in Figure 5.7, the QCD contributions are split into two, the Hadronic Vacuum Polarization (HVP) and the Hadronic Light by Light Scattering (HLbL). From these, the first one can be connected to experiment directly. The second one requires a deeper theoretical effort, since it cannot be obtained completely like that at the moment. We will use RχT to compute its main contribution, which is unambiguously defined and connected to measurable form factors within the dispersive formulation [11].

5.5.3.1 Hadronic Vacuum Polarization

The HVP is a two-loop QCD contribution (an hadronic loop is added to the Schwinger diagram), whose general topology is depicted in Figure 5.8.

The blob includes all possible intermediate hadronic states. The intermediate line can be connected with the $e^+e^- \rightarrow$ hadrons amplitude trough the spectral
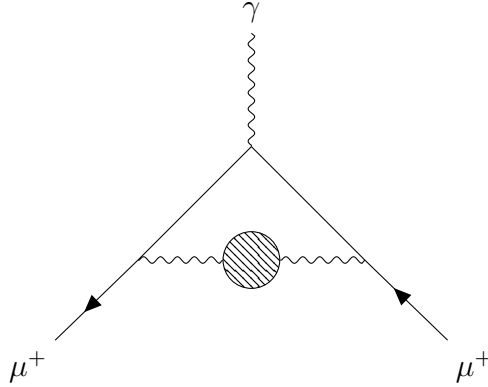
Figure 5.8. HVP general diagram.

theorem. The currently accepted value for the HVP contribution is [8]:

$$a_\mu^{HVP} = 6845(40) \times 10^{-11}. \tag{5.13}$$

5.5.3.2 Hadronic Light by Light Scattering

HLbL is the hardest calculation to perform, since it cannot be connected unambiguously to experimental data. An EFT approximation or dispersive methods can be employed in order to consider as many contributing processes as possible, which are in principle connected to measurable data. The bigger contributions to HLbL are the pseudoscalar pole ones, which will be discussed in the two last chapters. The general diagram for this is shown in Figure 5.9, that is order α suppressed with respect to the leading contribution to HVP.
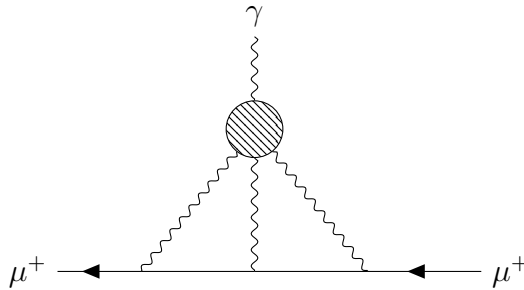
Figure 5.9. HLbL general diagram. The blob includes any type of hadron interactions.

The blob contains all possible intermediate hadronic states. It can be described by RχT by taking into account the most relevant hadronic states. The current value for HLbL is:

$$a_\mu^{HLbL} = 92(18) \times 10^{-11}. \tag{5.14}$$

This is consistent with the upper limit set in ref. [47] which is based on the fact that the hadron loop is almost saturated by parton level effects, this bound is $a_\mu^{HLbL} < 159 \times 10^{-11}$.

6. Contribution of the π^0 pole to a_μ

From all the contributions to the HLbL piece of the anomalous magnetic moment of the muon in the standard model, the most important one is the pseudoscalar-pole contribution [8]. Its computation cannot be performed in perturbation theory, so an EFT (or dispersive approach or model) must be used instead. The current tension between experiment and theory in a_μ has turned it into a precision problem, so evaluating this contribution with a reduced error is very important. The diagrams that describe this process are:
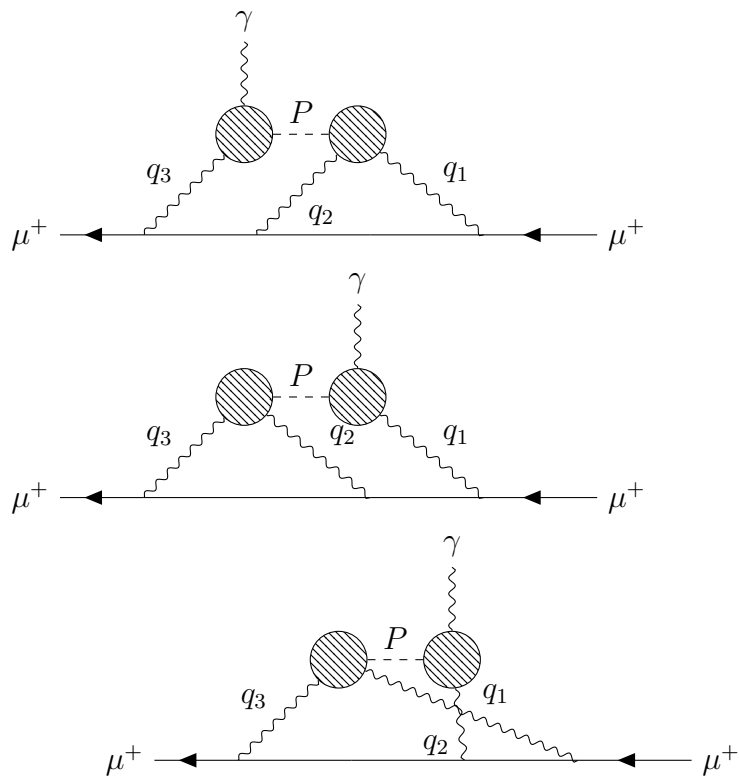
Figure 6.1. Feynman diagrams for the pseudoscalar-pole contribution to the HLbL piece of a_μ.

6.1 Pseudoscalar-pole contributions

The pseudoscalar pole contributions up to date [8] are:

P	$a_\mu^{P-pole} \times 10^{11}$
π^0	$63.0^{+2.7}_{-2.1}$
η	$16.3(1.4)$
η'	$14.5(1.9)$
$\pi^0 + \eta + \eta'$	$93.8^{+4.0}_{-3.6}$

Table 6.1. SM predictions for the pseudoscalar-pole contributions to the HLbL piece of a_μ.

The other contributions are smaller, these ones are π, K loops/boxes, S-wave $\pi\pi$ rescattering, scalars, tensors, axial vectors, u, d, s-loops/short-distance and c-loop. After summing up all these contributions, the magnitude remains similar but the error grows almost 5 times. Its current value is [8]

$$a_\mu^{HLbL} \times 10^{11} = 92 \pm 18. \tag{6.1}$$

6.2 π^0 pole contribution to the Hadronic light-by-light piece of a_μ

The pseudoscalar-pole contribution to the HLbL tensor can be easily obtained within the language of Green's functions. Inserting the identity as a sum over the QCD spectrum $((1 = \sum_X \int d\Pi_x |X\rangle \langle X|$, with $|X\rangle$ on-shell intermediate hadronic states) within the HLbL tensor [9, 48], it is obtained that such function exhibits well-isolated poles for the lightest pseudoscalar states. From here, the π^0 contribution can be taken from this sum with $X = \pi^0$. The γ with momenta q_i are off-shell, and the external γ is the only on-shell photon in the contribution. This procedure translates the diagrams in Figure 6.1 into the integral:

$$
a_\mu^{HLbL,\pi^0-\text{pole}} = -\frac{2\pi}{3} \left(\frac{\alpha}{\pi}\right)^3 \int_0^\infty dQ_1 dQ_2 \int_{-1}^{+1} dt \sqrt{1-t^2} Q_1^3 Q_2^3
$$
$$
\times \left[\frac{F_1 I_1(Q_1, Q_2, t)}{Q_2^2 + m_\pi^2} + \frac{F_2 I_2(Q_1, Q_2, t)}{Q_3^2 + m_\pi^2}\right], \tag{6.2}
$$

where $Q_3^2 = Q_1^2 + Q_2^2 + 2Q_1Q_2t$. F_i are expressed in terms of the transition form factors:

$$F_1 = \mathcal{F}_{\pi\gamma^*\gamma^*}(Q_1^2, Q_3^2)\mathcal{F}_{\pi\gamma^*\gamma^*}(Q_2^2, 0),$$
$$F_2 = \mathcal{F}_{\pi\gamma^*\gamma^*}(Q_1^2, Q_2^2)\mathcal{F}_{\pi\gamma^*\gamma^*}(Q_3^2, 0), \tag{6.3}$$

where I_i are defined as:

$$
\begin{aligned}
I_1(Q_1, Q_2, t) =& \frac{-1}{m_\mu^2 Q_3^2}\left[\frac{4m_\mu^2 t}{Q_1 Q_2} + (1 - R_{m1})\left(\frac{2Q_1 t}{Q_2}4(1 - t^2)\right)\right.\\
&\left. -(1 - R_{m1})^2\frac{Q_1 t}{Q_2} - 8X(Q_1, Q_2, t)(Q_2^2 - 2m_\mu^2)(1 - t^2)\right]\\
I_2(Q_1, Q_2, t) =& \frac{-1}{m_\mu^2 Q_3^2}\left[2(1 - R_{m1})\left(\frac{Q_1 t}{Q_2} + 1\right) + 2(1 - R_{m2})\left(\frac{Q_2 t}{Q_1} + 1\right)\right.\\
&4X(Q_1, Q_2, t)(Q_3^2 + 2m_\mu^2(1 - t^2))\Big],
\end{aligned}
\tag{6.4}
$$

in which $X(Q_1, Q_2, t)$ and R_{mi} are defined as:

$$X(Q_1, Q_2, t) = \frac{(1 - t^2)^{-1/2}}{Q_1 Q_2}\arctan\left(\frac{z\sqrt{1 - t^2}}{1 - zt}\right)$$
$$R_{mi} = \sqrt{1 + \frac{4m_\mu^2}{Q_i^2}}. \tag{6.5}$$

Finally, z is defined as:

$$z = \left(\frac{Q_1 Q_2}{4m_\mu^2}\right)(1 - R_{m1})(1 - R_{m2}). \tag{6.6}$$

According to this definition of the model independent computation of a_μ, the only input which is unknown is the transition form factor of the pion $\mathcal{F}_{\pi\gamma^*\gamma^*}(Q_1, Q_2)$, which will be calculated from our EFT, whose constants will be later set by asymptotic QCD constraints and experimental data. The resulting two loop integrals can be treated by first performing the angular integration analytically, using the method of Gegenbauer polynomials, followed by a numerical evaluation of the remaining two dimensional integration over the moduli of the Euclidean loop momenta [10]. The integral in eq. (6.2) can be performed as a double integral instead of a triple one [1]

---

[1]This can also be accomplished by setting the pion on-shell by means of a delta function, with good enough approximation in the numerical integration.

if the pole form factor is written in the form:

$$\mathcal{F}_{\pi^0\gamma^*\gamma^*}(q_1^2, q_2^2) = \frac{F_\pi}{3}\left[f(q_1) - \sum_{M_{V_i}}\frac{1}{q_2^2 - M_{V_i}^2}g_{M_{V_i}}(q_1^2)\right]. \tag{6.7}$$

After the angular integration in eq. (6.2), assuming -as it holds in physically motivated cases- that π^0-TFF has the shape in eq. (6.7), the pion pole contribution to the HLbL piece of a_μ is:

$$a_\mu^{HLbL:\pi^0-\text{pole}} = \left(\frac{\alpha}{\pi}\right)^3\left[a_\mu^{HLbL:\pi^0(1)} + a_\mu^{HLbL:\pi^0(2)}\right], \tag{6.8}$$

where $a_\mu^{HLbL:\pi^0(1)}$ and $a_\mu^{HLbL:\pi^0(2)}$ are defined as:

$$a_\mu^{HLbL:\pi^0(1)} = \int_0^\infty dQ_1 \int_0^\infty dQ_2\left[w_{f_1}(Q_1,Q_2)f^{(1)}(Q_1^2,Q_2^2) + \sum_{M_{V_i}}w_{g_1}(M_{V_i},Q_1,Q_2)g_{M_{V_i}}^{(1)}(Q_1^2,Q_2^2)\right],$$

$$a_\mu^{HLbL:\pi^0(2)} = \int_0^\infty dQ_1 \int_0^\infty dQ_2 \sum_{M=m_\pi,M_{V_i}}w_{g_2}(M,Q_1,Q_2)g_M^{(2)}(Q_1^2,Q_2^2), \tag{6.9}$$

with

$$f^{(1)} = \frac{F_\pi}{3}f(-Q_1^2)\mathcal{F}_{\pi^0\gamma^*\gamma^*}(-Q_2^2,0),$$

$$g_{M_{V_i}}^{(1)} = \frac{F_\pi}{3}\frac{g_{M_{V_i}}(-Q_1^2)}{M_{V_i}^2}\mathcal{F}_{\pi^0\gamma^*\gamma^*}(-Q_2^2,0),$$

$$g_{m_\pi}^{(2)} = \frac{F_\pi}{3}\mathcal{F}_{\pi^0\gamma^*\gamma^*}(-Q_1^2,-Q_2^2)\left(f(0) + \sum_{M_{V_i}}\frac{g_{M_{V_i}}(0)}{M_{V_i}^2 - m_\pi^2}\right),$$

$$g_{M_{V_i}}^{(2)} = \frac{F_\pi}{3}\mathcal{F}_{\pi^0\gamma^*\gamma^*}(-Q_1^2,-Q_2^2)\frac{g_{M_{V_i}}(0)}{m_\pi^2 - M_{V_i}^2},$$

$$\tag{6.10}$$

where the weight functions $w_{f_1}(Q_1^2, Q_2^2)$, $w_{g_i}(M^2, Q_1^2, Q_2^2)$ are:

$$
\begin{aligned}
w_{f_1}(Q_1, Q_2) =& \frac{\pi^2}{Q_2^2 + M_\pi^2} \frac{1}{6m_\mu^2 Q_1 Q_2} \Bigg\{ -4(2m_\mu^2 - Q_2^2)(Q_1^2 - Q_2^2)^2 \ln\Big[1+ \\
& \frac{(Q_1^2 + Q_2^2 - R^0)(Q_1^2 - R_1^{m_\mu})(Q_2^2 - R_2^{m_\mu})}{8m_\mu^2 Q_1^2 Q_2^2}\Big] + \Big[-4m_\mu^2 Q_1^2 Q_2^2 - \frac{1}{m_\mu^2 Q_1^4 Q_2^4} \\
& + \frac{1}{2m_\mu^4}Q_1^4 Q_2^6 + Q_1^6 - 3Q_1^4 Q_2^2 - Q_1^2 Q_2^4 + Q_2^6\Big]\left(1 - \frac{R_1^{m_\mu}}{Q_1^2}\right) - (Q_1^2 - Q_2^2)^2 \\
& \times R^0\left(1 - \frac{R_1^{m_\mu}}{Q_1^2}\right) + \frac{1}{m_\mu^2}Q_2^2(Q_2^4 - 4m_\mu^4)R_1^{m_\mu} - \frac{1}{2m_\mu^4}Q_1^4(Q_2^2 - 2m_\mu^2)R_2^{m_\mu} \\
& + \frac{1}{2m_\mu^4}(Q_2^2 - 2m_\mu^2)(Q_1^2 Q_2^2 - 2m_\mu^2 Q_1^2 - 2m_\mu^2 Q_2^2)R_1^{m_\mu} R_2^{m_\mu}\Bigg\}, \\
w_{g_1}(M, Q_1, Q_2) =& \frac{\pi^2}{Q_2^2 + M_\pi^2} \frac{1}{6m_\mu^2 Q_1 Q_2} \Bigg\{ -4(2m_\mu^2 - Q_2^2)(Q_1^2 - Q_2^2)^2 \ln\Big[1+ \\
& \frac{(Q_1^2 + Q_2^2 - R^0)(Q_1^2 - R_1^{m_\mu})(Q_2^2 - R_2^{m_\mu})}{8m_\mu^2 Q_1^2 Q_2^2}\Big] + 4(2m_\mu^2 - Q_2^2)[M^4 + (Q_1^2 - Q_2^2)^2 \\
& + 2M^2(Q_1^2 + Q_2^2)]\ln\Big[1 + \frac{(M^2 + Q_1^2 + Q_2^2 - R^M)(Q_1^2 - R_1^{m_\mu})(Q_2^2 - R_2^{m_\mu})}{8m_\mu^2 Q_1^2 Q_2^2}\Big] \\
& - \Big[M^6 + 3M^4 Q_1^2 + 3M^2 Q_1^4 + 3M^4 Q_2^2 + 2M^2 Q_1^2 Q_2^2 + 3M^2 Q_2^4 - \frac{M^2}{m_\mu^2}Q_1^2 Q_2^4\Big] \\
& \times \left(1 - \frac{R_1^{m_\mu}}{Q_1^2}\right) - (Q_1^2 - Q_2^2)^2 R^0\left(1 - \frac{R_1^{m_\mu}}{Q_1^2}\right) - \frac{M^2}{m_\mu^2}Q_1^2(Q_2^2 - 2m_\mu^2)R_2^{m_\mu}\Big(1 \\
& - \frac{R_1^{m_\mu}}{Q_1^2}\Big) + [M^4 + 2M^2 Q_1^2 + 2M^2 Q_2^2 + Q_1^4 + Q_2^4 - 2Q_1^2 Q_2^2]R^M\left(1 - \frac{R_1^{m_\mu}}{Q_1^2}\right)\Bigg\}, \\
w_{g_2}(M, Q_1, Q_2) =& \frac{\pi^2}{6m_\mu^2 M^2 Q_1 Q_2} \Bigg\{ -M^2 R_1^{m_\mu} R_2^{m_\mu} + 4[m_\mu^2(Q_2^2 - Q_1^2) + 2Q_1^2 Q_2^2](Q_1^2 - Q_2^2) \\
& \times \ln\Big[1 + \frac{(Q_1^2 + Q_2^2 - R^0)(Q_1^2 - R_1^{m_\mu})(Q_2^2 - R_2^{m_\mu})}{8m_\mu^2 Q_1^2 Q_2^2}\Big] + 4[M^2 m_\mu^2(Q_1^2 - Q_2^2) \\
& [-2Q_1^2 Q_2^2 + m_\mu^2(Q_1^2 - Q_2^2)] + 2M^2[Q_1^2 Q_2^2 + m_\mu^2(Q_1^2 + Q_2^2)]]\ln\Big[1+ \\
& \frac{(M^2 + Q_1^2 + Q_2^2 - R^M)(Q_1^2 - R_1^{m_\mu})(Q_2^2 - R_2^{m_\mu})}{8m_\mu^2 Q_1^2 Q_2^2}\Big] + M^4 Q_1^2 + 2M^2 Q_1^4 + M^4 Q_2^2 \\
& - M^2 Q_1^2 Q_2^2 + 2M^2 Q_2^4 + Q_1^2(Q_1^2 + Q_2^2)R^0\left(1 - \frac{R_1^{m_\mu}}{Q_1^2}\right) + Q_2^2(Q_2^2 - 3Q_1^2)R^0\Big(1 \\
& - \frac{R_2^{m_\mu}}{Q_2^2}\Big) - Q_1^2(M^2 + Q_1^2 + Q_2^2)R^M\left(1 - \frac{R_1^{m_\mu}}{Q_1^2}\right) - M^2(M^2 + 2Q_1^2 + Q_2^2)R_1^{m_\mu} - \\
& Q_2^2(M^2 - 3Q_1^2 + Q_2^2)R^M\left(1 - \frac{R_2^{m_\mu}}{Q_2^2}\right) - M^2(M^2 - 3Q_1^2 + 2Q_2^2)R_2^{m_\mu}\Bigg\},
\end{aligned}
$$

$$(6.11)$$

and the $R_i^{m_\mu}$, R^0 and R^M are:

$$R_i^{m_\mu} = \sqrt{Q_i^4 + 4m_\mu^2 Q_i^2} \quad i = 1, 2,$$

$$R^M = \sqrt{(M^2 + Q_1^2 + Q_2^2)^2 - 4Q_1^2 Q_2^2},$$

$$R^0 = \sqrt{(Q_1^2 + Q_2^2)^2 - 4Q_1^2 Q_2^2}.$$

(6.12)

This method, reduces the triple integral in eq. (6.2) into a double integral which can be computed by using numerical methods. Since the triple integral has inverse trigonometric functions of Q_1, Q_2, its evaluation becomes demanding even by using numerical methods, so the procedure of Gegenbauer polynomials becomes useful and convenient for $F_{\pi\gamma^*\gamma^*}$ with higher complexity, as in the case of two vector meson multiplets of resonances which we will be working in this thesis. In previous models for the construction of π-TFF this method was used for the computation of a_μ. For academical purposes, we performed the computation of them and reproduced correctly all values of ref. [10], see Table 6.2. The expressions for π-TFF in these models are:

$$\mathcal{F}_{\pi^0\gamma^*\gamma^*}^{WZW}(q_1^2, q_2^2) = -\frac{N_C}{12\pi^2 F_\pi},$$

$$\mathcal{F}_{\pi^0\gamma^*\gamma^*}^{VMD}(q_1^2, q_2^2) = -\frac{N_C}{12\pi^2 F_\pi} \frac{M_V^2}{(q_1^2 - M_V^2)} \frac{M_V^2}{(q_2^2 - M_V^2)},$$

$$\mathcal{F}_{\pi^0\gamma^*\gamma^*}^{LMD}(q_1^2, q_2^2) = \frac{F_\pi}{3} \frac{q_1^2 + q_2^2 - \frac{NC}{4\pi^2}\frac{M_V^4}{F_\pi^2}}{(q_1^1 - M_V^2)(q_2^2 - M_V^2)},$$

$$\mathcal{F}_{\pi^0\gamma^*\gamma^*}^{LMD+V}(q_1^2, q_2^2) = \frac{F_\pi}{3} \frac{q_1^2 q_2^2(q_1^2 + q_2^2) + h_1(q_1^2 + q_2^2)^2 + h_2 q_1^2 q_2^2 + h_5(q_1^2 + q_2^2) + h_7}{(q_1^2 - M_{V_1}^2)(q_2^2 - M_{V_1}^2)(q_1^2 - M_{V_2}^2)(q_2^2 - M_{V_2}^2)},$$

(6.13)

where the constants in the LMD+V are[10] $h_1 = 0$, $h_5 = 6.88 \pm 0.61 \text{GeV}^4$, $h_7 = -\frac{N_C}{4\pi^2}\frac{M_{V_1}^4 M_{V_2}^4}{F_\pi^2}$ and h_2 is unknown but will be taken from -10GeV^2 to 10GeV^2 and since in the WZW case the form factor integral is divergent, it is integrated just from 0GeV to 1GeV.

6.3 Pion Transition Form Factor (π^0 TFF)

As it can be seen in Table 6.1, the π^0 pole is the biggest contribution to the whole a_μ^{HLbL}, so the precise descriptions of the diagrams in Figure 6.1 in the case of $P = \pi$

Form Factor	$a_\mu^{\text{HLbL}:\pi(1)}$	$a_\mu^{\text{HLbL}:\pi(2)}$	$a_\mu^{\text{HLbL}:\pi-\text{pole}} \times 10^{10}$
WZW	0.095	0.0020	12.2
VMD	0.044	0.0013	5.6
LMD	0.057	0.0014	7.3
LMD+V ($h_2 = -10\text{GeV}^2$)	0.049	0.0013	6.3
LMD+V ($h_2 = 0\text{GeV}^2$)	0.045	0.0013	5.8
LMD+V ($h_2 = 10\text{GeV}^2$)	0.041	0.0013	5.3

Table 6.2. Results for the terms $a_\mu^{HLbL:\pi^0(1)}$, $a_\mu^{HLbL:\pi^0(2)}$ y $a_\mu^{HLbL:\pi^0-\text{pole}}$ for different models.
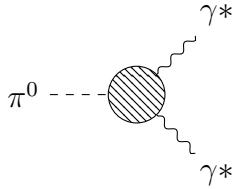
Figure 6.2. π^0 Transition Form Factor.

are fundamental for the precision in the calculation of the HLbL piece of a_μ. The vertex with two photons and one neutral pion is described by the π^0-TFF, as seen in Fig. 6.2.

The blob in Figure 6.2 can be described by RχT so that it ensures χPT at low energies and asymptotic QCD for high energies, in such a way that it can be used at all virtualities as the loop integrals go from 0 to ∞. Consequently, this vertex construction and computation are the building blocks for the theoretical calculation of $a_\mu^{HLbL:\pi^0-\text{pole}}$.

6.4 π^0-**TFF in** $R\chi T$

The calculation of π^0-TFF can be performed with all the formalism constructed in Chapter 3. The procedure is similar to the one for $\omega \to \pi\gamma$, with two important remarks: first, explicit chiral symmetry breaking terms are included (as they are necessary at the current level of precision); second, γ in this case are off-shell particles, since in the diagrams of Figure 6.1, the π^0-TFF is needed with one or two virtual γs.

6.4.1 $R\chi T$ Lagrangian for the π-TFF including the lightest meson resonances

The transition form factor can be computed explicitly in RχT, with the unconstrained constants coming from [2] the order p^6 chiral contributions in equation (4.6), the odd-intrinsic parity sector with 1 and 2 resonances in equations (4.3) and (4.8), respectively, and the pseudoscalar resonance $P \to P'$ transition vertex. In the 1 multiplet of resonances case, with chiral symmetry breaking, a set of relevant shifts on the couplings and masses are displayed on Table 6.3.

quantity	value with chiral symmetry breaking
$M^2_{\rho(\omega)}$	$M^2_V - 4e^V_m m^2_\pi$
$F_{V\rho}$	$(F_V + 8m^2_\pi \lambda_V)$
$F_{V\omega}$	$\frac{1}{3}(F_V + 8m^2_\pi \lambda_V)$

Table 6.3. Relevant shifts on masses and couplings caused by chiral symmetry breaking.

From the pseudoscalar resonance there are relevant processes which contribute to the π^0-TFF, these are recapitulated in the diagrams of Figure 6.3.

These diagrams contribute to the process, resulting in shifts on the constants introduced before:

$$C^W_7 \to C^{W*}_7 = C^W_7 + \frac{4d_m \kappa^P_5}{3M^2_{\pi_{(1300)}}},$$

$$c_3 \to c^*_3 = c_3 + \frac{d_m M_V \kappa^{PV}_3}{M^2_{\pi_{(1300)}}},$$

$$d_2 \to d^*_2 = d_2 + \frac{d_m \kappa^{PVV}}{2M^2_{\pi_{(1300)}}}. \tag{6.14}$$

6.4.2 π^0 TFF for LMD

LMD stands for lowest meson dominance. That is, only the pseudo-Goldstone bosons and the lightest vector (and, in this case, pseudoscalar) resonances are accounted for. The amplitude one gets with all these contributions is:

$$\mathcal{M}^{R\chi T:V,P,P'}_{\pi^0 \gamma^* \gamma^*} = ie^2 \epsilon^{\mu\nu\rho\sigma} q_{1\mu} q_{2\nu} \varepsilon^*_{1\rho} \varepsilon^*_{2\sigma} \mathcal{F}_{\pi^0 \gamma^* \gamma^*}(q^2_1, q^2_2), \tag{6.15}$$

---

[2]We recall that the Wess-Zumino-Witten part, calculated in equation (3.43, depends only on the pion decay constant and the number of colors.
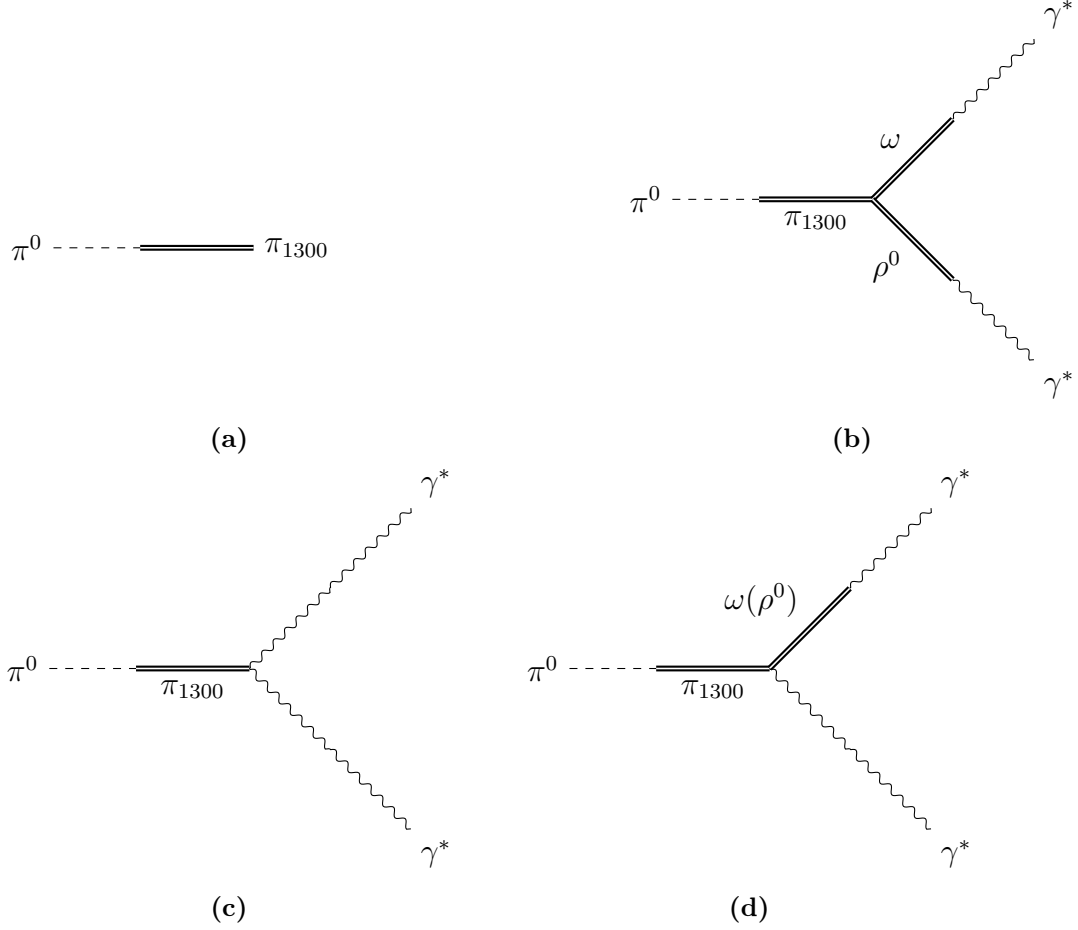
Figure 6.3. Feynman diagrams involving $\pi_{(1300)}$ relevant for π^0-TFF.

where $F_{\pi^0\gamma^*\gamma^*}^{R\chi T:V,P,P'}(q_1^2, q_2^2)$ is the π^0-TFF. And for the case of RχT with pGb(P), 1 vector meson resonance multiplet (V) and a pseudoscalar meson resonance multiplet (P') we get:

$$
\begin{aligned}
\mathcal{F}_{\pi^0\gamma^*\gamma^*}^{R\chi T:V,P,P'}(q_1^2, q_2^2) = \frac{2}{3F} &\left\{ \left(\frac{-N_C}{8\pi^2} - 8(q_1^2 + q_2^2)C_{22}^W + 32m_\pi^2 C_7^{W*} \right) \right. \\
&\left[\frac{-\sqrt{2}(F_V + 8m_\pi^2\lambda_V)}{M_V} \left(m\pi^2 c_{1235}^* + c_{125}q_1^2 - c_{1256}q_2^2 \right) \left(\frac{1}{M_\rho^2 - q_2^2} + \frac{1}{M_\omega^2 - q_2^2} \right) \right. \\
&\left. + 2(F_V + 8m_\pi^2\lambda_V)^2 \frac{m_\pi^2 d_{123}^* + d_3(q_1^2 + q_2^2)}{(M_\rho^2 - q_1^2)(M_\omega^2 - q_2^2)} \right] + (1 \leftrightarrow 2) \left. \right\},
\end{aligned}
$$
(6.16)

where the $1 \leftrightarrow 2$ implies both the exchange of momenta and polarizations, which leaves the non π^0-TFF part of equation (6.15) invariant because of the antisymmetry

65

properties of the Levi-Civita's symbol. The multi-index couplings are defined as:

$$c^*_{1235} = c_1 + c_2 + 8c^*_3 - c_5$$
$$c_{1256} = c_1 - c_2 - c_5 + 2c_6$$
$$c_{125} = c_1 - c_2 + c_5$$
$$d^*_{123} = d_1 + 8d^*_2 - d_3, \qquad (6.17)$$

and come from a similar procedure as in Tables 4.3, 4.4 and 4.5.

6.4.3 Short-Distance Constraints (LMD)

Perturbative expansions for g_s (or α_s) at high energies can be performed for QCD, and establish how some strong interacting observables must behave in this regime. These conditions are called short-distance constraints and their information for the π^0-TFF case can be split into three groups: vanishing π^0-TFF at high energies, correlator $\langle VVP \rangle$ at high energies and dominant behavior of π^0-TFF at high energies[56, 57, 58, 59]. The first group of constraints comes from the restrictions:

$$\lim_{Q^2 \to \infty} \mathcal{F}_{\pi^0 \gamma^* \gamma^*}(-Q^2, -Q^2) = 0, \quad \lim_{Q^2 \to \infty} \mathcal{F}_{\pi^0 \gamma^* \gamma^*}(-Q^2,) = 0. \qquad (6.18)$$

The second group of constraints comes from the behavior of the $\langle VVP \rangle$ QCD correlator:

$$(\Pi_{VVP})^{abc}_{\mu\nu}(p, q) = i^2 \int d^4x d^4y e^{i(px+qy)} \langle 0| T \left\{ V^a_\mu(x) V^b_\nu(y) P^c(0) \right\} |0\rangle, \qquad (6.19)$$

where V^a_μ and P^c are the even parity vector octet and the odd parity pseudoscalar conserved currents in (3.11), respectively. The two groups of constraints impose the

following relations between the RχT couplings[24, 7]:

$$c_1 = c_2 - c_5 = c_3 = c_{125} = c_{1235} = 0,$$

$$c_{1235}^* = 8c_3^* = \frac{8d_m\kappa^{PV}M_v}{m_{\pi_{(1300)}}^2} = \frac{N_C e_m^V M_V}{8\sqrt{2}\pi^2 F_V},$$

$$d_{123}^* = \frac{F^2}{8F_V^2} + \frac{4d_m\kappa^{PVV}}{m_{\pi_{(1300)}}^2}, \quad d_{123} = \frac{F^2}{8F_V^2},$$

$$d_3 = -\frac{N_C M_V^2}{64\pi^2 F_V^2}, \quad c_{1256} = -\frac{N_C M_V}{32\sqrt{2}\pi^2 F_V},$$

$$C_7^{W*} = \lambda_V = 0, \quad \kappa_5^P = 0, \quad C_7^W = C_8^W = C_{22}^W = 0. \tag{6.20}$$

This reduces the π^0-TFF to:

$$\mathcal{F}_{\pi^0\gamma^*\gamma^*}(q_1^2, q_2^2) = \frac{32\pi^2 m_\pi^2 F_V^2 d_{123}^* - N_C M_V^2 M_\rho^2}{12\pi^2 F_\pi(M_\rho^2 - q_1^2)(M_\omega^2 - q_2^2)}, \tag{6.21}$$

so that, in the chiral and large N_C limits, it matches previous results [32][10]:

$$\mathcal{F}_{\pi^0\gamma^*\gamma^*}(q_1^2, q_2^2) = -\frac{N_C M_V^2}{12\pi^2 F_0(M_V^2 - q_1^2)(M_V^2 - q_2^2)}. \tag{6.22}$$

6.5 Wrong asymptotic behavior of the LMD π^0 TFF

The third set of constraints to be imposed by asymptotic QCD is the one of the leading term at large $Q^2 = -q^2$:

$$\lim_{Q^2\to\infty} Q^2 \mathcal{F}_{\pi^0\gamma^*\gamma^*}(-Q^2, -Q^2) = \frac{2F}{3}, \quad \lim_{Q^2\to\infty} Q^2 \mathcal{F}_{\pi^0\gamma^*\gamma^*}(-Q^2, 0) = 2F. \tag{6.23}$$

From these, just the second one can be reproduced by the RχT working with the pGbs and the first multiplet of V and P resonances. There is not enough freedom left (undetermined coupling constants) in order to give the correct behavior. The doubly virtual π^0-TFF gives a $\frac{1}{q^4}$ leading contribution for high energies. This underestimates the π^0-pole's contribution to a_μ, since it falls faster than it should, so it induces an asymmetric systematic theory error in the evaluation of ref. [7]. This issue should be fixed including an additional multiplet of spin-one resonances in RχT: this is the aim of this work (here only the π^0 case is included, the η and η' contributions are left for future work).

6.6 Experimental input for π^0 TFF couplings

Experimental input can be used to fit the free parameters from equation (6.21), in this case, just one. For the case of η and η', there are more parameters. Information from CLEO [49], CELLO [50], LEP [51], BaBar [52, 53], Belle [54] and BESIII [55] experiments can be used for this purpose. Technical details on how to obtain these data are beyond the scope of this work, however a mention to the processes which give us information about the π^0-TFF is a good exercise to appreciate the basics of the involved experimental methods and ideas. One of these processes is the Dalitz decay of light pseudoscalar mesons, it gives information on the 1 virtual photon in the time-like sector as it can be seen in Figure 6.4. The double Dalitz decay $(\pi^0 \to 2(e^+e^-))$ gives access to the doubly virtual case[60].
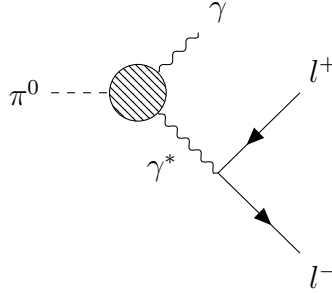
Figure 6.4. Dalitz decay of a π^0.

e^+e^- colliders also give information on the time-like region of π^0-TFF, the specific process which is useful for this observable is the one in Figure 6.5.
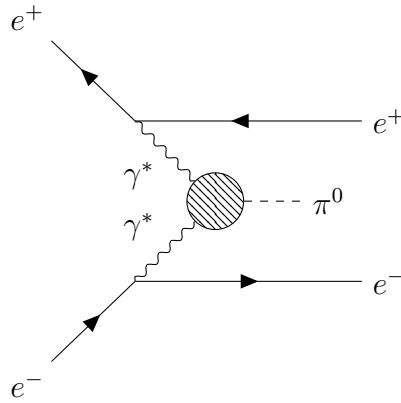
Figure 6.5. The $e^+e^- \to e^+e^-\pi^0$ process gives information about the π^0-TFF.

And finally two-photon collisions are studied at e^+e^- colliders. The cross section

of pseudoscalar meson production in two-photon collisions is proportional to the square of the respective spacelike TFF.

For this work and in [7], just the space-like information will be used. And only the one virtual γ case is used to estimate the values of the constants by comparison to experimental data from all experiments except BaBar [52] since π^0-TFF behaves differently (and seem to be at odds with the Brodsky-Lepage constraint) than the rest of high-energy data (particularly from Belle).

6.7 Results of π^0-pole contribution to a_μ (LMD)

In the RχT scheme with one multiplet of pseudoscalar and vector resonances, the results for fitting the constants in (6.21) to experimental data (except for BaBar), are gathered in Table 6.4 [7]. The fit is not sensitive to F_V^2, F_π^2 and d_{123}^* but only

constant	fit without BaBar data
$\bar{d}_{123}$	$(-2.3 \pm 1.5) \times 10^{-1}$
M_V	(791 ± 6)MeV
e_m^V	(-0.36 ± 0.10)

Table 6.4. Constants obtained from π^0-TFF experimental data to $\bar{d}_{123}$, M_V and e_m^V in (6.21).

to the combination $\frac{F_V^2 d_{123}^*}{F_\pi^2}$ which was called $\bar{d}_{123}$ in [7] [3]. With this information, the π^0-pole contribution to the HLbL piece of a_μ was calculated from (6.2) using the data of Table 6.4 in equation (6.21). The obtained value was [7] [4]:

$$a_\mu^{HLbL,\pi^0-\text{pole}} = (58.1 \pm 0.9) \times 10^{-11}. \tag{6.24}$$

This result is compatible with the dispersive one [11]

$$a_\mu^{HLbL,\pi^0-\text{pole}} = \left(6.26^{+0.30}_{-0.25}\right) \times 10^{-10}, \tag{6.25}$$

which is taken as the reference result in the White Paper [8], once updated by the final PrimEx measurement of $\Gamma(\pi^0 \to \gamma\gamma)$, to $\left(6.30^{+0.27}_{-0.21}\right) \times 10^{-10}$.

---

[3]Other fits are provided in this reference, and the minimization included η and η' TFF data as well, resulting in other couplings being fitted (which we do not display here).

[4]This result does not include the dominant systematic uncertainty, coming from the wrong asymptotic behaviour of the TFF, which amounted to $+0.5 \cdot 10^{-10}$ for the sum of the π^0, η and η' contributions (it is $\sim +0.3 \cdot 10^{-10}$ for the π^0-pole part).

7. $a_\mu^{\pi-\text{pole}}$ calculation via RχT in the two hadron saturation scheme

As mentioned in the section 6.5 and at the end of 6.7, the leading asymptotic contribution of the doubly virtual π^0-TFF lead to an underestimation of the total $a_\mu^{HLbL:\pi^0-\text{pole}}$ contribution. Aiming to confirm or refute the anomaly between experiment and the Standard Model prediction for a_μ is a precision problem, so fixing this systematic error is needed for the RχT computation to be competitive with those based on dispersion relations [11] and rational approximants [9]. These two are taken as the SM prediction for the π^0 and $\eta - \eta'$ cases, respectively.

7.1 Fixing the asymptotic behavior

As mentioned in ref. [32], the problem of wrong asymptotic behavior can be fixed if a second vector meson resonance multiplet is included with corresponding dynamical fields in RχT. This is the one including the first excitations of the ρ and ω states. It is also demonstrated that for all the correct asymptotic QCD predictions to be fulfilled, a second excitation of pseudoscalar mesons shall be included, although it will not modify the expression for the π^0-TFF (after couplings redefinition). For simplicity, just a second vector meson resonance multiplet (and only in the chiral limit) was added to the previous work in ref. [7], so that the short-distance constraints were fulfilled for this observable. This was just meant to estimate the associated uncertainty, as explained in this reference. Here this will be worked out consistently.

7.2 $R\chi T$ Lagrangian including two vector meson resonances

The Lagrangian of this scheme of RχT which is often called two hadron (multiplets) saturation (THS), is similar to the case of one hadron multiplet saturation (single

meson dominance or LMD). The chiral Lagrangian will be written just once, since the inclusion of new particles does not change the low-energy Lagrangian (it only modifies the numerical values of their couplings). The pseudoscalar resonance sector will just have duplicated κ^{PV} term ($V \to V'$) and triplicated the κ^{PVV} term ($VV \to V'V'$ and $VV \to \{V, V'\}$). The even and odd sector of RχT will be duplicated with the substitution $V \to V'$. The new terms which are more different are those of $VV'P$ type, which will be labeled $O^i_{VV'P}$ and will be 6, instead of the 4 of the VVP and $V'V'P$ cases. For summing up all that has been constructed so far, the complete $\mathcal{L}^{THS}$ is:

$$
\begin{aligned}
\mathcal{L}^{THS} =& \frac{F_\pi^2}{4} \langle u_\mu u^\mu + \chi_+ \rangle + \mathcal{L}_{\mathcal{WZW}} + \sum_{j=7,8,22} C_j^W O_j^W \\
& + \mathcal{L}_V^{kin} + \mathcal{L}_V^{even} + \mathcal{L}_V^{odd} + \mathcal{L}_{VV}^{even} + \mathcal{L}_{VV}^{odd} \\
& + \mathcal{L}_{V'}^{kin} + \mathcal{L}_{V'}^{even} + \mathcal{L}_{V'}^{odd} + \mathcal{L}_{V'V'}^{even} + \mathcal{L}_{V'V'}^{odd} \\
& + \mathcal{L}_{P'}^{even} + \mathcal{L}_{P'}^{odd} \\
& + \varepsilon_{\mu\nu\rho\sigma} \langle \kappa_3^{PV'} \{V'^{\mu\nu}, f_+^{\rho\sigma}\} P' + \kappa^{PV'V'} V'^{\mu\nu} V'^{\rho\sigma} P' + \kappa^{PVV'} \{V^{\mu\nu}, V^{\rho\sigma}\} P' \rangle \\
& + \sum_{n=a,b,c,d,e,f} d_n O^n_{VV'P},
\end{aligned}
$$
(7.1)

where -for the primed case-, the couplings will be correspondingly primed ($M_{V'}, F_{V'}, \lambda_{V'}, c_i', d_i', e_m^{V'}, \kappa_3^{PV'}, \kappa^{PV'V'}$) and there will be mixed V, V' terms too. The operators $O^n_{VV'P}$ are given in Table 7.1.

n	$O^n_{VV'P}$
a	$\varepsilon_{\mu\nu\rho\sigma} \langle \{V^{\mu\nu}, V'^{\rho\alpha}\} \nabla_\alpha u^\sigma \rangle$
b	$\varepsilon_{\mu\nu\rho\sigma} \langle \{V^{\mu\alpha}, V'^{\rho\sigma}\} \nabla_\alpha u^\nu \rangle$
c	$\varepsilon_{\mu\nu\rho\sigma} \langle \{\nabla_\alpha V^{\mu\nu}, V'^{\rho\alpha}\} u^\sigma \rangle$
d	$\varepsilon_{\mu\nu\rho\sigma} \langle \{\nabla_\alpha V^{\mu\alpha}, V'^{\rho\sigma}\} u^\nu \rangle$
e	$\varepsilon_{\mu\nu\rho\sigma} \langle \{\nabla^\sigma V^{\mu\nu}, V'^{\rho\alpha}\} u_\alpha \rangle$
f	$i\varepsilon_{\mu\nu\rho\sigma} \langle \{V^{\mu\nu}, V'^{\rho\sigma}\} \chi_- \rangle$

Table 7.1. Interaction terms with one vector meson resonance, one excited vector meson resonance and a pGb.

These terms include two resonances from different multiplets in the same diagrams of Figure 7.1. For π^0, just these crossed $\rho\omega'$ and $\omega\rho'$ contributions will appear, for η and η', crossed contributions do not appear, just $\rho\rho'$, $\omega\omega'$ and $\phi\phi'$.
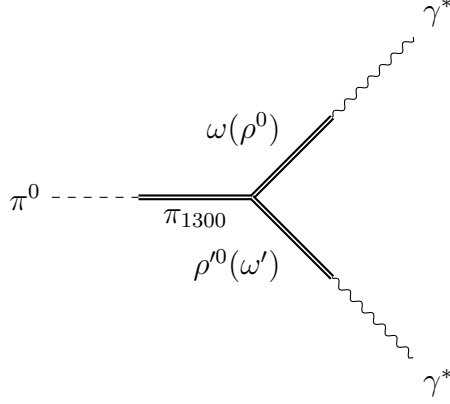
Figure 7.1. Contribution from a $\pi^0 \to \pi_{(1300)}$ transition and then a $\pi_{(1300)} \to \omega(\rho^0)\rho'^0(\omega')$ vertex.

7.3 π^0-TFF in THS RχT

With $\mathcal{L}^{THS}$, π^0-TFF can be obtained again in the same way as it was calculated in the last chapter. We got:

$$
\begin{aligned}
\mathcal{F}^{THS}_{\pi^0\gamma^*\gamma^*}(q_1^2, q_2^2) = \frac{2}{3F_\pi} &\left\{ \left(\frac{-N_C}{8\pi^2} - 8(q_1^2 + q_2^2)C_2 2^W + 32m_\pi^2 C_7^{W*} \right) \right. \\
&\left[\frac{-\sqrt{2}(F_V + 8m_\pi^2\lambda_V)}{M_V} \left(m\pi^2 c^*_{1235} + c_{125}q_1^2 - c_{1256}q_2^2 \right) \left(\frac{1}{M_\rho^2 - q_2^2} + \frac{1}{M_\omega^2 - q_2^2} \right) \right. \\
&+ 2(F_V + 8m_\pi^2\lambda_V)^2 \frac{m_\pi^2 d^*_{123} + d_3(q_1^2 + q_2^2)}{(M_\rho^2 - q_1^2)(M_\omega^2 - q_2^2)} \\
&- \frac{\sqrt{2}(F_{V'} + 8m_\pi^2\lambda_{V'})}{M_{V'}} \left(m_\pi^2 c'^*_{1235} + c'_{125}q_1^2 - c'_{1256}q_2^2 \right) \left(\frac{1}{M_{\rho'}^2 - q_2^2} + \frac{1}{M_{\omega'}^2 - q_2^2} \right) \\
&\left. + 2(F_{V'} + 8m_\pi^2\lambda_{V'})^2 \frac{m_\pi^2 d'^*_{123} + d'_3(q_1^2 + q_2^2)}{(M_{\rho'}^2 - q_1^2)(M_{\omega'}^2 - q_2^2)} + (1 \leftrightarrow 2) \right] \\
&+ 2(F_V + 8m_\pi^2\lambda_V)(F_{V'} + 8m_\pi^2\lambda_{V'}) \left(m_\pi^2 d^*_{abcf} + (q_1^2 + q_2^2)d_{abcd} \right) \\
&\left. \left(\frac{1}{(M_\rho^2 - q_1^2)(M_{\omega'}^2 - q_2^2)} + \frac{1}{(M_{\rho'}^2 - q_1^2)(M_\omega^2 - q_2^2)} \right) \right\},
\end{aligned}
$$

(7.2)

where the multi-index primed coupling constants have the same definition as the unprimed ones in (6.17), with corrections as the unprimed couplings in (6.14). The

mixed multiplet multi-index coupling constants are defined as:

$$d_{abcd} = d_a + d_b - d_c - 2d_d,$$

$$d_{abcf} = d_a + d_b - d_c + 8d_f^*,$$

(7.3)

where d_f gets corrections from the $\kappa^{VV'P}$ term in eq. (7.1):

$$d_f \to d_f^* = d_f + \frac{d_m \kappa^{PVV'}}{2m_{\pi(1300)}^2}.$$

(7.4)

7.4 Short Distance Constraints

Again, eq. (7.2) can be simplified, since the couplings in $\mathcal{F}_{\pi^0\gamma^*\gamma^*}^{THS}$ are constrained from QCD high-energy behavior. For the THS case in the chiral limit, short distance constraints have been computed in refs. [32, 61]. Corrections to the chiral limit case are order by order in the m_π^2 expansion, since π^0's mass is the scale of the symmetry breaking, furthermore the chiral counting is order by order in the p^2 expansion. These facts allow us to calculate the short distance constraints at both p^2 and m_π^2 orders.

7.4.1 $\lim_{Q^2 \to \infty} \mathcal{F}_{\pi^0\gamma^*\gamma^*}(-Q^2, -Q^0) = 0$ Constraints

For this limit to be satisfied, both quadratic and zeroth order terms in q^{2n} must vanish independently. Besides, the m_π^2 expansion allows us to obtain at most 4 independent short-distance constraints, which are shown in Table 7.2.

Q^{2n} order	m_π^2 order	constraint
Q^2	m_π^2	there is no term at this order
Q^2	m_π^0	$C_{22}^W = 0$
Q^0	m_π^2	$\lambda_V = \lambda_{V'} = 0$
Q^0	m_π^0	$(c_5 - c_6) + \frac{F_{V'}M_V}{F_V M_{V'}}(c_5' - c_6') = \frac{N_C M_V}{64\sqrt{2}\pi^2 F_V}$

Table 7.2. Two virtual photon constraints at different orders in Q^2 and m_π^2. In the third line we have used that that $C_7^* = 0$ from $\langle VVP \rangle$ short distance constraints [61, 24].

7.4.2 $\lim_{Q^2 \to 0} \mathcal{F}_{\pi^0\gamma^*\gamma^*}(-Q^2, 0) = 0$ Constraints

In the same way for this case, no more than 4 constraints can be obtained from different orders in the diverse expansions of the theory. The results for this case are

shown in Table 7.3.

Q^{2n} order	m_π^2 order	constraint
Q^2	m_π^2	$\frac{e_m^V}{M_V^2} = \frac{e_m^{V'}}{M_{V'}^2}$
Q^2	m_π^0	$c_{125} = -c'_{125}\frac{F_{V'}M_V^3}{F_V M_{V'}^3}$
Q^0	m_π^2	$c'^*_{1235} = -c^*_{1235}\frac{F_V M_{V'}^3}{F_{V'}M_V^3} + \frac{M_{V'}e_m^{V'}N_C}{8\sqrt{2}\pi^2 F_{V'}}$
Q^0	m_π^0	$8F_{V'}^2 M_V^2 d'_3 + 8F_V^2 M_{V'}^2 d_3 + 4F_V F_{V'}(M_V^2 + M_{V'}^2)d_{abcd}$
		$+4\sqrt{2}c_{125}F_V M_{V'}^2 M_V\left(1 - \frac{M_{V'}^2}{M_V^2}\right) = -\frac{M_V^2 M_{V'}^2 N_C}{8\pi^2}$

Table 7.3. One virtual photon constraints at different orders in Q^2 and m_π^2.

7.4.3 $\langle VVP \rangle$ Constraints

All $\langle VVP \rangle$ constraints at order m_π^0 are consistent with the chiral limit, they are found in [61]. The relevant ones for our work are:

$$C_7^* = c_{125} = c'_{125} = c_{1235} = c'_{1235} = 0. \qquad (7.5)$$

7.4.4 Constraints from Dominant $\frac{1}{Q^2}$ behavior in the space-like region.

The constraints on the leading behavior of the π-TFF at high energies is set by refs. [56][57] in the single virtual photon case and by refs. [58][59] in the doubly virtual photon case, they are given by:

$$\lim_{Q^2\to\infty} -Q^2 \mathcal{F}_{\pi^0\gamma^*\gamma^*}(-Q^2,-Q^2) = \frac{2F}{3},$$
$$\lim_{Q^2\to\infty} -Q^2 \mathcal{F}_{\pi^0\gamma^*\gamma^*}(-Q^2,0) = 2F, \qquad (7.6)$$

are at $\frac{1}{Q^2}$ order, and are collected in Table 7.4. With $c_5 - c_6 = c_{56}$.

7.5 $\mathcal{F}^{THS}_{\pi^0\gamma^*\gamma^*}(q_1^2, q_2^2)$

After applying all short-distance constraints from the previous section, 3 independent (combination of) couplings remain, $d^*_{123} \propto \bar{d}_{123}$, $d_3 \propto \bar{d}_3$ and $F_{V'}d^*_{abcf} \propto \bar{d}_{abcf}$

75

virtual photons	m_π^2 order	constraint
2	m_π^2	$c_{56} = \frac{c^*_{1235}}{8e_m^V}$
2	m_π^0	$d_3' = \left(8F^2\pi^2 M_V^3 + 64d_3\pi^2 F_V^2 M_V^3 + 64\sqrt{2}c_5 6\pi^2 F_V M_V^4\right.$ $+8F^2\pi^2 M_V M_{V'}^2 - 64d_3\pi^2 F_V^2 M_V M_{V'}^2 - 64\sqrt{2}c_{56}\pi^2 F_V M_{V'}^4$ $\left. - M_V^3 M_{V'}^2 N_C + M_V M_{V'}^4 N_C\right) / \left(64\pi^2 F_V^2 M_V (M_V^2 - M_{V'}^2)\right)$
1	m_π^2	$d_{123}'^* = -\frac{F_V\left(2d^*_{123}F_V M_{V'}^2 + d^*_{abcf}F_{V'}(M_V^2 + M_{V'}^2)\right)}{2F_{V'}^2 M_V^2}$
1	m_π^0	$c^*_{1235} = -e_m^V\left(4F^2\pi^2 M_V^4 + 32d_3\pi^2 F_V^2 M_V^4 + 24F^2\pi^2 M_V^2 M_{V'}^2\right.$ $-64d_3\pi^2 F_V^2 M_V^2 M_{V'}^2 + 32d_3\pi^2 F_V^2 M_{V'}^4$ $\left. + M_V^2 M_{V'}^4 N_C\right) / \left(4\sqrt{2}\pi^2 F_V M_V (M_V^4 - M_{V'}^4)\right)$

Table 7.4. Short-distance constraints obtained by the dominant behavior of singly and doubly virtual photons in the π^0-TFF.

(see table 7.5). The final $\mathcal{F}^{THS}_{\pi^0\gamma^*\gamma^*}(q_1^2, q_2^2)$ is:

$$\mathcal{F}^{THS}_{\pi^0\gamma^*\gamma^*}(q_1^2, q_2^2) = \left[32\pi^2 F_V^2 m_\pi^2 \left(1 - \frac{M_{V'}^2}{M_V^2}\right)\left(q_1^2 q_2^2 - \frac{M_{V'}^2}{M_V^2}M_\rho^4\right)d^*_{123}\right.$$

$$+ 64\pi^2 q_1^2 q_2^2 F_V^2 \left(1 - \frac{M_{V'}^2}{M_V^2}\right)^2 M_\rho^2 d_3$$

$$+ 16\pi^2 F_V F_{V'} m_\pi^2 \left(1 - \frac{M_{V'}^2}{M_V^2}\right)\left(q_1^2 q_2^2 - M_\rho^4\right)d^*_{abcf}$$

$$+ 4F_\pi^2\pi^2 q_1^2 q_2^2(q_1^2 + q_2^2 - 2M_\rho^2) + 24F_\pi^2\pi^2\frac{M_{V'}^2}{M_V^2}M_\rho^2((q_1^2 + q_2^2)M_\rho^2 - 2q_1^2 q_2^2)$$

$$\left. + N_C\frac{M_{V'}^4}{M_V^2}M_\rho^2(q_1^2 q_2^2 - M_\rho^4)\right]$$

$$/ \left[12\pi^2 F_\pi(q_1^2 - M_\rho^2)(q_2^2 - M_\omega^2)(q_1^2 - M_{\rho'}^2)(q_2^2 - M_{\omega'}^2)\right].$$

(7.7)

In the LMD scheme, it was not possible to obtain short distance constraints from the dominant behavior of π-TFF (as the ones in Table 7.4), since the couplings were not enough for these asymptotic behavior to be reproduced.

If we stop the constraining of eq. (7.2) with only the relations in Tables 7.3 and 7.2 (for the LMD case, only these conditions were able to be satisfied), after setting all couplings and masses from the second vector meson multiplet to zero, the result in ref. [7] is correctly reproduced.

In the chiral limit, this result is in contradiction with the expression found in ref. [7] by a sign in the d_3 term. However, the behavior of $\mathcal{F}^{THS}_{\pi^0\gamma^*\gamma^*}(q_1^2, q_2^2)$ in the doubly virtual photon case in that work is unphysical, since it becomes highly oscillatory and acquires negative values. This is corrected if the sign is taken positive, consequently,

new coupling	expression in terms of previous couplings
$\bar{d}_{123}$	$\dfrac{F_V^2 d_{123}^*}{3F_\pi^2}$
$\bar{d}_3$	$\dfrac{F_V^2 d_3}{3F_\pi^2}$
$\bar{d}_{abcf}$	$\dfrac{F_V F_{V'} d_{abcf}^*}{6F_\pi^2}$

Table 7.5. Redefinition of coupling constants.

the result in eq. (7.7) will be taken as correct.

The multi-index coupling constants are set from LMD for d_{123}^* and d_3, while fit to available data on one virtual photon π-TFF will be used to get d_{abcf}^*. Since there are more couplings which are only sensitive to the doubly virtual photon case, and there is no data in that sector, only an estimation on $a_\mu^{HLbL,\pi^0-\text{pole}}$ can be done. For fitting these couplings, the η and η' TFFs must be computed since there is information on η-TFF available from $e^+e^- \to \pi^+\pi^-\eta$ for the doubly virtual case [62]. The multi-index couplings are multiplied by different coupling constants, it will be convenient to redefine them as it was done for d_{123}^* in the LMD case, see Table 7.5.

With this redefinition of the coupling constants, the expression for π^0TFF is:

$$
\begin{aligned}
\mathcal{F}_{\pi^0\gamma^*\gamma^*}^{THS}(q_1^2, q_2^2) = & \left[96\pi^2 F_\pi^2 m_\pi^2 \left(1 - \frac{M_{V'}^2}{M_V^2} \right) \left(q_1^2 q_2^2 - \frac{M_{V'}^2}{M_V^2} M_\rho^4 \right) \bar{d}_{123} \right. \\
& + 192\pi^2 q_1^2 q_2^2 F_\pi^2 \left(1 - \frac{M_{V'}^2}{M_V^2} \right)^2 M_\rho^2 \bar{d}_3 \\
& + 96\pi^2 F_\pi^2 m_\pi^2 \left(1 - \frac{M_{V'}^2}{M_V^2} \right) \left(q_1^2 q_2^2 - M_\rho^4 \right) \bar{d}_{abcf} \\
& + 4F_\pi^2 \pi^2 q_1^2 q_2^2 (q_1^2 + q_2^2 - 2M_\rho^2) + 24F_\pi^2 \pi^2 \frac{M_{V'}^2}{M_V^2} M_\rho^2 ((q_1^2 + q_2^2)M_\rho^2 - 2q_1^2 q_2^2) \\
& \left. + N_C \frac{M_{V'}^4}{M_V^2} M_\rho^2 (q_1^2 q_2^2 - M_\rho^4) \right] \\
& / \left[12\pi^2 F_\pi (q_1^2 - M_\rho^2)(q_2^2 - M_\omega^2)(q_1^2 - M_{\rho'}^2)(q_2^2 - M_{\omega'}^2) \right].
\end{aligned}
\tag{7.8}
$$

7.6 $\mathcal{F}_{\pi^0\gamma^*\gamma^*}^{THS}(q_1^2, q_2^2)$ couplings and parameters

The still free parameters will be fitted to available data, coming from CLEO [49], BaBar [52], Belle [54] and CELLO [50] and probe the space-like region for one virtual photon. The data set has the format $(Q^2, -Q^2 \mathcal{F}_{\pi^0\gamma\gamma^*}(-Q^2, 0))$, from our expression

of π^0-TFF, we get:

$$-Q^2 \mathcal{F}_{\pi^0 \gamma^* \gamma^*}^{THS}(-Q^2, 0) = \frac{\left[M_{V'}^2 M_\rho^2 N_C Q^2 + 24 F_\pi^2 \pi^2 Q^4 \right.}{\left. -96 F_\pi^2 \pi^2 m_\pi^2 Q^2 \left(1 - \frac{M_V^2}{M_{V'}^2}\right) \left(\bar{d}_{abcf} + \frac{M_{V'}^2}{M_V^2} \bar{d}_{123}\right)\right]}{12 F_\pi \pi^2 (Q^2 + M_\rho^2)(Q^2 + M_{\rho'}^2)} \tag{7.9}$$

We can redefine again the combination of coupling constants since the fit will not be available to distinguish between $\bar{d}_{abcf}$ and $\bar{d}_{123}$, entering the linear combination $\bar{d}_{fit}$:

$$\bar{d}_{\text{fit}} = \bar{d}_{abcf} + \bar{d}_{123} \frac{M_{V'}^2}{M_V^2}. \tag{7.10}$$

Because this is a preliminary work, the couplings (some of them to be fitted, too, in future work) are set as follows:

- $\bar{d}_{123}$ will be taken from the fit to experimental data in ref. [7].

- $\bar{d}_3$ will be taken from the consistent set of short-distance constraints on the odd-intrinsic parity sector [24]:

$$\bar{d}_3 = -\frac{N_C M_V^2}{192 F_\pi^2 \pi^2}. \tag{7.11}$$

- M_V will be taken from the fit to experimental data in ref. [7].

- $M_{V'}^2$ will be set as the isospin average of the involved particles in this process from the second multiplet of vector resonances, which masses will be taken from the PDG [30].:

$$M_{V'}^2 = \frac{M_{\rho'0}^2 + 2M_{\rho'\pm}^2 + M_{\omega'}^2}{4} = (1448 \,\text{MeV})^2. \tag{7.12}$$

- In the model, the masses of $M_{\rho(\omega)}$ are the same and can be calculated with the data in Table 6.4.

- $M_{\rho',\omega'}^2$ are equal in the simplified model, so they will be taken as $M_{V'}^2$.

- m_π will be taken from PDG [30], in the isospin symmetry limit, in which we are computing.

- $N_C = 3$ is the number of colors.

- F_π is the pion decay constant, and its value is $F_\pi = 92.2$ MeV [30].

- $\bar{d}_{\text{fit}}$ will be fitted to available data. From it and the value of $\bar{d}_{123}$ (which will be taken as an initial guess for $\bar{d}_{\text{fit}}$) in ref. [7], $\bar{d}_{abcf}$ will be obtained.

This gives an estimate for the parameters and couplings of $\mathcal{F}_{\pi^0 \gamma^* \gamma^*}^{THS}$ since the fit will be complete until all constants are fitted to experimental data (in a joint fit together with the η and η' channels). In refs. [6, 7], π^0-TFF is fitted with and without BaBar data [52], since this set of measurements differs with respect to the rest of data at high energies. Eq. (7.9) will be fitted with and without BaBar data.

7.7 Fit results

For the initial guess, we set to zero the value of d_{abcf} since it is there where the information of the second multiplet is mainly present, the comparison with ref. [7] and experimental data can be observed in Figure 7.2. At low energies, it can be seen that its behavior is very close to the LMD case, but at higher energies it approaches the asymptotic behavior prescribed by QCD.

The values obtained from the fit of eq. (7.9) to available data are collected in the table 7.6.

As it can be seen in eq. (7.9), the constant to be fitted is multiplied by the symmetry

	$\bar{d}_{\text{fit}}$	$\chi^2/d.o.f.$	$\bar{d}_{abcf}$
Initial guess	$\bar{d}_{123} \frac{M_{V'}^2}{M_V^2} = -0.778$	0.170	0
With Babar Data	3.16 ± 1.31	0.167	3.94 ± 1.40
Without Babar Data	4.74 ± 1.06	0.170	5.51 ± 1.18

Table 7.6. Fit results of eq. (7.9) to available data on the $\pi^0 - TFF$.

breaking parameter m_π^2, so its contribution is highly suppressed compared with the other terms. As a consequence, the fit is not very sensitive to small changes on $\bar{d}_{\text{fit}}$ as it shows the comparison between the different $\chi^2/d.o.f.$, see Table 7.6. As mentioned before, a similar structure will appear in the $\eta - \eta'$ case, but since their masses are much higher than π^0's, the fit will be more sensitive to changes in the shared parameters. In contrast with ref. [7], no accuracy improvement is obtained by taking out BaBar data [52]. This can be due to the parameters that we are borrowing from this analysis (instead of fitting them).

The plots resulting for 1 virtual π-TFF of eq. (7.9) with the data in Table 7.6 are
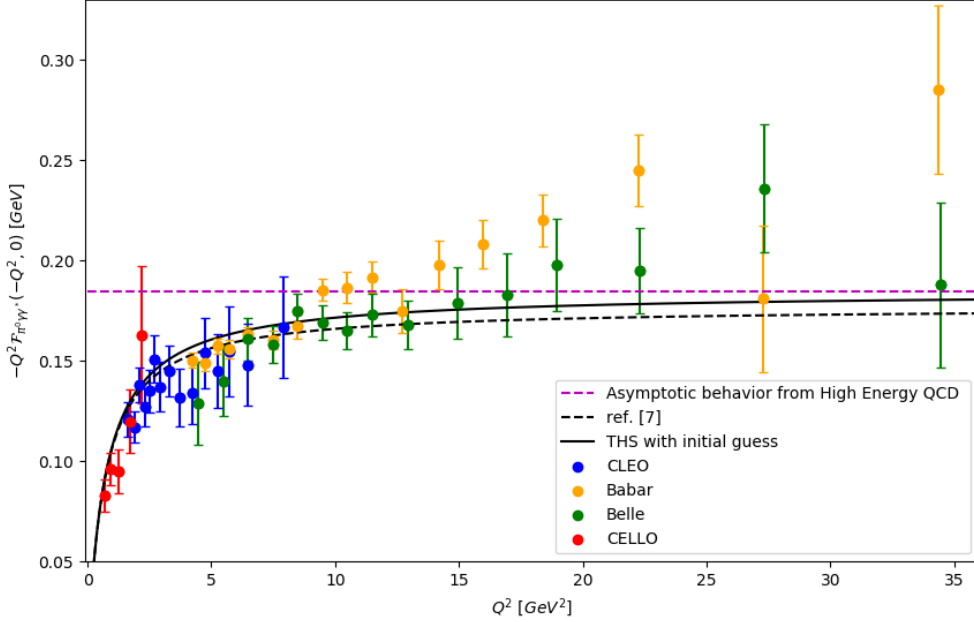
Figure 7.2. π-TFF for the initial guess value $\bar{d}_{abcf} = 0$(solid black line), compared with all available data from CLEO[49](blue), BaBar[52](yellow), Belle[54](green), CELLO[50](red). Also, the LMD model from ref.[7](dashed black line) is plotted.

shown in Figure 7.3 for all data and without BaBar[52] data.

The 1 virtual photon case of π-TFF reproduces the high energy behavior which could not be reproduced in the LMD case, this is possible due to the number of new couplings coming from including a second multiplet of vector meson resonances. However, there are two problems. The first one is that the coupling available to fit in π-TFF is chirally suppressed, as it is multiplied by m_π^2, therefore the experimental data on π-TFF is not good to probe its value. The second problem is the fact that $\bar{d}_{abcf}$ and $\bar{d}_{123}$ appear in a single linear combination in the 1 virtual photon case, but they appear in two different linear combinations in the 2 virtual photons case, where there is no experimental data yet.

The first problem still has another consequence: even though the data is not very sensitive to $\bar{d}_{\text{fit}}$, the integral in eq. (6.2) is. Therefore, a better approach to its calculation must be done: the $\eta - \eta'$-TFF computation will help in this regard, since the corresponding mass is comparable with the scale of the mass of the first multiplet of vector meson resonances.

The contribution arising from the second problem is suppressed with respect to the first one since the doubly virtual photon π-TFF just appears in the second integral

80

of eq. (6.2), which weight function is 2 orders of magnitude smaller. However, in a precision problem the small details count. The solution for this issue is the same as in the first case: there is information about the doubly virtual transition form factor for η [62], which will probe very valuable.

There is no available data for the doubly virtual form factor in the pion case, and the parameter $\bar{d}_3$ is sensitive to this case only. By taking the parameters and couplings as mentioned in the past section, the plot on Figure 7.4 is obtained. As it can be seen, and has been widely mentioned during this work, the asymptotic QCD condition was not correctly reproduced in ref. [7], and now it is fulfilled. However, the fit to $\eta - \eta'$ data is still necessary to get the couplings unavailable for π and improve the calculations (nevertheless its computation has higher difficulty and will be addressed in future work).

7.8 π^0 pole contribution to HLbL piece of a_μ with two meson resonance multiplets in the $R\chi T$

For the evaluation of eq. (6.8), partial fractions of the general $f(q_2^2)$ expressions in (7.8) (using the fact that $M_\rho = M_\omega$ and $M_{\rho'} = M_{\omega'}$ in THS) are:

expression	partial fraction
$\frac{h_0(q_1^2)}{(q_2^2-M_\rho^2)(q_2^2-M_{\rho'}^2)}$	$\frac{h_0(q_1^2)}{(q_2^2-M_\rho^2)(M_\rho^2-M_{\rho'}^2)} + \frac{h_0(q_1^2)}{(q_2^2-M_{\rho'}^2)(M_{\rho'}^2-M_\rho^2)}$
$\frac{q_2^2 h_2(q_1^2)}{(q_2^2-M_\rho^2)(q_2^2-M_{\rho'}^2)}$	$\frac{h_2(q_1^2)M_\rho^2}{(q_2^2-M_\rho^2)(M_\rho^2-M_{\rho'}^2)} + \frac{h_2(q_1^2)M_{\rho'}^2}{(q_2^2-M_{\rho'}^2)(M_{\rho'}^2-M_\rho^2)}$
$\frac{q_2^4 h_4(q_1^2)}{(q_2^2-M_\rho^2)(q_2^2-M_{\rho'}^2)}$	$h_4(q_1^2) + \frac{h_4(q_1^2)M_\rho^4}{(q_2^2-M_\rho^2)(M_\rho^2-M_{\rho'}^2)} + \frac{h_4(q_1^2)M_{\rho'}^4}{(q_2^2-M_{\rho'}^2)(M_{\rho'}^2-M_\rho^2)}$

Table 7.7. Partial fraction splitting of all q_2^2 contributions in eq. (7.8) .

$\mathcal{F}_{\pi^0\gamma^*\gamma^*}(q_1^2, q_2^2)$ in terms of $h_{2i}(q_1^2)$ is:

$$\mathcal{F}_{\pi^0\gamma^*\gamma^*}(q_1^2, q_2^2) = \frac{F_\pi}{3}\left[\frac{h_0(q_1^2) + q_2^2 h_2(q_1^2) + q_2^4 h_4(q_1^2)}{(q_2^2 - M_\rho^2)(q_2^2 - M_{\rho'}^2)}\right]. \tag{7.13}$$

The $h_1(q_1^2)$ can be obtained rearranging eq. (7.8):

$$
\begin{aligned}
h_0(q_1^2) = & -\left[24\bar{d}_{123}m_\pi^2\frac{M_{V'}^2}{M_V^2}\left(1-\frac{M_{V'}^2}{M_V^2}\right)M_\rho^4 + 24\bar{d}_{abcf}m_\pi^2\left(1-\frac{M_{V'}^2}{M_V^2}\right)M_\rho^4 \right. \\
& \left. + \frac{-6q_1^2M_\rho^4\frac{M_{V'}^2}{M_V^2} + \frac{M_\rho^6 M_{V'}^4 N_C}{4M_V^2 F_\pi^2 \pi^2}}{(q_1^2-M_\rho^2)(q_1^2-M_{\rho'}^2)}\right],
\end{aligned}
$$

$$
\begin{aligned}
h_2(q_1^2) = & \left[24\bar{d}_{123}q_1^2 m_\pi^2\left(1-\frac{M_{V'}^2}{M_V^2}\right) + 24\bar{d}_{abcf}q_1^2 m_\pi^2\left(1-\frac{M_{V'}^2}{M_V^2}\right) + 48\bar{d}_3 q_1^2\left(1-\frac{M_{V'}^2}{M_V^2}\right)^2 M_\rho^2 \right. \\
& \left. + \frac{q_1^2(q_1^2-2M_\rho^2) + 6\frac{M_{V'}^2}{M_V^2}M_\rho^2(M_\rho^2-2q_1^2) + \frac{q_1^2 M_{V'}^4 M_\rho^2 N_C}{4M_V^2 F_\pi^2 \pi^2}}{(q_1^2-M_\rho^2)(q_1^2-M_{\rho'}^2)}\right],
\end{aligned}
$$

$$
h_4(q_1^2) = \frac{q_1^2}{(q_1^2-M_\rho^2)(q_1^2-M_{\rho'}^2)},
$$

$$(7.14)$$

$g_{M_{V_i}}(q_1^2)$ and $f(q_1^2)$ in eq. (6.7) are related to $h_i(q_1^2)$ by:

$$
f(q_1^2) = h_4(q_1^2),
$$
$$
g_{M_\rho}(q_1^2) = -\frac{h_0(q_1^2) + M_\rho^2 h_2(q_1^2) + M_\rho^4 h_4(q_1^2)}{M_\rho^2 - M_{\rho'}^2},
$$
$$
g_{M_{\rho'}}(q_1^2) = -\frac{h_0(q_1^2) + M_{\rho'}^2 h_2(q_1^2) + M_{\rho'}^4 h_4(q_1^2)}{M_{\rho'}^2 - M_\rho^2}.
$$

$$(7.15)$$

Given $f(q_1^2)$ and $g_{M_{V(V')}^2}$, and eq. (6.9), $a_\mu^{HLbL:\pi^0-\text{pole}}$ was calculated. Although the integrals go from zero to infinity, the changes in their values reached the numerical error around the scale $\Lambda = 10 GeV^2$, so the integral was performed up to $30 GeV^2$. This integration was performed for all combinations of limits in the values of $\bar{d}_{123}$[7] and $\bar{d}_{abcf}$ in order to get the limits of our estimation. Using the obtained coupling and the ones set in section 7.6, the obtained bounds to the value of the pion pole contribution to the HLbL piece of a_μ in the two vector meson resonance multiplets scheme estimate are:

$$
4.93 \pm 0.06 \leq a_\mu^{\pi^0-\text{pole},HLbL} \times 10^{10} \leq 5.72 \pm 0.08 \,(\text{All data}),
$$
$$
4.60 \pm 0.06 \leq a_\mu^{\pi^0-\text{pole},HLbL} \times 10^{10} \leq 5.30 \pm 0.07 \,(\text{Without BaBar}),
$$
$$
5.97 \pm 0.09 \leq a_\mu^{\pi^0-\text{pole},HLbL} \times 10^{10} \leq 6.26 \pm 0.09 \,(\text{Initial guess}).
$$

$$(7.16)$$

The values of a_μ are much more sensitive to changes in $\bar{d}_{\text{fit}}$ than the single virtual π-TFF, so the analysis should be completed by studying higher pseudoscalar poles ($\eta - \eta'$). The results from all possible combinations of the $\bar{d}_{123}$ and $\bar{d}_{fabc}$, considering the initial guess and the errors of both values can be seen in Table 7.8 which is

	$\bar{d}_{123}$	$\bar{d}_{abcf}$	$a_\mu \times 10^{10}$
All Data	-0.40	2.54	5.72 ± 0.08
		3.94	5.43 ± 0.07
		5.34	5.15 ± 0.07
		0	6.26 ± 0.09
	-0.25	2.54	5.60 ± 0.08
(Central Value)		3.94	5.32 ± 0.07
		5.34	5.03 ± 0.07
(Initial guess)		0	6.14 ± 0.09
	-0.10	2.54	5.49 ± 0.08
		3.94	5.20 ± 0.07
		5.37	4.93 ± 0.06
		0	6.02 ± 0.09
Without BaBar	-0.38	4.34	5.30 ± 0.07
		5.52	5.06 ± 0.07
		6.70	4.82 ± 0.06
		0	6.22 ± 0.09
	-0.23	4.34	5.18 ± 0.07
(Central Value)		5.52	4.94 ± 0.07
		6.70	4.71 ± 0.06
(Initial guess)		0	6.09 ± 0.09
	-0.08	4.34	5.06 ± 0.07
		5.52	4.83 ± 0.06
		6.70	4.60 ± 0.06
		0	5.97 ± 0.09

Table 7.8. a_μ values for all combinations of errors of $\bar{d}_{123}$[7] and $\bar{d}_{abcf}$. Results with $\bar{d}_{abcf} \sim 0$ are the most realistic estimates.

consistent with previous calculations [8, 7, 6, 9, 10, 11, 12], provided $\bar{d}_{abcf} \sim 0$, corresponding to our educated guess. This is not yet an improvement over the systematic error in ref. [7] because the high sensitivity of a_μ to changes in the coupling constants (particularly $\bar{d}_{abcf}$) contrasted with the little sensitivity to these couplings of the available data considered in this work. However, when all necessary constants get fitted to the complete set of data, a more precise and reliable value of $a_\mu^{HLbL,\pi^0-\text{pole}}$ will be obtained. Specifically, the computation of $\eta - \eta'$-TFF is expected to improve drastically the calculation.
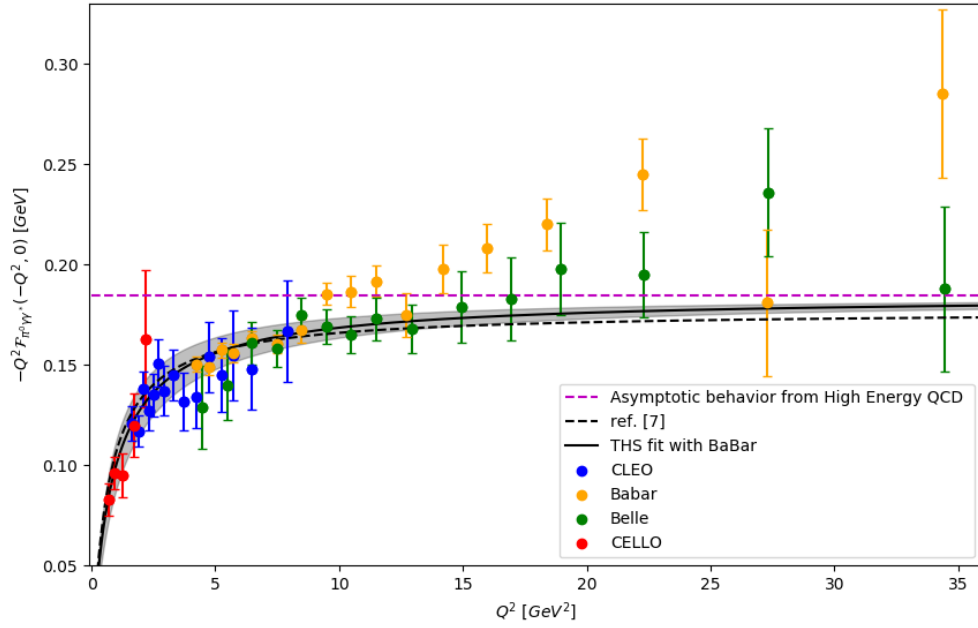
(a)
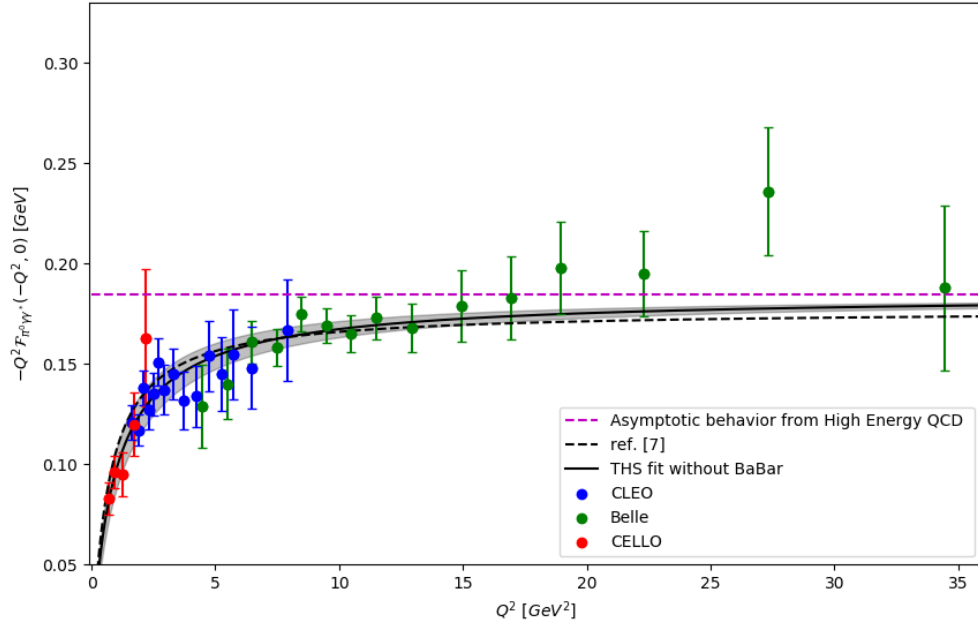
(b)

Figure 7.3. Fit of eq. (7.9) to experimental data (black solid line) **a)** from CELLO [50], CLEO [49], BaBar [52] and Belle [54] **b)** All data except BaBar [52]. The blue data is from CLEO, the orange data is from BaBar, the green data is from Belle and the red data is from CELLO. The shaded region is the 5σ confidence interval of each fit. The purple dotted line is the limit of high energies and the black dotted line is the fit from LMD in ref. [7].
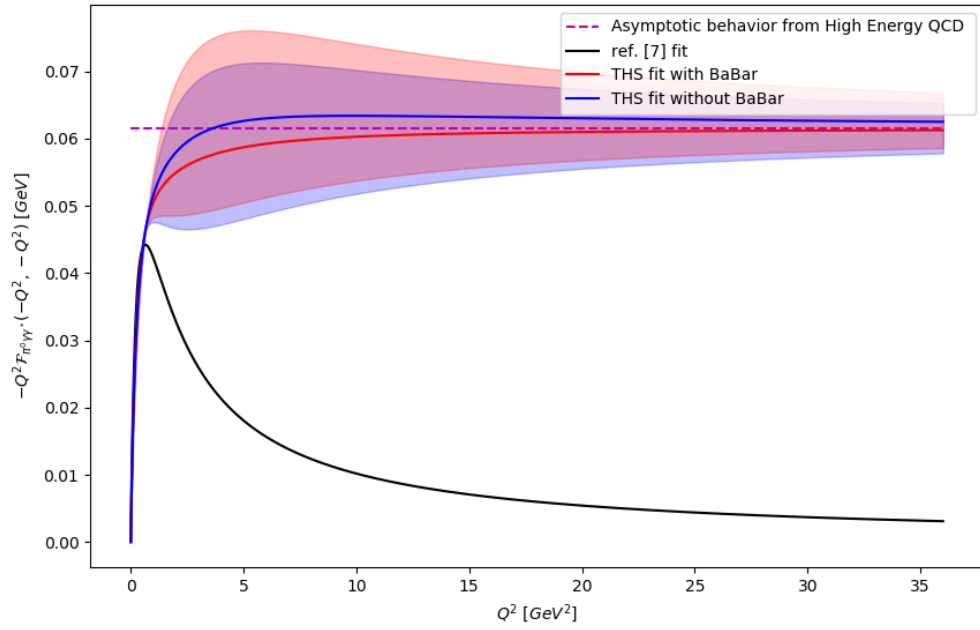
Figure 7.4. THS doubly virtual photon π-TFF with the parameters and couplings from section 7.6 and the fit values of Table 7.6 compared with the LMD case in ref. [7].

Conclusions and Perspectives

Conclusions

QCD fundamental theory cannot be used for performing analytical calculations as it can be done with EW theory. From this fact, an EFT is required. An EFT based on the symmetries of the underlying theory can be constructed and used to reproduce QCD observables at different regimes: χPT for low energies and $R\chi T$ for intermediate and high energies.

Although χPT reproduces and predicts many QCD observables at low energies with very good precision and accuracy, as energy increases, perturbativity is lost. For this reason, in the regime of intermediate energies, the lowest vector meson resonance multiplet should be included ($R\chi T$) as it is shown in [27], still reproducing low energy behavior. However, it is not enough for verifying particular high energy limits. This gets fixed by adding a second vector meson resonance multiplet (THS).

The main source of error in a_μ comes from the hadronic part, specifically (for the relative error) in the Hadronic Light by Light piece. From this part, the π-pole is the highest lone contribution, so it is important to work on a precise calculation of it.

On a previous work using EFT's [7], π-pole contribution was calculated, however, the theory did not have enough couplings to reproduce all high energy predictions, resulting in a systematic error, underestimating the calculation of $a_\mu^{HLbL:\pi-\text{pole}}$. This problem was addressed successfully in this work by the THS scheme.

An expression for π-TFF was found within the THS scheme. By imposing short distance constraints on this expression, a small number of couplings and parameters remained free. As a preliminary work, these couplings and parameters except one (which was fitted to single virtual photon experimental data) were taken from the

LMD+V results on ref.[7], PDG[30], and the LMD+V constraints[24]. The results for different approximations are bounded between $46.0\pm0.6 \leq a_\mu^{\pi^0-\text{pole},HLbL} \times 10^{11} \leq 62.2 \pm 0.9$, which is consistent with other references [8, 7, 6, 9, 10, 11, 12] but at this stage, is not competitive given its large uncertainty (we recall that the White Paper result for this contribution is $\left(63.0^{+2.7}_{-2.1}\right) \times 10^{-11}$) [8].

The unique parameter that was fitted, was chirally suppressed with respect to the rest of contributions, so its variation did not affect substantially the correlation between the model and the experimental data. However, the variation of this coupling was important for the π-pole contribution, so the results of this work are not conclusive and will be improved.

A systematic error is unavoidable in this work as no information on doubly virtual photon π-TFF has been measured. Some of the couplings are sensitive only to this case, so an approximation to $LMD + V$ values was the best we could do for this work.

Perspectives

There is more work to be done in the same direction and we expect that this new computations will increase the accuracy and, in consequence, the relevance of what was done for this thesis. The first improvement to the methodology will be to fit all parameters and data in eq. (7.9). This will increase the sensitivity of the model to data.

Second, as mentioned in the conclusions above, the results can be improved since η and η' belong to the same multiplet (the couplings to vector mesons will be the same) but their masses are around 4 and 7 times the mass of π, which means that chirally suppressed couplings in the π case will be around 16 and 49 times more sensitive to data (which are a bit less precise than for π^0, however).

Third, there is information for doubly virtual photons in the η-TFF[62], which will give us light on the parameters which cannot be obtained from π data and this will allow us to avoid using LMD+V constraints. As they are calculated in different schemes, this approximation has a systematic error which we will evade by performing the computation of $\eta - \eta'$ within the THS scheme.

Finally, we can say that this work is incomplete until $\eta - \eta'$-TFF is computed, constrained by short distance behavior and fitted to available data. This work can be important when finalized, as it solves systematic errors in the $R\chi T$ past computations, possibly rendering it competitive with the current state of the art calculations of the pseudo-Goldstone pole contributions to a_μ^{HLbL}.

Bibliography

[1] Ch. Utpal and N. Pran, *Phys. Rev. D*, **66** (2002) 093001.

[2] B. Abi et al. (Muon g-2 Collaboration)*Phys. Rev. Lett.* **126** (2021), 141801

[3] D. Gross and F. Wilczek, *Phys. Rev. Lett.* **30** (1973), 1343

[4] G. Ecker, J. Gasser, A. Pich and E. de Rafael, *Nucl. Phys. B* **321** (1989) 311.

[5] J. Portolés, *AIP Conference Proceedings* **1322**(2010) 178.

[6] P. Roig, A. Guevara, and G. López Castro, *Phys. Rev. D* **89**(2014), 073016.

[7] A. Guevara, P. Roig, J.J. Sanz-Cillero *JHEP* **06**(2018), 160.

[8] T.Aoyama et al. *Phys.Rept.* **887** (2020) 1-166.

[9] P. Masjuan, P. Sánchez-Puertas *Phys. Rev. D* **95** (2017) 054026.

[10] M. Knecht, A. Nyffeler, *Phys. Rev. D* **65**(2002) 073034.

[11] M. Hoferichter, B. L. Hoid, B. Kubis, S. Leupold and S. P. Schneider, *JHEP* **10** (2018) 141.

[12] K. Raya, A. Bashir, P. Roig, *Phys. Rev. D* **101** (2020) 7, 074021.

[13] P. Langacker, *The Standard Model and Beyond* (CRC Press, 2010). ISBN:9781420079067.

[14] Aitchison, Hey. *Gauge Theories in Particle Physics: A practical introduction*, (CRC Press, 2013). ISBN: 9781466513020.

[15] M. Peskin, *Concepts of Elementary Particle Physics* (Oxford University Press, 2019). ISBN: 9780198812197.

[16] T.D. Lee and C.N. Yang, *Phys. Rev.* **104** (1956) 254-258.

[17] C.S. Wu et al. *Phys.Rev.* **105** (1957) 1413-1414.

[18] F. Mandl, G. Shaw, *Quantum Field Theory* (John Wiley & Sons, 1993). ISBN: 9780471105091.

[19] ATLAS Coll., Georges Aad et al., *Phys.Lett.B* **716** (2012) 1-29.
CMS Coll., Serguei Chatrchyan et al., *Phys.Lett.B* **716** (2012) 30-61.

[20] S. Scherer, M. Schindler, *A Primer for Chiral Perturbation Theory* (Springer, 2012). ISBN: 9783642192531.

[21] P. Pal, *An Introductory Course of Particle Physics* (CRC Press, 2014). ISBN: 9781482216998.

[22] D. Gross *Proc.Nat.Acad.Sci.* **102** (2005) 5717-5740.

[16] S. Weinberg, *Physica* **96A** (1979) 327-340.

[23] J. Gasser, H. Leutwyler, *Nucl. Phys. B* **250** (1985) 465.

[24] J. Bijnens, L. Girlanda and P. Talavera, *Eur. Phys. J.* C**23** (2002) 539.

[25] J. Wess, B. Zumino, *Phys. Lett. B* **37** (1971) 95.

[26] E. Witten, *Phys. Lett. B* **223** (1983) 422.

[27] G. Ecker, J. Gasser, H. Leutwyler, A. Pich, E. de Rafael, *Nucl. Phys. B* **321** (1989) 311-342.

[28] M. Knecht and A. Nyffeler, *Phys.Rev.D* **65** (2011) 073034.

[29] P. D. Ruiz-Femenía, A. Pich and J. Portolés, *JHEP* **07** (2003) 003.

[24] P.Roig, J.J. Sanz-Cillero, *Phys.Lett.B* **733** (2014) 158-163.

[30] Particle Data Group, P.A. Zyla et al. *PTEP* **2020** (2020) 8, 083C01.

[31] K. Kamp, J. Novotny, *Phys.Rev.D* **84** (2011) 014036.

[32] T. Kadavy, K. Kampf, J. Novotny, [arXiv:2206.02579 [hep-ph]](2022).

[33] J.D. Jackson *Classical Electrodynamics* (Jhon Wiley & sons, 1999) ISBN: 047130932X.

[34] J.J. Sakurai, J.J. Napolitano, *Modern Quantum Mechanics* (Pearson, 2014). ISBN: 9789332519008.

[35] P. Escribano, J. Terol-Calvo, A. Vicente, *Phys.Rev.D* **103** (2021) 11, 115018.

[36] Muon g-2 Collaboration, G.W. Bennett et al. *Phys.Rev.D* **73** (2006) 072003.

[37] Muon g-2 Collaboration, B. Abi et al. *Phys. Rev. Lett.* **126**, 141801.

[38] FNAL, (2021) *First results from Fermilab's Muon g-2 experiment strengthen evidence of new physics*, [visited in 12/Feb/2023] `https://news.fnal.gov/2021/04/first-results-from-fermilabs-muon-g-2-experiment-strengthen-evidence-of-new-physics/`.

[39] P. Sánchez-Puertas, (2021) *Current progress in the muon g-2*, [visited in 12/Feb/2023] `https://indico.nucleares.unam.mx/event/1717/session/39/material/0/0.pdf`.

[40] J. Schwinger, *Phys. Rev.* **82** (1951) 664-679.

[41] A. Petermann *Nucl.Phys.* **1** (1956) 5, 357-359.

[42] C.M. Sommerfeld *Phys. Rev.* **107** (1957), 328

[43] S. Laporta, E. Remiddi, *Phys. Rev.* **107** (1996) 328.

[44] S. Laporta *Phys.Lett.B* **772** (2017) 232-238.

[45] T. Kinoshita et al. *Phys.Rev.D* **97** (2018) 3, 036001

[46] C. Gnendiger, D. Stöckinger, H. Stöckinger-Kim *Phys.Rev.D* **88** (2013) 053005.

[47] J. Erler, G. Toledo-Sánchez *Phys. Rev. Lett.* **97** (2006), 161801.

[48] F. Jegerlehner, A. Nyffeler, *Phys.Rept.* **477** (2009) 1-110.

[49] J. Gronberg et al. [CLEO Collaboration], *Phys. Rev. D* **57** (1998) 33.

[50] H. J. Behrend et al. [CELLO Collaboration], *Z. Phys. C* **49** (1991) 401.

[51] M. Acciarri et al. [L3 Collaboration], *Phys. Lett. B* **418** (1998) 399.

[52] B. Aubert et al. [BaBar Collaboration], *Phys. Rev. D* **80** (2009) 052002.

[53] P. del Amo Sanchez et al. [BaBar Collaboration], *Phys. Rev. D* **84** (2011) 052001.

[54] [Belle Collaboration]: S. Uehara et al. *Phys. Rev. D* **86** (2012) 092007.

[55] BES III Coll., M. Ablikim *et al.* **Chin. Phys. C 37** (2013) 123001.

[56] S. J. Brodsky and G. R. Farrar, *Phys. Rev. Lett.* **31** (1973) 1153.

[57] G. P. Lepage and S. J. Brodsky, *Phys. Rev. D* **22** (1980) 2157.

[58] V. A. Nesterenko and A. V. Radyushkin, *Phys. Lett.* **B128** (1983) 439.

[59] A. Novikov, Mikhail A. Shifman, A. I. Vainshtein, M. B. Voloshin, V. I. Za-kharov, *Nucl. Phys. B* **237** (1984) 525.

[60] Yining Xian a, Bo-Qiang Ma, *Nucl. Phys. A* **1027**(2022) 122497.

[61] V. Mateu, J. Portolés, *Eur.Phys.J.C* **52** (2007) 325-338.

[62] S. Holz, J. Plenter, C. W. Xiao, T. Dato, C. Hanhart, B. Kubis, U.-G. Meißner & A. Wirzba *Eur. Phys. J. C* **81** (2021), 1002.